The Design of Radio-over-Fibre (RoF) and Free Space optics (RoFSO) Systems for The Indoor and Outdoor Building Networks

Hassan K. Al-Musawi

A thesis submitted in partial fulfilment of the requirements of the University of Northumbria at Newcastle for the degree of

Doctor of Philosophy

Research undertaken in the Faculty of Engineering and Environment

March 2017

Abstract

The 4th generation- long term evolution (4G-LTE) mobile technology is widely adopted that offer both higher capacity and efficient bandwidth usage at a global level. However, considering that in cellular networks the major data traffic mostly occurs indoor, providing high quality can be a daunting task. 4G-LTE provides strong support for both outdoor and indoor coverage by adopting enhanced NodeB (eNB) and home eNB (HeNB), respectively. This research work presents (*i*) a single-mode filtering technique (SMFT) as a simple design, low cost scheme to degrade the dispersion behaviour of the hybrid radio over the multi-mode fibre (MMF) and free space optics (RoMMF-FSO); (*ii*) the hybrid radio-over-fibre and radio-over-FSO (RoF-FSO) system as a solution to extend the indoor coverage of 4G-LTE; and (*iii*) the use of perfluorinated graded-index polymer-optical fibre (PF-GI-POF) for in-building networks. The results show that SMFT may increase RoMMF-FSO bandwidth by 2 GHz and enhance the error vector magnitude (EVM) performance by 4%. The proposed system was also made to experience weak turbulence and thick fog for transmission of 67.2 Mbps 16-QAM 4G-LTE. A design for the residential gateway is proposed as the interface between the 1550 and 850 nm wavelengths. The 100 m of PF-GI-POF is adopted as in-building network with 4G-LTE being transmitted over the proposed hybrid radio-over-POF and FSO (RoPOF-FSO) link under the thick fog condition. The proposed system can transmit 4G-LTE at a data rate of up to 33.6 Mbps and 100.8 Mbps, with the latter encountering a power penalty of ~8 dB to compensate for the induced fog loss. Furthermore, the successful transmission of 60 Mbps at 2.6 GHz was reported to have achieved the EVM of 3.5% and BER 10^{-5} for 300 m of PF-GI-POF.

Acknowledgements

In the name of Allah, the Beneficent and the Merciful. Praise and Gratitude be to Allah for upholding me with perseverance, wisdom and strength throughout this journey, and allowing everything to happen miraculously such that this thesis can be finished accordingly. The journey through my PhD studies, which bears enlightening life and research experiences, fruitful technical achievements and timely completion of this thesis, is impossible without the wonderful people who have walked with me and uplifted me through numerous good and difficult moments. First of all, I would like to express my heartfelt gratitude to my supervisors, namely Dr. Wai Pang Ng and Professor Zabih Gassemlooy for their support, inspiring comments and guidance through my studies. I wish you all the best and further success and achievements in your life.

Moreover, I would like to convey my sincere acknowledgement to my parents and sisters for their continuous support, encouragement and prayers throughout my life. My deepest gratitude goes to my dearest wife, who has persistently accompanied me in completing this journey, I am grateful for her immense patience and support and encouragement during my research. Also, I dedicate this thesis to my lovely children, and I appreciate all their patience and support during father's study.

I am also grateful to the members of the Optical Communications Research Group (OCRG) at the Faculty of Engineering and Environment, Northumbria University for their support during my study. Finally, I also thank the Iraqi Ministry of Higher Education and Scientific Research, the Iraqi Cultural Attaché in London and Kufa University for supporting me during my study abroad.

Declaration

I declare that the work contained in this thesis has not been submitted for any other award and that it is all my own work. I also confirm that this work fully acknowledges opinions, ideas and contributions from the work of others.

Any ethical clearance for the research presented in this thesis has been approved. Approval has been sought and granted by the Faculty Ethics Committee on 24/06/2015.

I declare that the Word Count of this Thesis is 35,772 words

Name: Hassan K. Al-Musawi

Signature:

Date:

Table of Contents

Glossary of Acronyms

1G	1st generation
2G	2nd generation
3D	Three-dimension
3G	3rd generation
3GPP	3rd Generation partnership project
4G	4th generation
5G	5th generation
ADM	Add/drop multiplexer
AEL	Accessible emission limits
AMPS	Advanced mobile phone system
ANSI	American national standards institute
APD	Avalanche photodiode
ASE	Amplified spontaneous noise
AWGN	Additive white Gaussian noise
B2B	Back-to-back
BER	Bit error rate

BS	Base station
BW.L	Bandwidth-length product
CATV	Community antenna television
CDMA	Code division multiple access
CENELEC	European committee for electrotechnical standardization
C-H	Carbon- hydrogen bonds
CO_2	Carbon dioxide
CP	Cyclic prefix
CS	Central station
DAC	Digital-to-analogue
DAS	Distributed antenna system
DFB	Distributed feedback laser
DFE	Decision feedback equalizer
DIY	Do-it-yourself
DL	Downlink network
DM	Direct modulation
DMA	Differential mode attenuation
DWDM	Dense wavelength division multiplexing

E/O	Electrical-to-optical
EDFA	Erbium-doped fibre amplifier
EDGE	Enhanced data rates for GSM
EM	External modulation
eNB	Enhanced NodeB
EVM	Error vector magnitude
F	Fluorine atoms
FCC	Federal communication commission
FDMA	Frequency division multiple access
FEC	Forward error correction
FP	Fabry-Perot laser
FSO	Free space optics
FTTH	Fibre-to-the-home
FTTx	Fibre-to-the-x
FWHM	Full width at half maximum
GI-POF	Graded index POF
GPRS	General packet radio service
GRIN	Gradient index lens

GSM	Global System for Mobile Communications
H	Hydrogen atoms
H_2O	Water vapour
HeNB	Home eNB
He-Ne	Helium-Neon
HSPA	High speed packet access
ICT	Information and communication technology
IEC	International electrotechnical commission
IF	Intermediate frequency
IFFT	Inverse fast Fourier transform
IM	Intensity modulation
IM/DD	Intensity modulation with direct detection
IMT-2000	International mobile telecommunication-2000
InGaAsP	Indium Gallium Arsenide Phosphide
IoT	Internet of Things
IR	Infrared
ISI	Intersymbol interference
J-TACS	Japanese total access communication system

LD	Laser diode
LED	Light emitting diode
LOS	Line of sight
LTE	Long term evolution
MIMO	Multiple-input multiple-output
MLM	Multilongitudinal modes
MMF	Multimode fibre
MMSE	Minimum mean square error
MZM	Mach–Zehnder electro-optical modulator
NA	Numerical aperture
NEC	Nippon Electric Company
NMT	Nordic mobile telephone
O/E	Optical-to-electrical
Ofcom	Office of communication
OFDM	Orthogonal frequency division multiplexing
OFL	Overfilled launch condition
OLP	Optical launch power
OM	Optical mode

OOK	On-off keying
P/S	Parallel-to-serial
PAM	Pulse amplitude modulation
PC	polarization controller
PD	Photodetector
PDF	Probability distribution function
PER	Packet error rate
PFC	Positive frequency chirp
PF-GI-POF	Perfluorinated graded-index polymer optical fibre
PIN	p-i-n photodetector
PMMA	Polymethyl methacrylate
POF	Polymer optical fibre
PON	Passive optical network
PP	Power penalty
QAM	Quadrature amplitude modulation
QoS	Quality-of-service
QPSK	Quadrature phase shift keying
RF	Radio frequency

RG	Residential gateway
RML	Restricted mode launch
RN	Relay node
RoF	Radio-over-fibre
RoFSO	Radio over FSO
RoMMF	Radio over MMF
RoMMF-FSO	Radio over MMF and FSO
RoPOF-FSO	Radio over POF and radio over FSO
RU	Remote unit
Rx	Receiver
SC-FDMA	Single-carrier frequency division multiple access
SCM	Single-carrier modulation
Si-APD	Silicon avalanche photodiode
SI-POF	Step index POF
SMF	Single mode fibre
SMFT	Single-mode filtering technique
SNR	Signal-to-noise ratio
TACS	Total access communication system

TDMA	Time division multiple access
TIA	Trans-impedance amplifier
Tx	Transmitter
UE	User equipment
UL	Uplink network
UMTS	Universal mobile telecommunication system
UWB	Ultra-wideband
VCSEL	Vertical cavity surface emitting laser
VOA	Variable optical attenuator
VoIP	Voice over internet protocol
VSA	Vector signal analyser
VSG	Vector signal generator
WCDMA	Wideband division multiplexing access
WDM	Wavelength division multiplexing
WiMAX	Worldwide Interoperability for Microwave Access
WLAN	Wireless local area network
ZF	Zero forcing

Glossary of Symbols

A_{rx}	Receiver aperture area in free space link
A_{21}	Spontaneous emission coefficient
A_{geo}	Geometric spreading loss of the FSO propagation
a	Optical fibre core radius
B_i	Sellmeier oscillator strength coefficient
B_{21}	Stimulated emission coefficient
C_i	Sellmeier oscillator wavelength coefficient
C_n^2	Refractive index structure parameter
C_T^2	Temperature structure constant
D	Chromatic dispersion parameter
d_{MMF}	Core diameter of the MMF
d_i	Free space link distance
d_{tx}	Transmitter aperture dimeter in free space link
d_{rx}	Receiver aperture dimeter in free space link
dN/dt	Rate of change of carrier density
dS/dt	Rate of change of photon density
E_1	Energy at ground state
E_2	Energy at excited state
$E_i(t)$	Input optical field of MZM
$E_o(t)$	Output optical field of MZM
e	Electronic charge

$erfc(x)$	Complementary error function
$erfcinv(x)$	Complementary inverse error function
f	Operating frequency of the propagating signal
$f_{h_s}(h_s)$	PDF of the atmospheric turbulence
f_{RF}	Carrier frequency of the OFDM signal
f_{UL}	Uplink carrier frequency
g	Refractive index exponent
g_o	Optical gain
g_{th}	Threshold optical gain
$g(x_s)$	Multiplication channel impairment
h	Planck's constant
h_l	Atmospheric loss
h_{FSO}	Channel state of the FSO system
h_s	Attenuation due to scintillation
$h\nu$	Photon energy
$H_{POF}(f)$	Total transfer function of the GI-POF
$H_{SMF}(f)$	Total transfer function of the GI-POF
$H_{MMF}(f)$	Total transfer function of the MMF
$H_{total}(f)$	Total transfer function of the hybrid RoMMF-FSO
$H_{ch}(f)$	Chromatic dispersion frequency response of the GI-POF
$H_{mod}(f)$	Modal dispersion frequency response of the GI-POF
I_{dc}	Biasing current
I_{th}	Threshold current
I_{rf}	Amplitude of the sinusoidal modulation current

I_s	Input signal current
I_p	p^{th}-order modified Bessel function
I_{op}	Received optical intensity
k	Mode group index
k_o	Fitting constant of Bessel function
K	Total number of the mode groups in MMF or POF
k_m	Modulation format-dependent factor
L	Transmission length
L_0	Outer scale of turbulence
L_{cavity}	Laser cavity length
L_{focal}	Lens focal length
L_{total}	Total channel distance in the hybrid RoMMF-FSO
L_M	Link Margin
l_0	Inner scale of turbulence
M	Constellation size
m	Subcarrier index
n_{eff}	Effective refractive index
N	Carrier density
N_0	Noise power spectral density of the RF system
N_1	Ground state
N_2	Excited state
N_s	Total subcarriers number
N_{th}	Threshold carrier density
N_{tr}	Transparency carrier density

NA	Numerical aperture
n_1	Refractive index of core
n_2	Refractive index of cladding
P	Atmospheric pressure
P_o	Received power
P_i	Input power
P_{opt}	Optical power
P_{max}	Maximum magnitude of the ideal transmitted symbol
$P_{MZM}(t)$	MZM power transfer function
P_{fund}	Input power of the fundamental mode in MMF
P_k	Input power of the k^{th} mode group
P_R	Receiver sensitivity
$\rho(v)$	Spectral density of electromagnetic energy
q	Particle size parameter
Q	Q-function
r	Distance from the core centre of the optical fibre
R_o	Reflectivity of n-type Bragg reflector
R_p	Vector displacement between two observation points
S	Photon density
S_{21}	Gain coefficient
$S_{cp}(x)$	OFDM signal with CP
$S_{cp}(t)$	Continuous OFDM signal with CP
$S(x)$	OFDM signal
$S_{RF}(t)$	Up-converted RF OFDM signal

$S_r(x)$	Received OFDM signal
$S_r(x_s)$	Received symbol
$S_t(x)$	Transmitted OFDM signal
$S_t(x_s)$	Transmitted symbol
T	Absolute temperature
T_1, T_2	Temperature at two points separated by distance R_p
T_{th}	Transmittance threshold
t	Continuously varying time of the input signal
t_B	Temporal boundary condition
v	Optical frequency
V_f	Normalized frequency
V_{act}	Volume of the active region
V_{bias}	MZM biasing voltage
V_π	Half-wave voltage
V	Visibility
v_g	Group velocity
w	Radius of the mode distribution
W_B	Beam waist radius of the FSO link
w	Optical wavenumber
x	Time domain index
x_s	Symbol index
$X(m)$	Composite subcarriers of modulated symbols
α	Attenuation coefficient
α_{fund}	Attenuation of the fundamental mode in MMF

α_k	k^{th} mode dependent attenuation
α_{MZM}	MZM insertion loss
α_{total}	Total attenuation in the hybrid RoMMF-FSO
β	Fraction of spontaneous emission
β_l	Atmospheric attenuation coefficient
Γ	Lateral confinement factor
Γ_z	Longitudinal confinement factor
Δ	Refractive index contrast
ϵ	Profile dispersion parameter
ζ	Gain saturation coefficient
η	Internal quantum efficiency
$\eta\ (x_s)$	Additive white Gaussian noise (AWGN)
η_w	Weighting constant of Bessel function
θ	Laser divergence angle
θ_B	Tx lens divergence angle
λ	Propagating wavelength
λ_o	Maximum sensitive wavelength for human eye
μ_0	Mean value of the zero symbol level
μ_1	Mean value of the one symbol level
σ_λ	Laser linewidth
σ_I^2	Scintillation index
σ_R^2	Rytov variance
σ_X^2	Log-amplitude variance
σ_0	Standard deviation of the zero symbol level

σ_1	Standard deviation of the one symbol level
τ_c	Carrier life time
τ_{fund}	Group delay of the fundamental mode in MMF
τ_k	k^{th} mode group delay
τ_p	Photon life time
ω_{RF}	Carrier frequency converted from Hz to rad
ω_m	Modulation frequency for the sinusoidal modulation current

List of Figures

List of Tables

Chapter 1

Introduction

1.1 Growth and Evolution in the Field of Communications

The rapid development of the mobile communications in recent years and the implications it may possibly have on the mobile operators to fulfil the increasing demand in terms of coverage and data services have widely been discussed. In this regard, a massive growth and considerable deployment of optical systems may offer some workable solutions to cope with the wireless traffic bottleneck [1].

Figure 1.1 illustrates a statistical data which was measured and predicted by Ericsson [2]. It specifically highlights the global subscription growth for both the fixed and mobile broadband services from the year of 2011 till 2021. It can be seen that the growth rate for the mobile services is relatively more significant than to those of the fixed services. Notably, the total mobile subscriptions until the year of 2016 were about 7.4 billion, from which 63 million were new subscribers in the first quarter of

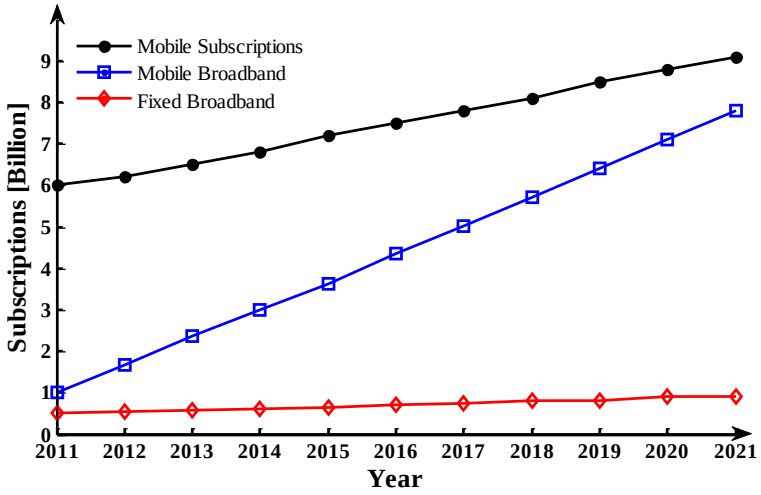

Figure 1.1: The growth of both mobile and fixed broadband services [2]

2016. More interestingly, it is projected to reach an estimated 9 billion by the end of 2021. The increase of the mobile broadband is due to the large bundles of data services that offered by the mobile operators [3].

A direct inference which can be drawn from the discussion in the foregoing is that the ever increasing demand for the mobile broadband usage is one of the most important issues that may adversely affect the mobile communication sector. In reference to the above-mentioned figure, the global data traffic growth is reportedly up by 63% between the year of 2015 and 2016 [4] and it is predicted to increase 10 fold by the year of 2021 [2]. A recent study reported in [3] shows that the use of smart phones and tablets are increased from 86% to 95% in a population of 1.27 billion people between the year of 2015 and 2016 in the Europe and United States. It is noteworthy that the recently increased smart phone subscription in addition to the trend of adopting the concept of the internet of things (IoT) and an aggregate increment of the average data volume per device may account for such a rapid increase observed in data traffic. In order to cope with the increasing demand for larger volume of data

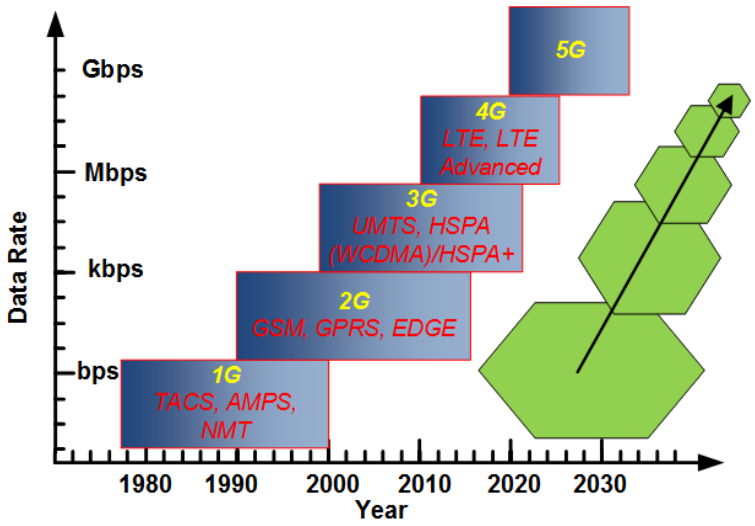

Figure 1.2: The evolution of mobile communication technologies

more efficiently, a number of mobile network topologies have recently been developed by the mobile operators as indicated in Figure 1.2. It has to be noted that the first generation (1G) of the international mobile communication system, which was established in the 1980s utilizes an analogue technology. The most established systems associated with the 1G were the Total Access Communication System (TACS) in Europe, Nordic Mobile Telephone (NMT) in the Nordic or Scandinavian countries, Analogue Mobile Phone System (AMPS) in the USA, and the Japanese Total Access Communication System (J-TACS) in both Japan and Hong Kong. It is worth highlighting that their standards were narrowband, mostly designed for voice services and they support low bandwidth, for which the peak data rate was just at 9.6 kbps [5]. In contrast, the second generation (2G) was the next stage of wireless system development. Notably, it was the first digital mobile system which came to be known as the Global System for Mobile Communications (GSM), which provided data services over the mobile systems by means of enabling transmission of text messages, emails, and other data applications. The GSM technology was further developed later to support relatively higher data rate of up to 114 kbps by means of transmitting packet data using General Packet Radio Services (GPRS) technology. Subsequently, the Enhanced Data Rates for GSM Evolution (EDGE) technology that supports relatively faster data rates and higher throughput capacity i.e., 3 to 4 times in comparison with the GPRS was adopted [6, 7]. It was not the end as further improvement continued to be made in order to provide better services such as video calling, streaming, and gaming. Such services were made available by means of the 3rd generation (3G) system which was better known as the Universal Mobile Telecommunication System (UMTS). This system was developed to provide the subscribers with services which are of better quality such as the ones involving data

and multimedia [8]. It is also worth highlighting that the 3G UMTS wideband networks managed to fulfil the requirements of the International Mobile Telecommunications-2000 (IMT-2000), which were introduced by the 3rd generation partnership project (3GPP) organisation in the year of 2001 [5, 9]. The roles of 3GPP involve to help enhancing and defining the mobile system standards from almost every region of the world and to provide the updated standards using system of "Releases", which are delivered to the mobile network operators as a work plan [10]. Accordingly, the 3GPP introduces High Speed Packet Access (HSPA) based on the Wideband Code Division Multiple Access (WCDMA) technology to help enhance the capacity of the mobile systems, support the voice over internet protocol (VoIP), and achieve higher data rate of up to 14 Mbps, which is presently further improved to 28 Mbps in HSPA+ systems [6, 11]. In its 8th release, 3GPP developed the 4th generation-long term evolution (4G-LTE) as a framework for it to further develop the existing radio technologies, which may help meet the rapid increase observed in the data requirements [12]. The work plan within 3GPP has continued to develop LTE towards the culmination of the LTE-Advanced in Release 10 and beyond, which can be considered as a giant step in the evolution of LTE over the years. The 4G-LTE is supporting 69% of the total mobile data traffic in 2016 [4]. As the demand by both new and existing users has always been one the rise, it is more likely that the 4G technology and its infrastructure may have to migrate to fifth-generation (5G) mobile systems [13], which is designed to supply multi-gigabit broadband services such as ultra-high definition video [14]. The growth of the mobile communication technologies can be seen in the targeted peak rate, range, and cell size as presented in Table 1.1, in which the data were obtained from [5, 14, 15].

Table 1.1: The outline of the main mobile technologies

Technology	Multiplexing Protocol	Spectrum [MHz]	Peak Data Rate	Cell Radius [km]
AMPS/NMT	FDMA	150/450	9.6 kbps	40
GSM	TDMA	900 / 1800	9.6 kbps	35
GPRS	TDMA	900 / 1800	171.6 kbps	35
EDGE	TDMA	900 / 1800	473.6 kbps	26
UMTS	CDMA	873 / 1900	2 Mbps	2
HSPA	CDMA	2100	14.4 Mbps	1.23
LTE	SC-FDMA (UL)/OFDM (DL)	800 /1800 / 2600	100 Mbps	1 km
LTE-A	SC-FDMA (UL)/OFDM (DL)	800 /1800 / 2600	1 Gbps	1 km
5G-Multi-radio access	MIMO OFDM	3-90 GHz	>1 Gbps	<100 m

1.1.1 LTE Concepts

As it was highlighted in the earlier section, the 4G-LTE mobile technology is widely adopted by almost every mobile operator in their attempts to offer higher capacity and efficient bandwidth usage on a global scale [16].

It is worth highlighting that the shift from the 3G technologies into the 4G was primarily due to the remarkable advancement made within the communication technology. It is particularly about the advancement in the mobile devices, which have been developed with their processor performance, power consumption, and relatively larger memory size. Besides, the huge bandwidth backbone based on the optical fibre has further led to the rapid increase of using internet services unconventionally over the smart phones. In this regard, the 4G-LTE introduced a network architecture that included enhanced NodeB (eNB) and home eNB (HeNB) for both outdoor and indoor wireless applications, respectively [17]. Despite such a positive development, the increasing demand for the mobile broadband usage and the possible implications such

an increase may have on the mobile communication sector have been one of the mostly discussed issues. The LTE which many consider as a sophisticated technology was introduced into the market to meet the rapid increase observed in the number of users and broadband applications by providing relatively higher data rates, better coverage, lower latency and more importantly, maintain the quality of service (QoS) [18].

It has to be noted that the main objectives of the LTE technology are to, inter alia, enhance data throughput for both downlink (DL) and uplink (UL) scenarios in comparison with the previous mobile technologies. In this regard, LTE uses the adaptive modulation and coding scheme, in which the modulation scheme is altered in line with the channel condition for user equipment (UE). In addition, the LTE uses single carrier modulation (SCM) of the quadrature phase shift keying (QPSK), 16-quadrature amplitude modulation and 64-QAM modulation. One of these SCM schemes is adopted to generate number of subcarriers. The SCM subcarriers are then multiplexed using orthogonal frequency division multiplexing (OFDM) and single carrier frequency division multiple access (SC-FDMA) as a multiple access in the DL and UL, respectively. At first, the LTE data rate capability was to deliver 100 Mbps with 2x2 multiple input multiple output (MIMO) antenna configuration, which at present has been increased to 300 Mbps using 4×4 MIMO. An increased demand for a relatively higher data rate over long distance links may account for the adoption of MIMO OFDM communication systems. It is noteworthy that another increase in the peak rate was observed in the year of 2015 up to 450 Mbps by adopting of LTE-Advanced, which is targeted to reach 1 Gbps transmission rate [19]. Moreover, LTE technology is designed to support high mobility communications such as while travelling in trains and cars, particularly, for the transportations moving at a speed of up to 350 km/h [20].

1.2 Problem Statement

The targets discussed in the foregoing sections can be achieved by means of increasing the density of the base stations (BSs), which may in turn help enhance the system performance. Most of the recent BSs have been used for either the macro or micro cells with the cell radius of 1 km by relying on the framework of eNB. More specifically, eNB assigns the resources to the UE for both DL and UL. Taking a closer look at the smart LTE architecture, shows that the radio access network uses a single type of node i.e., eNB, which is designed with built-in operation of the central station (CS) [5]. In addition, eNB is responsible for all signal processing functions such as the modulation to the higher order format, and up-conversion of the carrier frequency and amplification [21]. Note that, such integrated functions make the design of eNB rather complex with costly structure [22]. Furthermore, the allocated LTE spectrum for the urban areas is 1.8 GHz and 2.6 GHz in contrast to the LTE spectrum for the rural areas i.e., 800 MHz [22, 23]. It is also worth highlighting that there is a need to address the significant traffic growth by means of adopting relatively higher frequency bands as proposed in the next generation 5G technology, which is designed to operate in a spectrum of between 3 - 90 GHz [14]. Notwithstanding such potentials, the transmitted radio frequency (RF) signals beyond the 2 GHz will possibly experience high propagation losses, which will result in low penetration levels to the walls and buildings. According to [24], the propagation path loss for the signal at 2.6 GHz transmitted for 1 km in urban area is ~107 dB. Note that, such losses along with high multipath losses in the urban environment have reportedly resulted in providing rather poor indoor coverage [25], which is also worsened by the degradation in the signal-to-noise ratio (SNR). In order to overcome high penetration loss, it is sensible to adopt multiple scenarios such as increasing the number of eNB or emitting more power from

both the eNB and UE using high power amplifiers. However, both solutions may reportedly have a number of drawbacks such as the high cost, complexity and its potential impact on the UE battery lifetime as the amplifiers may consume most of the battery power [25]. On the other hand, the higher modulation schemes, which are required for relatively higher data rates can be difficult to achieve for indoor networks owing to the deterioration observed in the channel conditions within eNB cell edge locations [26]. In [27], it was demonstrated that the indoor UE may consume an estimated 80% of all mobile broadband traffic. In addition, a recent estimation by [28] and [26] indicated that 45% of households and 30% of businesses have equally experienced poor indoor coverage.

Enhancing the indoor coverage can be a real challenge for the indoor radio planning between the operating networks and the mobile users, for which there rises a need for the adoption of some special techniques such as the distributed antenna systems (DAS) and femtocell technology. Historical records reveal that the DAS idea was founded in the 1980s and was subsequently developed by the operators to split the transmitted power between separated low power antenna units, which cover the in-building areas [26]. DAS system was proposed by using passive components such as the splitters and coaxial cables. However, such components were used for the GSM only as the 3G and beyond technologies on the other hand, use relatively higher frequencies, for which the signal is degraded greatly owing to the high attenuation of the passive components in such frequencies. The estimated loss for the 0.5-inch coaxial cable is about 11 dB per 100 m on frequencies beyond 2 GHz [29], for which the use of coaxial cable for bigger buildings is not always possible. This is because of the installation problems and limited positions for the antennas due to the weight and cable rigidity.

It is worth highlighting that one of the most promising candidates to overcome the drawbacks of the passive DAS system is the integration with the optical technology using radio-over-fibre (RoF) [30]. In recent years, the fibre-to-the-x (FTTx) technology has already widely been implemented on a global scale to provide the broadband services to the premises and buildings. The FTTx links may serve as the ideal infrastructure for the in-building network by means of implementing the RoF networks without having to fulfil any significant hardware requirements [31]. The RoF technology has notably drawn a growing interest for in-building applications owing to a number of advantages such as enhancing the coverage by using the low power DAS systems and the tremendous bandwidth of the optical fibre, which can handle bandwidth-hungry applications [32]. In the RoF-DAS, active components are used such as the master unit or residential gateway (RG), remote unit (RU) and the optical fibre. It has to be noted that the RG is the interface between the access and in-building networks, in which controlling the signals and adjusting the power levels can be performed by means of the internal converters and amplifiers. In the RU, optical-to-electrical conversion and vice versa is performed prior to beaming the radio signal by means of the antenna. The optical fibre is used for transmitting the optical signal between the RG and RU for relatively longer distance in comparison with the conventional copper cables and it is also capable of supporting multi-radio services simultaneously. RoF-DAS technology can be considered the optimal solution to extend the indoor coverage owing to factors such as providing scalable architecture, flexibility and easier installation [33].

On the other hand, the 3GPP LTE is capable of addressing the indoor coverage by means of the HeNB in the promising small cells technology, which was suggested in Release 12 [5] and Release 13 [19]. The small cells refer to the femtocells (i.e., home

base stations) and picocells, which are both capable of covering distances of up to 30 m and ~100 m, respectively. They are able to do so owing to the relatively lower power that is transmitted from their base stations along with the effects of reflections and deflections from the walls and other indoor obstacles [26]. It has to be noted that the pico/femtocells are cellular network access points, which are proposed for the indoor applications to connect the standard mobile UE to the mobile operators. It can be done by means of either the residential broadband access such as copper cable, which is capable of offering a transmission of 3 Mbps and 128 kbps for DL and UL, respectively [34], or using optical fibres along with the wireless last-mile technologies [26]. The pico/femtocells are usually operated under the coverage of the larger cells such as microcells or macrocells and they may deploy the same licence spectrum [35].

Despite the similarities between the DAS and small cell scenarios, particularly in the output power and coverage area, both technologies differ in terms of the operation techniques. DAS operates as point-to-multipoint solution, where all the distributed antennas connected to main node (i.e. RG). Additionally, DAS performs the process of optical to electrical conversion and converting the DL radio signal to the UE, and simultaneously carries the UL radio signal from the UE back to the RG. On the hand, small cell technology uses small indoor base stations (i.e HeNB), which have the ability of performing all the complicated signal processing such as the modulation, multiplexing and coding. In RoF-DAS, the HeNB operates as RU to extend the indoor coverage with less complicated design.

The use of RoF-DAS technology offers several advantages for both mobile users and operators. As for the users, this technology offers better mobile coverage in the indoor environments, relatively higher data transfer performance, lower transmission of power and an extended UE battery life. In contrast, the benefits for the operators

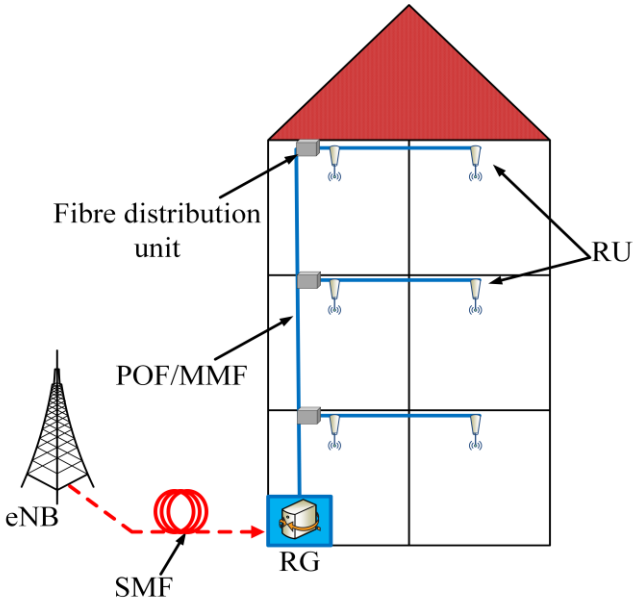

Figure 1.3: Indoor coverage using RoF-DAS technology

are such as the enhancement of the indoor coverage, which may help increase the network capacity and number of users. In addition, it also helps decrease the growth of the macrocell backhaul costs [36]. Furthermore, in a recently reported study [35], it was shown that the use of the residential DAS in the urban areas may decrease the total energy consumption by 60% among the high data traffic users. Linking this with the LTE, it has to be noted that the femtocells include the HeNB, which operates as RU to extend the indoor coverage. As the femtocell are considered as the secured extension to the mobile services within buildings, therefore they are linked over the IP broadband that can be provided by the FTTx technology, which can be extended to the in-building RoF to help reduce the small cell architecture complexity. The process of wireless signal generation and modulation can be carried out within the eNB, at which the optical fibre is used to distribute the signals to the antenna stations [37].

Figure 1.3 illustrates an example for such an extension by means of a typical RoF application of the DAS for in-building network, in which the RG and RU are used to

enhance the indoor 4G-LTE coverage. The single-mode fibre (SMF) connects the RG with the eNB, upon which most of the signal processing is performed. Traditionally, a SMF is used for the long-haul backbone networks due to factors such as its huge bandwidth, low attenuation and low chromatic dispersion. It is also worth highlighting that the SMF offers a bandwidth of at least 25 THz, for which the transmitted signal may experience an attenuation and chromatic dispersion of ~0.2 dB/km and ~17 ps/nm.km at 1550 nm optical wavelength, respectively [38, 39]. However, the requirements for cost-effective solutions of in-building networks are seen as part of the main constraints for adopting the SMF fibres. For the indoor applications, the multi-mode-fibre (MMF) and polymer optical fibre (POF) are commonly used for both the local area networks and the last mile access networks. Presently, the MMF is identified by their optical mode (OM) as outlined in the ISO/IEC 11801 standard [40]. It is considered as a fibre backbone infrastructure in the existing buildings, particularly the OM1 and OM2 that are capable of supporting data rate up of up to 1 Gbps or OM3 and OM4, which on the other hand are capable of supporting data rate of up to 10 Gbps [41]. The global MMF infrastructure, which is currently installed in-buildings, is about 17 million km [42]. Moreover, the promising solution for such networks uses the POF as a channel in order to transport the wireless signals due to the conveniences in relation to the installation, maintenance, connectorization, and small bending radius [43]. The POF notably offers the potential low cost solution for indoor networks in terms of devices along with the possibility of sharing the existing ducts with the electrical cables [44]. However, it has to be borne in mind that the POF channels may however experience relatively higher attenuation levels for around 100 dB/km [45], which may in turn lead to a substantial signal attenuation because of the reduction observed in the received power and SNR. In relation to such a scenario,

a practical investigation was reported in [46], which showed a transmission of 53.3 Mbps over 200 m of POF using OFDM for the ultra-wideband (UWB) applications in RoF networks.

Additionally, the multi-mode propagation phenomenon, which means the simultaneous excitation of various modes inside the fibre core may generate the modal dispersion, which may typically take place at the rate of ~10 ns/km [47]. Such a modal dispersion is capable of limiting the MMF or the POF bandwidth significantly owing to the pulse broadening that may potentially lead to the intersymbol interference (ISI). Consequently, the fibre capacity and bandwidth may remain limited for relatively shorter distance applications such as the residential building with a typical distance of between 100 m and 300 m [48, 49]. A serial transmission of 64 Gbps and 56 Gbps was reported to take place over 57 m and 157 m MMF, respectively, achieving bit error rate (BER) less than 10^{-12} using on-off keying (OOK)[50, 51]. In the study of [52], the same BER for a rate of 48.7 Gbps was presented for 200 m MMF by means of using pulse modulation scheme along with the signal processing formats for dispersion compensating. In this regard, several techniques have already been proposed to mitigate the modal dispersion using signal processing or electronic equalizer schemes within the receiver. Such equalizers are, inter alia, the zero forcing (ZF) or the minimum mean square error (MMSE) equalizer, or even nonlinear equalizers like decision feedback equalizer (DFE). However, such techniques are not exempt from major drawbacks for either. They include the inefficient performance owing to the significant noise enhancement, particularly to the linear schemes, or relatively higher complexity designs which may increase exponentially with the received data rate along with the channel estimation requirements [47, 53]. An electronic equalizer was adopted in [54] to target the data rate of 1.25 Gbps over 50 m of POF achieving BER

of 10^{-9}. Moreover, a transmission of 2.1 Gbps over 100 m POF by means of using DFE was reported in [55]. However, it is worth highlighting that these techniques included additional complexities to the system in terms of the pre-channel characterization. Besides, in some applications, there is no guarantee that the typical equalizer methods such as the ZF or the MMSE equalizer are capable of compensating the effect of the modal dispersion totally as was reported in [56]. Therefore, several physical techniques have been proposed to reduce the number of propagating modes at the receiver such as the single-mode filtering technique (SMFT) [57], and the offset launch technique [58].

Along with the wireless RF and RoF technologies, the free space optics (FSO) has also equally drawn attention to provide relatively higher data rate wireless connectivity. The transmission of RF signals over the FSO channel, which is known as radio-over-FSO (RoFSO), is an attractive option in the existing "last mile" access networks [59] along with the wireless local area networks (WLANs) [60, 61]. The FSO technology notably offers higher bandwidth, free license, low deployment cost, and immunity to the electromagnetic. However, the performance of FSO links can be degraded severely owing partly to the atmospheric channel conditions such as smoke, fog, and turbulence [53]. It is noteworthy that the combination of RoF and RoFSO technologies can be adopted to extend the multi wireless services for access, WLAN and in-building networks in rural and urban environments. The RoF technology has already been proposed for both networks while the RoFSO link can be deployed in places where there is no fibre optic infrastructure in place (i.e., mostly in rural areas).

1.3 Aims and Objectives

Considering the discussion in the foregoing, the aim of the present study therefore is to introduce the RoF and RoFSO systems to help enhance the performance of the indoor 4G-LTE communication networks for the inter and intra-building networks. The RoF is expected to be a more suitable design to help enhance the indoor coverage for the 4G-LTE networks, while the RoFSO technology is adopted to extend and connect multi-indoor RoF links for both the rural and urban environments. The integration between both systems may culminate in a hybrid system of RoF and RoFSO (RoF-FSO).

The objectives of this research include:

1. The simulation of the hybrid RoF-RoFSO using 4G-LTE at 800 MHz and 2.6 GHz for the rural and urban areas, respectively.
2. Evaluate the system performance using the quality metrics such as the error vector magnitude (EVM), and BER.
3. Propose an efficient and simple design technique to compensate the modal behaviour of the MMF channel in the hybrid radio over MMF and FSO channels (RoMMF-FSO).
4. Experimental implementation of the proposed hybrid RoMMF-FSO system to verify the theoretical model along with validating the system design under real weather conditions such as turbulence and fog.
5. Propose and design a practical system to transmit the 4G-LTE signal over longer possible POF channel for the indoor environment, which can be affected by limiting factors of the relatively higher attenuation and modal dispersion.

1.4 Original Contribution

The original contributions to the world of knowledge from this study are summarised in the following:

- A hybrid RoMMF-FSO optical system is proposed in chapter 3, which includes both MMF and FSO channels as a solution to extend the transmission of the LTE signals. The hybrid system is intended to connect multi building networks in the last metre (inter-room networks) and the last mile of the access networks in urban areas. A system performance is investigated to look into the potential impact of the modal dispersion in the transmission system. In this regard, the SMFT filtering technique is adopted to enhance the hybrid system performance under a weak turbulence effect. In the SMFT, a simple patchcord of SMF was used in order to attenuate the modal effects in such hybrid systems. It is noteworthy that the investigation was carried out in terms of the of the total system transfer function, laser beam profile at the receiver and the EVM results of the received LTE signal. The results have been published in [C1], [C2] and [J1].
- In chapter 4, the performance of the hybrid RoMMF-FSO optical system is investigated under the impact of atmospheric fog in the rural areas. The SMFT was used to enhance the performance of the 4G-LTE signal and verified by means of using link budget and EVM analysis. These results have been published in [C3].

- A design for the RG is proposed in chapter 4 as a workable solution to connect indoor mobile users to the backbone core network particularly, for the rural environments. The proposed system employed the hybrid radio over POF and radio over FSO (RoPOF-FSO) in sparsely populated regions with low cost solutions in comparison with the existent coaxial copper cables. These results have been published in [C4].
- As the QoS of the 4G-LTE for in-building networks degraded at a relatively higher frequency, a practical RoF system is therefore proposed in chapter 5 in order to help optimise the indoor coverage by adopting the low cost vertical cavity surface emitting laser (VCSEL) as a direct modulated (DM) laser and PF-GI-POF as an optical channel. The resulting output has been published in [C5].

The overall contribution of this research is graphically illustrated with a research road map as depicted in Figure 1.4.

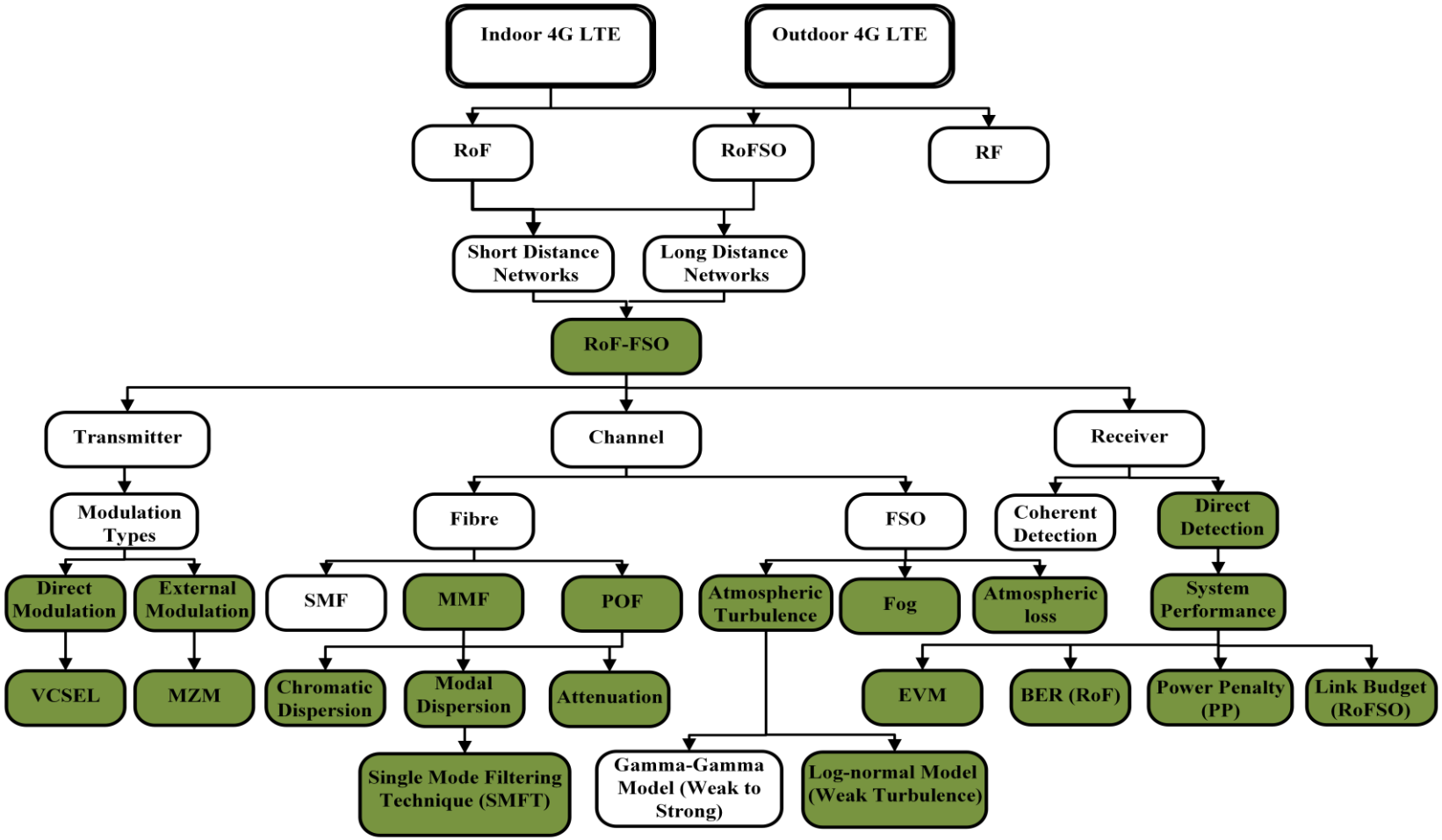

Figure 1.4: Block diagram of the original contributions of the study

1.5 Research Outcome

The outcomes of the research programme have either been published or peer-reviewed for publications in journals and conferences. They are enlisted in the following:

Journals

[J1] H. K. Al-Musawi, T. Cseh, J. Bohata, W. P. Ng, Z. Ghassemlooy, S. Zvanovec, E. Udvary and P. Pesek, " Adaptation of mode filtering technique in 4G-LTE hybrid RoMMF-FSO for last-mile access netrwork," *Journal of Lightwave Technology*, vol. PP, pp. 1-1, 2017.

Conferences

[C1] H. K. Al-Musawi, T. Cseh, J. Bohata, P. Pesek, W. P. Ng, Z. Ghassemlooy, E. Udvary, T. Berceli, and S. Zvanovec, "Experimental optimization of the hybrid RoMMF-FSO system using mode filtering techniques," in *2016 IEEE International Conference on Communications Workshops (ICC)*, 2016, pp. 405-410.

[C2] H. K. Al-Musawi, T. Cseh, J. Bohata, P. Pesek, W. P. Ng, Z. Ghassemlooy, E. Udvary, S. Zvanovec, and M. Ijaz, "Fundamental investigation of extending 4G-LTE signal over MMF/SMF-FSO under controlled turbulence conditions," in *2016 International Symposium on Communication Systems, Networks and Digital Signal Processing (CSNDSP)*, 2016, pp. 1-6.

[C3] T. Cseh, H. K. Al-Musawi, M. M. Abadi, Z. Ghassemlooy, W. P. Ng, E. Udvary, T. Berceli, and S. Zvanovec, "Improvements in combined radio over multimode fibre and radio over FSO systems by applying mode filtering," in *2015 17th*

International Conference on Transparent Optical Networks (ICTON), 2015, pp. 1-4.

[C4] H. K. Al-Musawi, T. Cseh, M. M. Abadi, W. P. Ng, Z. Ghassemlooy, E. Udvary, and T. Berceli, "Experimental demonstration of transmitting LTE over FSO for in-building POF networks," in 2015 *17th International Conference on Transparent Optical Networks (ICTON)*, 2015, pp. 1-4.

[C5] H. K. Al-Musawi, W. P. Ng, Z. Ghassemlooy, C. Lu, and N. Lalam, "Experimental analysis of EVM and BER for indoor radio-over-fibre networks using polymer optical fibre," in *2015 20th European Conference on Networks and Optical Communications- (NOC)*, 2015, pp. 1-6.

[C6] N. Lalam, W. P. Ng, X. Dai, and H. K. Al-Musawi, "Characterization of Brillouin frequency shift in Brillouin Optical Time Domain Analysis (BOTDA)," in *2015 20th European Conference on Networks and Optical Communications- (NOC)*, 2015, pp. 1-4

1.6 Thesis Organization

This thesis is mainly focused on the research work dedicated to the integration between the RoF and RoFSO networks in terms of the indoor coverage for the 4G-LTE at 2.6 GHz and 800 MHz. The organisation of this thesis is divided into six main chapters focusing on the outcomes of the research including a review of literature, original contributions, conclusions and the implications for future works. More specifically, chapter one outlines the principle introduction and provides an overview of the recent developments in the mobile communications including the related mobile technologies, particularly the 4G-LTE. In addition, the problem statement, aims and objectives, original contributions of this research as well as the resulting publications are provided in the same

chapter. Moving on, chapter two presents a detailed introduction on both RoF and RoFSO covering the significant parts which are required to construct a hybrid RoF-RoFSO network including MMF, POF and FSO channels, and as well as the main challenges in relation to the hybrid system performance. Also, the theoretical expressions that can be used to model the hybrid RoMMF-FSO and RoPOF-FSO networks are discussed too. Next, chapter three delineates the modal behaviour of the MMF in the Hybrid RoMMF-FSO in the last-mile access networks. Theoretical and experimental models are presented including the use of the SMFT as a physical solution to mitigate the modal dispersion under atmospheric weak turbulence effect. This is followed by the chapter four, which is divided into two main sections. The first section addresses a further practical investigation of using the SMFT on the hybrid RoMMF-FSO but under foggy weather. In contrast, the second section is dedicated to the RG design in the hybrid RoPOF-FSO. Next, chapter five introduces the theoretical and experimental models for the RoF, which can be used to help enhance the 4G-LTE indoor coverage including the use of the VCSEL along with the PF-GI-POF as the most suitable low cost candidates. Finally, chapter six concludes this study and outlines some recommendations for future works in the field to help enhance the indoor coverage for the next generation mobile technology, namely the 5G technology.

Chapter 2

Fundamentals of Hybrid Radio-Over-Fibre and Free-Space Optics Communication Systems

2.1 Introduction

In the ancient history, light was mostly used by most of the civilizations on record for communication purposes. Their optical signalling methods varied from mirrors, smoke signals, and fire beacons to convey messages to their intended audience. The underlying ideas of such methods were taken to another level with the invention of the first optical telegraph in the year of 1794 based on visible coded signals. The newly invented optical telegraph served two French cities which were 200 km apart by means of relay stations [47]. However, the use of this method was found ineffective due to its relatively higher cost but lower efficiency in comparison with the electrical telegraph. It has to be noted that the first free space optics (FSO) channel was the Photo-phone patent, which was demonstrated by Alexander Graham Bell in the year of 1880 [62, 63]. In this regard, the main idea of the experiment was using intensity-modulated sunlight beam to transmit voice data over the air for 200 m. Despite such an effort, the patent did not succeed due to the irregular nature of sunlight along with weaknesses of the devices used. With the earliest use of Light Amplification by Stimulated Emission of Radiation device (LASER) by T. H. Maiman at the Hughes research laboratory in 1960s, the era of optical technology has therefore transformed [64]. The invention of the LASER has been one of the most

significant scientific achievements in the twentieth century. The FSO demonstrations which were recorded within the span of 1960s and 1970s include the first TV over FSO in the year of 1963 [65].

It is also worth highlighting that the significant contribution of both Charles K. Kao and George Hockham who jointly found a way to reduce the losses incurred through fibres by an estimated 20 dB/km for inter-office communications was another major development. It was suggested that a dielectric fibre which uses cladding with a relatively lower refractive index than the core could a potentially practical solution for the guiding of light [66]. More related studies looking into reducing the fibre losses incurred were carried out in the 1970s. Such studies began with the use of light wave systems operating at 800 nm wavelength and subsequently shifting to the 1310 nm by means of which, the losses were reduced to ~1 dB/km, in addition to the chromatic dispersion at a zero level. However, the capacity of the optical systems was limited only to ~100 Mbps owing to the modal dispersion in the multi-mode fibre (MMF) [47]. Such a limitation was overcome in the 1980s by means of single-mode fibre (SMF), in which the modal dispersion was eliminated. The next step was about shifting the optical system to operate at the 1550 nm, which was capable of keeping the fibre loss at the lowest i.e., as low as 0.2 dB/km and enabling longer span between the repeaters. Also, the appearance of an erbium-doped fibre amplifier (EDFA), which operates at the 1550 nm window, drew the attention of scholars for long distance optical systems. However, fibres at this wavelength window exhibited a chromatic dispersion of ~17 ps/(nm.km), which can be considered as the major linear impairment in the SMF systems [39].

Three main infrastructures are part of traditional terrestrial telecommunication networks, namely the access network, the metropolitan area and the core network. By means of the access network, the end users are able to connect to the rest of the network system within the range of a few kilometres. In contrast, the metropolitan network is

capable of covering metropolitan areas of up to a few hundred kilometres, and it notably consists of both the access and in-building networks. Better still, the core network is capable of aggregating the traffic from multiple metropolitan networks and it may route the data to the backbone channel of the network for a few thousands of kilometres [67, 68].

With the advent of relatively higher volume of internet applications, which rely on data streaming, an explosive growth of data communication traffic has in turn been observed over the years. Such a development has culminated in a substantial increase for the network capacity. In addition, the bandwidth requirements in this regard may equally have to cope with such an increasing traffic demand, failing which may lead to the radio frequency (RF) spectrum congestion. It is noteworthy that the shift from the RF carrier into the optical carrier can be considered as a workable solution due to the latter's huge bandwidth and a relatively lower energy consumption [69, 70]. The technology of transmitting information signals to the end users over the optical fibre is known as the radio-over- fibre (RoF). In employing 4^{th} generation- long term evolution (4G-LTE) technology, there is a need for the adoption of a framework to help improve the coverage and capacity of both the outdoor and indoor wireless applications by using the enhanced NodeB (eNB) and distributed antenna system (DAS), respectively [17]. In this regard, the SMF has been proposed as an effective channel for the long-haul networks due to its huge bandwidth, low attenuation and low chromatic dispersion [71]. Notwithstanding, as the coverage of the eNB base stations is limited to 1 km only, expanding the wireless coverage for relatively longer distance can be quite challenging. Alternatively, a relay node (RN) was proposed in [72] as a more efficient solution for further outdoor coverage extension. In relation to its mechanism, the RN is located in the RF cell edge in order to link the end users with the eNBs by means of the SMF based network, and the RoF may deal with the

interface between the eNB and RN. In addition, the RoF technology can be effectively used for the in-building networks to help strengthen the 4G-LTE indoor signal coverage, which is considered relatively weaker indoors owing to low penetration levels [26]. On the other hand, within the terrestrial communication systems, the radio-over-free-space optics (RoFSO) technology can be adopted for the last mile access networks in order to extend the broadband connectivity to the regions, in which the fibre may not be available.

This chapter therefore discusses the terrestrial access networks using both RoFSO and RoF technologies and their specifications in terms of their features, applications, system block diagram and challenges for each technology. Figure 2.1 depicts a scenario of using both technologies in both densely and sparsely populated areas. The RoF technology uses the SMF for the long-haul networks, while the polymer optical fibre (POF) or the MMF is deployed for the short distance in-building networks for connecting the residential gateway (RG) with the remote unit (RU). The FSO links with the line-of-sight (LOS) links are used to inter-connect buildings as part of the “last mile” connectivity.

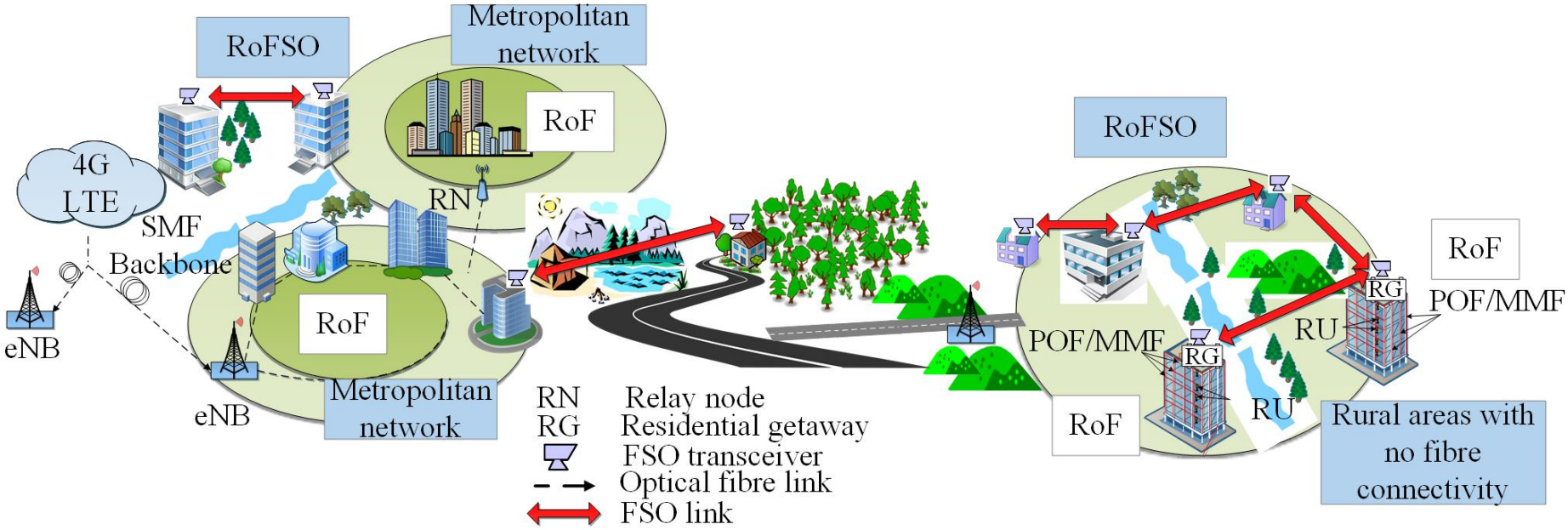

Figure 2.1: A scenario of deployment of RoF and RoFSO in both urban and rural areas

2.2 An Overview of Radio-Over-Fibre

Both fixed and mobile wireless networks in recent years have intended to deliver high-speed broadband services. Notwithstanding, owing partly to the insufficient bandwidth of the low frequency ranges, the wireless systems have been operating in the high microwave frequency band (usually in GHz). In the cellular systems, a considerable amount of attention has been turned to use small cell architectures to simultaneously help improve the coverage and increase the traffic capacity. Therefore, both the 4G and 5th generation (5G) cellular systems are now widely adopting either the picocell or femtocell as their framework in line with the predicted future data traffic. It is worth highlighting that the complexity and the cost of the BSs for such systems can be considered as critical parameters. The RoF technology, which many scholars consider as a promising technique to deliver broadband services is the main part of the emerging optical-wireless networks [72].

RoF refers to the technology, by means of which light is modulated by RF signal and it is subsequently propagated through an optical fibre channel. In general, three methods are mostly applied for transmitting radio signals over fibre by means of direct intensity modulation (IM) i.e., baseband, intermediate frequency (IF) and RF band transmission [73]. In relation to baseband, data are transmitted in digital format into the base stations (BSs), at which the signal processing is carried out including the modulation of the appropriate format (i.e., quadrature phase shift keying (QPSK), quadrature amplitude modulation (QAM), and orthogonal frequency division multiplexing (OFDM)), up-conversion to the microwave carrier frequency and amplification prior to being radiated by means of the antenna to the user equipment (UE) eventually. In such a scenario, the central station (CS) may have to be equipped

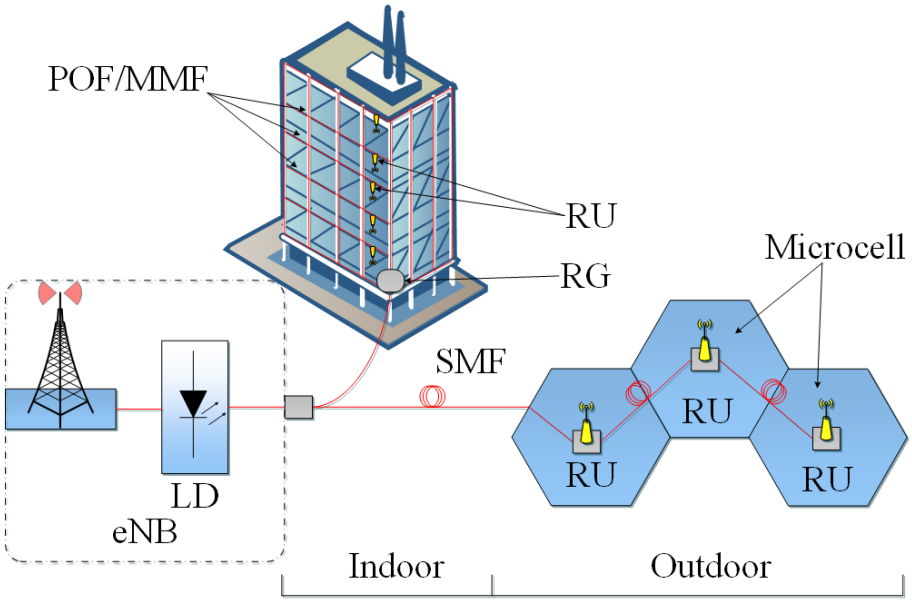

Figure 2.2: The RoF systems for indoor and outdoor LTE applications

with relatively simpler optoelectronic devices. However, it has to be noted that the BSs require complex equipment with signal modulation circuitry, which are particularly specified for high frequency mobile networks. In addition, in the event of any system upgrade, these equipment may require replacement, too. In the IF transmission, the data modulation on IF band is implemented in the CS but the other signal processing may still take place in the BSs. In the RF transmission in contrast, all complex processing is shifted from the multiple BSs to the CS. At the BS, the received signal has to be down-converted into the electrical domain, which is followed by an amplification and subsequently radiated by the antenna. In the event of the amplifier and antenna having been designed to operate in a broad frequency range, the upgraded system may not require any replacement of the devices. In such a scenario, the adoption of the RF transmitting the data can therefore be considered as the most effective solution to deal with the overall network complexity.

Upon looking into the 4G-LTE, it can be discovered that the RoF is adopted to facilitate the wireless access and distribute the downlink (DL) RF signals from the

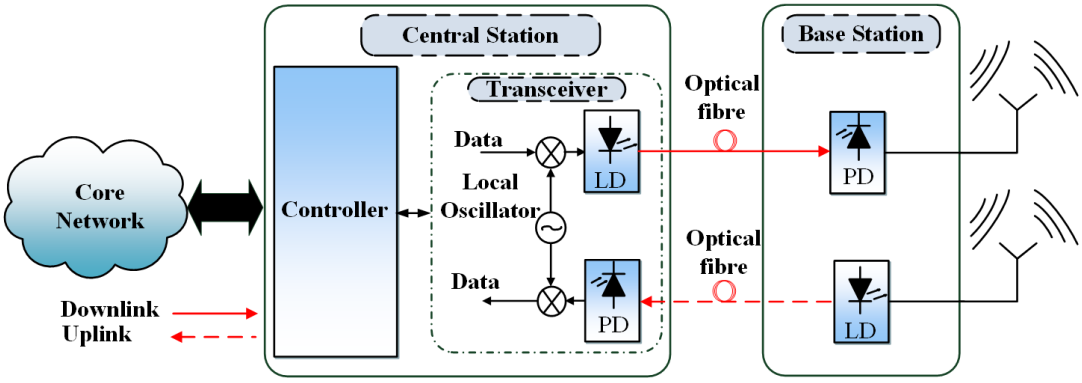

Figure 2.3: Overview of RoF system

eNB to the RUs for both the outdoor and indoor applications, respectively. The signals are then transmitted to the UEs by means of wireless connectivity. Simultaneously, the RoF carries the uplink (UL) signals from the UEs back to the eNB, as it is illustrated in Figure 2.2. It is noteworthy that the SMF is mostly used to extend the signal coverage for longer distances, whereas the POF or MMF is adopted for the dead zones such as the in-building and tunnels. In the traditional telecommunication systems, the RF signal processing such as the carrier modulation, frequency up-conversion and the multiplexing are carried out at the BSs and are subsequently fed back to the antenna. Upon looking into similar mechanisms in the RoF, it can be discovered that such complicated processing functions can be transferred to the eNB instead of the multi BSs, which help simplify the design of BSs significantly and therefore reduce the installation and maintance costs [74].

As illustrated in Figure 2.3, a typical RoF is used as an interface between the CS and the BSs. The DL electrical data are delivered by the core network and are subsequently collected by the CS, at which the signal processing is performed including the frequency up-conversion and the electrical-to-optical conversion by means of modulating the laser diode (LD). The modulated optical signal is then transmitted through an optical fibre prior to its launch at the BS. At the BS, following

the process of optical into electrical conversion by means of a photodetector (PD), the electrical signal is eventually transmitted to the UEs through an antenna. On the contrary, the UL signal is the reverse process of the DL signal.

2.2.1 RoF Applications

In relation to the scenario of small cells, the distributed antenna system (DAS) may appealingly serve as a suitable source to create hotspot points, which are distributed throughout the small cells and linked to a centralized station [26]. It has been empirically proven in related studies that the RoF is the most successful technique, which is capable of fulfilling the requirements of small cell topology, including the DAS topology for both outdoor and indoor applications. The outdoor access networks which adopts the SMF and the indoor access networks which on the other hand uses the POF or MMF, are equally preferred for the short communication links [75]. It is worth highlighting that the deployment of optical fibre links for telecommunication distribution purposes was first introduced in the year of 1991 using term of microwave photonics [74]. The RoF networks have since then been used because of the increasing demand required for massive bit rate communication applications. Related previous works in cellular systems have introduced a multi-service operation using RoF such as in [74], where both global system for mobile communications (GSM) and universal mobile telecommunication system (UMTS) performance were evaluated theoretically using 50 km of SMF acting as an optical link between the centralised station and remote unit (RU). In [76], an analysis of the RoF system that can support both wideband code division multiple access (WCDMA) operating at 900 MHz and wireless local area network (WLAN) operating at 2.4 GHz was carried out. Another experimental work by [32] explored the possibility of transmitting multi-wireless services such as the ultra-wideband (UWB), worldwide interoperability for

microwave access (WiMAX) and UMTS over SMF and MMF for 50 km and 400 m distances, respectively. Moreover, the integration of 4G-LTE with the RoF system was investigated both theoretically and practically by [72], the findings of which indicated an error-free transmission of 2.6 GHz LTE signal with 64-QAM modulation over 60 km SMF achieving ~6 % error vector magnitude (EVM). Additionally, in the study of [77], radio-over-MMF (RoMMF) based on distributed feedback laser (DFB) with IM was demonstrated to support the transmission of RF carrier of up to 20 GHz. Besides, another experimental presentation of transmission OFDM multi-standard signals for both UWB and WLAN was reported in [78] using low cost vertical cavity surface emitting laser (VCSEL) and graded-index-POF (GI-POF). In the study of [79], it was reported about other recent works demonstrating the transmission of 8 LTE-A at 64-QAM and 4-pulse amplitude modulation (PAM) achieving a throughput of 479 Mbps and 1.4 Gbps, respectively, over 20 m of GI-POF used to fed the 5G small cells.

It is noteworthy that several practical applications for the RoF systems have already been carried out ranging from in-building distribution such as shopping malls, tunnels and wireline links to military radar systems and broadcasting of cable TV signals using fibre-to-the-home (FTTH) systems [80]. In this regard, the RoF systems have already been proposed by some of the commercial investors such as Commscope corporation [81], Zinwave corporation [82] and TE connectivity [83]. The above-mentioned examples for applying the RoF were in Osaka station in Japan, the 2000 Olympic Games in Sydney, and the Bluewater shopping centre, UK respectively [73]. Also, several European operators such as France Telecom, Telecom Italia, and Telefonica adopted the POF as a link for indoor communication systems a few years ago [84].

2.3 An Overview of Radio-Over-FSO

Presently, the FSO technology has widely drawn the attention of scholars in the domain of communication. It is worth highlighting that the FSO-laser based system is considered as a well-established technology, in which the transmission of information laden optical radiation happens through the atmosphere from point to point. The first commercial laser link was presented in Japan by Nippon Electric Company (NEC) in the year of 1970 using Helium-Neon (He-Ne) laser for a distance of 14 km [65]. However, owing to high security purposes, the use of FSO for a few decades was restricted to military communication purposes only in comparison with the other RF links [85]. In this regard, the FSO technology in the 1970s experienced rather a slow penetration into the civil commercial market because of the existing RF networks were adequate enough to cope with the users' demands along with a lack of accurate tracking and pointing optical schemes, which were required to handle the atmospheric effects of this technology.

The rapid growth of the optoelectronic devices along with a number of other factors such as the rise of optical infrastructure, cost-effective compared to the other technologies, and the ease of deployment are among the reasons for the rebirth the FSO technology [85]. The FSO technology has recently emerged as a commercially applicable solution, which is considered as a complementary technology to the RF systems due to its capacity to meet the ever-increasing data demands within the access networks. It is also noteworthy that the RF technology has reached its bandwidth limitations owing to the spectrum congestion, interference and licence issues [86]. The FSO system in this regard has attracted the attention of many to support the 'last mile' access networks serving as a bridge between the local networks or between the local and wide networks [87].

2.3.1 Features of FSO Communications

The following key features associated with the FSO technology have helped make it more applicable in comparison with the other existing conventional RF technologies, such as microwave and millimetre wave (mm-wave), as outlined in the following:

- **High data rate:** With the drastic increase observed in wireless data traffic, quite a number of independent reports have therefore warned of the potential RF spectrum crises looming on the horizon [88]. In such a scenario, the FSO technology has alternatively offered a large data bandwidth of up to 400 THz [89], which is capable of coping with the future broadband demand. At present, available commercial FSO products reportedly offer transmitting relatively higher data rates of up to 10 Gb/s such as the TereScope 10GE produced by MRV [90],whereas the experimental research have achieved transmission of up to 1.6 Tbit/s using just a single FSO link [91].
- **Unlicensed spectrum:** The congestion of the RF spectrum and the interference between the adjacent carriers are some of the major obstacles for the wireless RF communication systems. Therefore, some of the relevant authorities, such as the federal communication commission (FCC) in the US and office of communication (Ofcom) in the UK, have devised stringent regulations to allocate the RF spectrum slices in their attempts to keep such interferences minimal [92]. Notwithstanding, the large fee along with the limited spectrum has necessitated complementary solutions such as adopting the optical channels. It has to be noted that the commercial FSO structures work within the infrared (IR) spectral range to achieve minimum signal absorption and scattering i.e., between 850 and 1550 nm, which are mostly

around the frequencies of 200 THz [85]. Furthermore, the above-mentioned wavelengths are reportedly used in the fibre optic communication systems. Therefore, the devices of industrial standards can be used for both technologies, particularly in the transmitter and receiver. At present, the FSO spectrum band is not regulated as licensing is not a requirement for frequencies beyond 300 GHz [93].

- **Narrow beam size:** An extremely narrow beam is known for the laser beam with the diffraction of limited divergence ranging between 0.01-0.1 mrad [63], which indicates the optical power confinement happening within the narrow area. Therefore, the FSO links may have an adequate spatial isolation from the potential interference, and consequently, the FSO systems may have the capacity to operate independently, allowing for unlimited degrees of frequency reuse applications. Furthermore, the narrow beam may also make it difficult for the interception of the transmitted data by the unintended users. However, this feature implies precise and tight alignment requirements [94].
- **Power efficient:** One of the major challenges of advancing the future information and communication technology (ICT) systems is the energy efficiency particularly, about the power consumption of the devices and infrastructure of indoor and outdoor networks. It is projected that the total power consumption of the ICT networks may increase annually by 13% due to the rapid growth of the communication industry [95]. Moreover, the ICT sector is one of targeted applications to mitigate the carbon emission due to its contribution of 3% of the total global energy consumption. An estimation study which was reported in [96] showed the carbon emission increasing at a 5% incremental rate annually, which was caused by the expected growth of the

extensive mobile networks and power-hungry BSs. The use of the FSO technology is therefore deemed as a promising solution to resolve such power efficiency issues, as FSO links reportedly use rather low power schemes. Hence, the FSO technology is considered as a "green" technology as it helps minimize energy consumption, which makes it an environment-friendly technology compared to the conventional RF systems [96, 97].

- **Cost effective:** The relatively lower cost of the FSO systems is another advantage of this technology in comparison to other communication schemes. Mostly, FSO links do not require the common installation operations such as trenching of roads and digging up tunnels, in addition to the free licence [98]. Owing to the smaller size of the optical transceivers, they do not require much space to be installed compared to the RF antenna [99]. A related market study carried out by [100] revealed that the monthly cost per Mbps in the RF systems was about double that of the FSO based networks.
- **Ease and fast installation:** The key requirement to establish FSO link is to ensure LOS between the transmitters and receivers. However, the expected time for FSO link establishment may take up to a few hours [101]. Moreover, a recent survey which sampled the operators in Europe and the USA indicated that the FSO links were installed faster than the other communication schemes [102].
- **Inherent security:** Considerations for security issues in relation to data communications are of utmost importance. It is in order to ensure that there is no access for unauthorised parties to the communication link. In this regard, the LOS FSO technology allows relatively higher transmission security, which can be considered as very useful for both military and banking sectors [103].

The confined FSO beam provides a significant degree of covertness, with inherent physical layer, which is immune to eavesdropping. The malicious interception is almost impossible owing to the optical beam obstruction, which may lead to link failure for the intended recipients. Furthermore, IR FSO links may jam the resistant owing to laser's narrow foot print, which again may make interception and detection very difficult [94].

2.3.2 Area of FSO Applications

The FSO technology has a wide range of applications, which include short and long distances terrestrial applications, in addition to the space applications. In recent years, most of the FSO applications were limited to immovable terminals (i.e. transmitter and receiver are fixed) with a minimum level of mobility only. There are two main connecting topologies: i) point-to-point links such as those used to connect two buildings, and ii) point-to-multipoint links such as those used on campuses and hospitals [104]. Typically, the FSO applications include the links of ground-to-ground, ground-to-aircraft, satellite-to-satellite, and satellite-to-ground stations [93].The main FSO applications are described in the following:

- **Last mile access links:** The adoption of the FSO technology in the last mile networks is motivated by the unique features associated with the FSO systems in addition to the rapid demand for delivering high-speed data to the end users. The FSO links represent an efficient solution for the 'last mile' bottleneck, which helps bridge the gap between the existing fibre optic infrastructure and the end users. The deployment of the fibre optic technologies as a backbone network has in recent years been increased to address the tremendous bandwidth broadband requirements. Such a development indicates a shift from

the reliance on bandwidth bottleneck towards the last mile access network. It has to be noted that by means of deployment of the FTTH, an excellent performance can be observed but it may require massive investments to be made [105]. The capacity of the wireless networks to offer high data rates (i.e., giga per second) still has some limitations due to a relatively lower carrier frequency being used, in addition to the RF broadcast nature and the available regulated spectrum [106]. Moreover, the lack of wired/wireless infrastructure especially in rural areas is observed due to lower density of population and number of potential users [67]. It is because of such obstacles, the FSO systems have been proposed as a cost-effective and high performance solution [70]. In addition, the FSO links can be deployed in point-to-point, point-to-multipoint, and ring or mesh connections. At present, most of the commercial FSO products which are widely available offer transmitting high data rates of up to 2.5 or 10 Gb/s such as SONAbeam 2500-E introduced by fSONA and TereScope 10GE produced by MRV, respectively [90].

- **Hybrid RF-FSO systems:** The hybrid link refers to using the FSO in combination with non-optical wireless technology. Some practical limitations associated with the RF networks and potential adverse influences from the weather such as fog, rain, and smoke have necessitated a hybrid scheme to overcome the limitations of both technologies. The integration between the RF and FSO systems is one of the proposed solutions to cope with the RF-FSO challenges and to achieve 99.9 % availability in severe atmospheric conditions [107].Therefore, some of the recent studies have looked into the hybrid RF-FSO system in terms of investigating the modulation techniques [108], hybrid

system measurements [109], diversity schemes [110], coding techniques [111, 112], and channel modelling [113].

- **Long range FSO links:** An outdoor LOS FSO network providing 2.5 Gbps over a distance of 4.4 km was reported in [114], whereas in [115], 10 Gbps were transmitted over 16 channels using wavelength division multiplexing (WDM) up to 2.16 km link distance. The first commercial outdoor FSO system was introduced in the year of 2008 which delivered 10 Gbps [87]. In the same year, a terrestrial FSO communication system was reported experimentally in [116] highlighting the transmission of 8-channels with 40 Gbps per channel data rate (i.e., 320 Gbps as total data rate). Another study by [117] demonstrated a practical investigation of transmitting a digital TV based RF signal over a 1 km FSO link at a wavelength of 1550 nm.
- **Cellular communications:** One of the important issues in the 4G and the next generation 5G cellular networks is designing a backhaul featuring both high capacity and cost effective, which may enable it to cope with a massive predicted future traffic. It is also worth highlighting that the FSO link is a promising candidate technology that can be deployed between the BSs and the mobile switching centres or to connect inter-building optical networks, allowing for much higher throughput in comparison with the wireline connections and microwave links [118]. Some recent practical investigations which were reported in [119-121] illustrated a successful transmission of 4G–LTE signals over FSO link under fog or turbulence fading effects.
- **Redundant link and disaster recovery:** Temporary FSO links are required for disaster and emergency situations ranging from both natural and man-made ones, which may potentially lead to the collapse of the local communications

infrastructure. The FSO links can therefore be utilised within hours due to lightweight, low power and easy to install [53, 118].

- **Back up to optical fibre link:** The FSO link can be used in the event of the optical fibre either linking down or unavailable. Moreover, the FSO links are mostly used where the optical fibres are impractical due to the physical obstacles [53, 85].

In addition, a growing interest in FSO technology has been observed in both the military and homeland security applications owing partly to its installation processes which can be carried out within 24 hours or even less. It is noteworthy that a very high bandwidth FSO link can be deployed to connect remote non-permanent sites, difficult territories, border control and battlefields. Besides, an equal increase in commercial interest to adopt the FSO in the optical sensing applications has also been observed. These applications are notably favoured in the security and military applications too [122-124]. In the case of the present work however, the focus is on the terrestrial FSO applications for the last mile access networks.

2.4 Hybrid RoF-FSO System

The combination of RoF and RoFSO may offer an appealing option for distributing radio signals and connecting multi-indoor RoF networks in places where the underground fibre may not be available, particularly in rural and sparsely populated areas. It is worth highlighting that this option is even more interesting, since it requires no digging between two buildings and thus the cost of installation is relatively lower. In this regard, a theoretical study by [67] highlighted the most efficient technologies, which can be used to enhance the wireless last-mile access links such as adopting the optical fibre in addition to the FSO as complementary technologies for the RF based

technology. The integration between the RoF and RoFSO systems was demonstrated theoretically in [125] and experimentally in [117] to indicate the transmission of OFDM signal between two RoF links using 1 km FSO under the turbulence effect. Either POF or MMF is adopted for the in-building RoF technology as both types are equally preferable for short span communication systems. According to the prediction made in [126], an estimated 17 million kilometres worldwide had already been installed as indoor links. The POF channel on the other hand has drawn more attention for the indoor networks as a cost competitive channel, less brittle, durable and more flexible compared to the silica based optical fibres [127, 128]. In [80], a hybrid community antenna television (CATV) and QPSK-OFDM signals were demonstrated practically over a link of 60 km SMF and 25 m GI-POF. It represented the long reach passive optical network (PON) and end users' premises network, respectively. A transmission of 40 Gbps over a hybrid optical links including FSO and POF is proposed in [129] using adaptive OFDM coding format.

2.4.1 System Model

The block diagram of the hybrid RoF-FSO system as shown in Figure 2.4 has used: (a) direct modulation (DM) that refers to intensity modulation with direct detection (IM/DD) modulation technique, which is widely used for the most cost-effective typical systems [22, 118] and (b) external modulation (EM), which is proposed for high data rate applications that may require relatively lower noise levels [130]. The FSO link requires a LOS path, which indicates that no obstacles are found between the transmitter and receiver. The typical deployment of the FSO network architectures are point-to-point in a ring, mesh and star structure. Almost every communication system includes the following three parts: transmitter, channel and the receiver. For the hybrid RoF-FSO system proposed in the present study, the optical channel consists of the optical fibre in addition to the FSO channel. Further details of each part are introduced in the following sections.

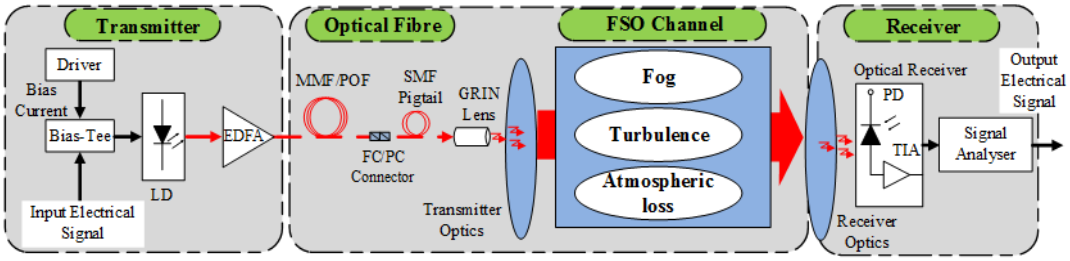

(a)

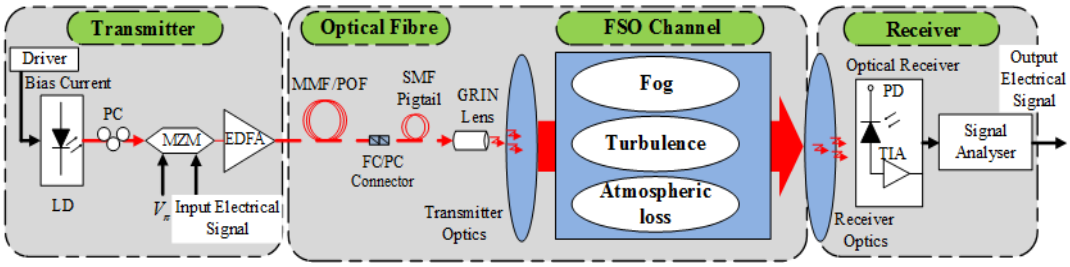

(b)

Figure 2.4: Block diagram of the Hybrid RoF-FSO communication model using (a) Direct modulation, and (b) External modulation

2.4.2 Optical Transmitter

The transmitter side consists of a driver, light source, modulator and amplifier. A driver circuit is deployed to regulate the biasing current of laser and to stabilise its performance. It is worth highlighting that a Bias-Tee can be used to change the bipolar analogue signal into unipolar form.

The input electrical signal is a passband signal based on OFDM at 800 MHz or 2.6 GHz LTE frequency band [5]. In the base band, the signal is composed of the QPSK, 16-QAM or 64-QAM as a single carrier modulation (SCM) at analogue radio bandwidth of 5 MHz, 10 MHz, 15 MHz and 20 MHz, which are the standard values for the LTE technology [18]. The electrical signal converts into optical signal using laser diode either by means of DM as shown in Figure 2.4 (a) or the EM as shown in Figure 2.4 (b). In this regard, the DM is considered as a cost effective technique and is used widely for most of the commercial optical systems [22, 118]. In addition, the source electrical signal is modulated into the intensity of the optical radiation only. On the contrary, in the EM, both intensity and phase/frequency of the light can be modulated. The EM can be performed by means of Mach–Zehnder electro-optical modulator (MZM). In comparison with the DM, the MZM is proposed for high-frequency digital applications to decrease the signal distortion and noise. Moreover, MZM-based transmitters are preferred to operate at dense wavelength division multiplexing (DWDM), due to their wavelength range flexibility, which are capable of providing relatively higher system capacity [130]. The modulated signal is amplified using the EDFA in order to compensate for the link loss and simultaneously, ensure sufficient link power budget prior to being launched into the optical channel.

Many factors affect the selection of the proper light source for the high data rate short distance networks such as the transmission modes and the signal spectral width. The light emitting diode (LED) and LD are the most popular transmitters as both can be deployed for the optical communication systems. The LED is used commonly for low data and short range communications [131], whereas the LD is more widely used for the optical communication links as it can be used for higher data rate and longer transmission span for the indoor and outdoor networks [97]. There are three main laser types, namely fabry-perot (FP) laser, the DFB, and the VCSEL. The key properties for these sources include the narrow linewidth, high optical power, and transmitting efficient coupling light to the optical fibre [132]. Table 2.1 provides a comparison of basic properties (i.e., typical values) for the main light sources [45, 133]. The LED emits light with wide spectral width [134], and improvement power of up to 0.2 m W at a relatively lower cost. However, the large numerical aperture (NA) and broad spectral width of LED may result in transmission distortion in of the event of networks employing multimode fibres as a backbone [135]. The signal distortion caused by the intersymbol interference (ISI) and accumulated modal dispersion [136]. On the other hand, using multilongitudinal modes (MLM) FP laser may increase the signal distortion by the enlargement of chromatic dispersion effect [38]. By contrast, VCSELs have a narrow spectral output and a low threshold current i.e., about 1 mA,

Table 2.1: Typical specification of the main light sources [45, 133]

Specification	**LED**	**FP**	**VCSEL**	**DFB**
Linewidth (nm)	35	30	3	< 1
Optical power (mW)	0.2	7	10	10
Modulation (Gbps)	0.25	1.7	1	4

which means that VCSELs can operate at a constant current even with inconsistent temperatures [45]. In addition, an acceptable bandwidth, about 10 GHz, can be supplied by VCSELs for the short-distance networks [45, 135]. Therefore, a VCSEL effectively strikes a balance between the cost and quality and therefore makes itself a real candidate for short distance transmission systems, such as RoF polymer based links [136]. The recent trend is to employ DFB for long haul systems, as this device emits a single longitudinal mode with a high transmission power and a narrow wavelength band. As the typical operating power of the DFB laser is 10 mW [134], its capability in recent years has improved to deliver more than 200 mW [47, 137]. However, high costs may possibly limit their applications within building network, which is why the need for employing the DFB mainly in the long span outdoor applications [136].

For the FSO networks, there are several transmission wavelength bands, which are designed mainly to operate within the spectral window ranges of 780-900 nm and 1520-1600 nm. The former range is usually adopted for the major FSO applications because of the components being available for relatively lower cost, but it cannot be assured for the eye safety that it may keep the emission power at lower levels. On the other hand, the 1550 nm band is attractive for a number of reasons: i) compatibility with the 3rd window wavelength band that is adopted by the wavelength-division multiplexing networks and EDFA technology; ii) eye safety with approximately 50-to-100 times more than 800 nm, which means transmitting higher power [138, 139]; iii) low atmospheric attenuation; iv) lower levels of the solar background radiation and v) lower Doppler shift. Therefore, the 1550 nm transmitted signal over the FSO may have more power that can overcome relatively some of the atmospheric fading effects, particularly the fog. However, relatively higher cost of the components, stricter

alignment requirements and lower detector sensitivity are the main drawbacks associated with the 1550 nm band. Typically, the detectors that operate at 1550 nm are reportedly less sensitive, relatively smaller surface area compared to the silicon avalanche photodiode (Si-APD) at 850 nm [138]. Finally, the transmitter optics such as the telescope or lens are deployed to collimate the light towards the receiver to keep the divergence angle smaller, which may help reduce the geometrical loss [140].

In the present work, the author has adopted the VCSEL at 850 nm and DFB at 1550 for both the indoor and outdoor applications, respectively. Figure 2.5 illustrates the internal structure of the DFB and VCSEL laser diodes. The DFB laser is a type of edge-emitting lasers, which operates in a dominant single mode, while suppressing other modes of oscillation. The optical feedback can be accomplished by an internal grating that exists within the active region as it can be seen in Figure 2.5 (a). The Bragg gratings may cause spatially periodic variations in the effective refractive index of the laser waveguide culminating in an effective selection of one longitudinal mode. In this regard, the DFB is considered as a suitable candidate for the outdoor communication applications such as long haul optical fibre and FSO networks owing to its capability to radiate single mode with high output power and narrow linewidth. In [141], a transmission of 10 Gbps was demonstrated for a distance of more than 80 km SMF using the DFB at 1550 nm wavelength.

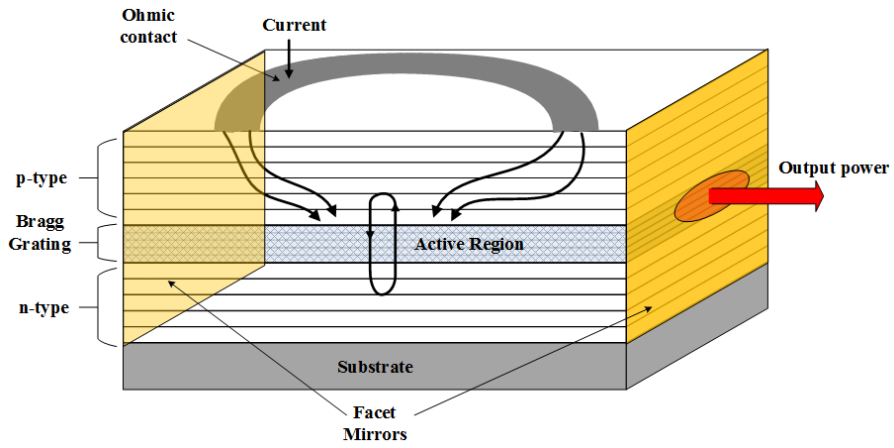

(a)

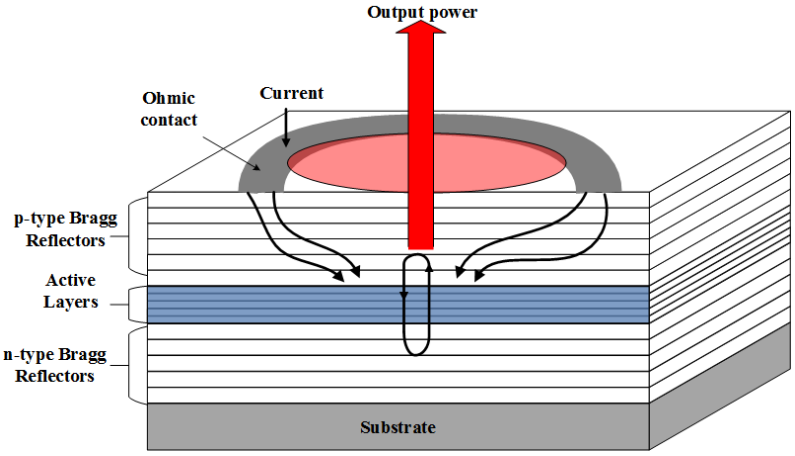

(b)

Figure 2.5: Schematic layer structure of (a) DFB and (b) VCSEL laser

Figure 2.5 (b) illustrates the typical structure of the VCSEL laser diode, in which the lasing is achieved vertically either at the top or bottom of the diode. The inner cavity consists of the amplifying layers that are fabricated on top of each other on the substrate. The active region sandwich consists of multiple quantum wells and is surrounded by highly reflectivity mirrors within the range of ~99.5 to 99.9% [142]. These mirrors are located at the top and bottom of the structure and they contain the distributed Bragg reflectors, which are made from altering material of several quarter-wavelength thick layers with different refractive indices. It has to be noted that the

VCSEL is capable of operating in a single longitudinal mode due to its extremely short cavity, which is about 1 μm. The emitted light is perpendicular to the surface and in circular form, which may help improve the coupling efficiency into the optical fibre.

Thereby, the use of the VCSEL in the optical communication has increased rapidly [47]. The first commercial VCSEL emerged in the year of 1996, which was initiated by Honeywell for 850 nm emissions. Subsequently, many companies started to produce the VCSEL in other wavelength windows, i.e., 1330 and 1550 nm [142]. It is also noteworthy that several techniques were developed in the last decade to control the transverse VCSEL modes such as the oxide-confinement technique, in which a layer of aluminium-oxide is used as a directional aperture to confine the optical mode. This type of laser is capable of replacing the DFB in multiple optical applications as long as the output power is efficient for the system budget. The most common application is the indoor optical application because of its low cost compared to the DFB. Moreover, VCSEL is considered suitable for the WDM applications owing to its capability for wavelength tuning over a wide range in addition to its capacity of creating VCSEL arrays [143-145].

2.4.2.1 Laser Fundamental Concepts

To understand the mechanism of light generation within light sources, which are employed in the hybrid optical communication system, it is of utmost importance to consider both the basic atomic concepts and the device structure. It is worth highlighting that laser is a device that amplifies the light, where it operates in line with the stimulated emission producing highly coherent radiation and highly monochromatic. In other words, it has a narrow linewidth and highly directional beam [146].

The laser operation is relative to the interaction observed between the light and materials such as Indium Gallium Arsenide Phosphide (InGaAsP) or other ternary and quaternary semiconductor compounds that are used to fabricate the PN junction [47, 135]. The PN junction is considered as a barrier between the p-type and n-type semiconductors. The basic mechanism responsible for the light emission is the recombination of the electrons and holes in PN junction, where the electrical field is generated owing to the potential differences observed between the two materials leading to create a depletion region with a width depending on the doping concentrates of each P and N type. It is therefore, a forward current is required to overcome such a barrier. This current is the threshold point at which the laser conducting begins, where it starts to emit light when the current is increased beyond this point. The diffusion of electrons and holes across the depletion region may lead to present both in the same region simultaneously. Thus, a recombination may begin between both the carriers, which in turn may generate the spontaneous and stimulated emission as a result of optical feedback and optical gain. The lasing process is a consequence of the positive optical feedback that may potentially lead to the oscillation inside the laser cavity. The stimulated emission can be fulfilled when the optical gain equals the loss, in addition to the positive optical feedback, which can be achieved by providing cleaved facets in the active region or by the distributed grating [135, 146].

Despite the different laser types, the basic principle under which they operate is almost the same. Laser operation is a result of interaction of quanta of energy, better known as photons, with the material atoms. Based on the quantum theory, these atoms are distributed in certain discrete energy states. The process of light absorption or emission

may lead to make an atomic transition between these states. Figure 2.6 represents a simple two energy levels, in which a transition between these states involves an absorption or emission of a photon with energy of $h\nu = E_2 - E_1$, where h is Plank's constant, ν is optical frequency, E_1 and E_2 is the ground state energy and excited state energy, respectively. In the thermal equilibrium condition, the system is in the ground state, which means $N_1 > N_2$ [147], where N_1 and N_2 is the number of electrons on the ground and excited states, respectively. The absorption may occur when a photon incident on the material leading to an electron transition from E_1 to E_2 as shown in Figure 2.6 (a). This electron may return to the ground state shortly after due to the instable condition, thereby a photon is emitted for the process of spontaneous emission (see Figure 2.6 (b)). The photons are emitted in a random phase and arbitrary polarization. The spontaneous emission rate is explained by $dN_2/dt = -N_2A_{21}$, where A_{21} is the spontaneous emission coefficient. Figure 2.6 (c) illustrates the process of the stimulated emission. Here, the system is exposed by an incident photon while an electron remains in the excited state. Thereby, the electron is dropped immediately to the ground state with the same phase of the incident photon. The stimulated emission is essentially negligible in thermal equilibrium condition considering that the most incident photons are absorbed. It can be achieved in the event

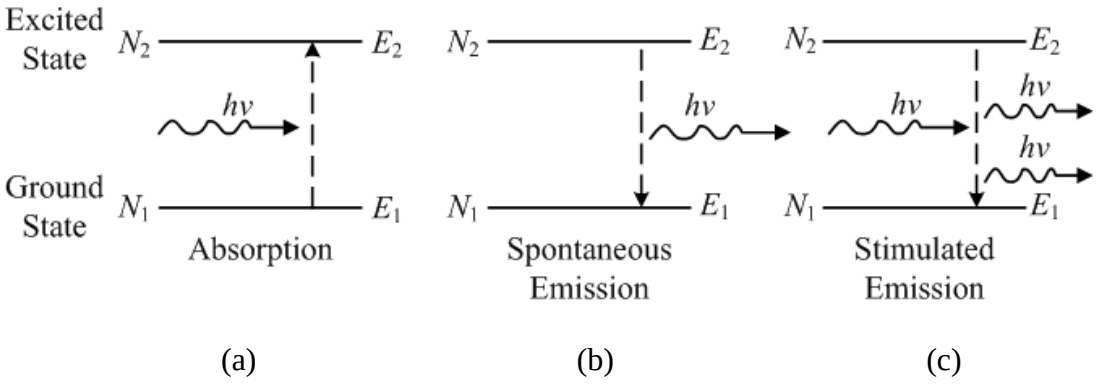

Figure 2.6: Energy state diagram: (a) Absorption, (b) Spontaneous emission, and (c) Stimulated emission

of the electron population in the excited state being greater than that of the ground state, i.e., $N_2 > N_1$. This condition is known as the population inversion, which can be obtained by injecting the electrons into the device contacts. This process is called "pumping" technique. The total rate at which the N_2 population decreases due to the stimulated emission is $dN_2 / dt = -N_2 \rho(v) B_{21}$, where $\rho(v)$ is the energy density of the external applied field, B_{21} is the stimulated emission coefficient [148]. The negative sign may denote the decrease of the population at the N_2 level.

The operation of the semiconductor laser can be described in terms of the carrier density level. Figure 2.7 shows the growth of the carrier density N and photon density S against the injected biasing current I_{dc}. N_{th} represents the threshold carrier density, which is required to start the lasing process. N_{tr} is the transparency carrier density i.e., the minimum density, for which the material starts to be transparent to the photons, i.e. starting optical gain g_o. At the condition of below transparent, i.e., $N < N_{tr}$ the optical gain is negative, which indicates a relatively higher photon decay rate in comparison with the spontaneous emission photons that may deteriorate due to the effect of the cavity and reflectors loses. At the $N_{tr} < N \ll N_{th}$, as I increases, the N equally increases as well. Laser gain is positive but $g_o \ll g_{th}$, where g_{th} is the threshold gain. Hence, the photon rate is not large enough to balance the decay rate. At $N \approx N_{th}$, when I is increased beyond the threshold I_{th}, the optical gain begins to be more than the decay rate. The S increases and becomes so large due to a relatively higher recombination rate resulting from the stimulated emission, which in turn preventing N from increasing beyond the N_{th}.

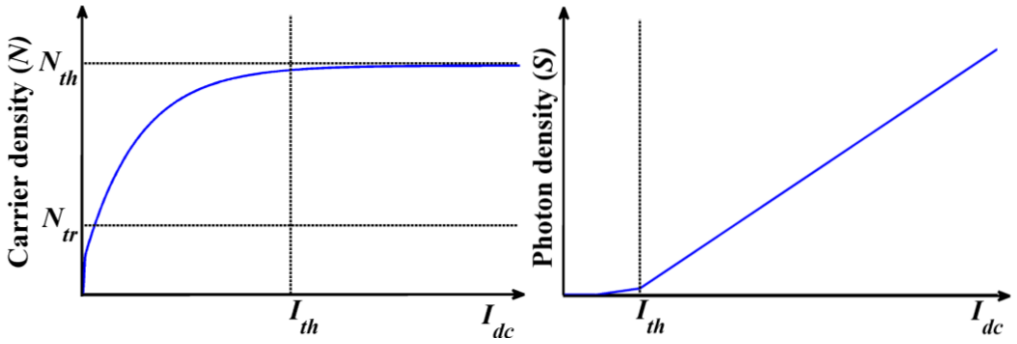

(a) (b)

Figure 2.7: Semiconductor laser operation in terms of: (a) Carrier density and (b) Photon density versus the biasing current

Figure 2.7 (b) displays a linear increment of *S* when the injected current exceeds the threshold point i.e., the lasing point.

The semiconductor laser behaviour can be defined using differential rate equations, which may better describe the interaction observed between the *N* and *S* in the active region in terms of the rate of change with time evolution. Basic form of the rate equations is:

$$\frac{dN}{dt} = \text{Injected carrier - Spontaneous emission - Stimulated emission}$$

$$\frac{dS}{dt} = \text{Stimulated emission + Spontaneous emission - Photon loss}$$

In the present study, the DFB is used as a light source for the EM scheme, for which the transfer function of the MZM is required to model the optical signal. In the indoor application, the VCSEL diode is adopted in IM-DD scheme, which required to be modelled using differential rate equations. The detailed rate equations for a VCSEL working at 850 nm can be expressed as in the following equations [149-151]:

$$\frac{dN(t)}{dt} = \frac{\eta I_s(t)}{eV_{act}} - \frac{N(t)}{\tau_c} - g_o \frac{N(t) - N_{tr}}{1 + \xi S(t)}, \tag{2.1}$$

$$\frac{dS(t)}{dt} = \Gamma v_g g_o \frac{N(t) - N_{tr}}{1 + \xi S(t)} S(t) + \Gamma \beta \frac{N(t)}{\tau_c} - \frac{S(t)}{\tau_p}, \tag{2.2}$$

where η is the internal quantum efficiency, I_s is the input signal current, e is the electronic charge, V_{act} represents the volume of the active region, τ_c is the carrier life time, g_o is the optical gain coefficient, ξ is the gain saturation coefficient, Γ is the lateral confinement factor, v_g is the group velocity, β represents the fraction of spontaneous emission, τ_p is the photon life time.

The output optical power P_{opt} can be obtained by [150]:

$$P_{opt} = \frac{1}{2} h\nu\pi v_g w^2 \Gamma_z \left(1 - R_o^{\,2}\right) S(t), \tag{2.3}$$

where w is the radius of the mode distribution, Γ_z is the longitudinal confinement factor, R_o is the reflectivity of n-type reflector. The parameter values are listed in Table 2.2, which are adopted from [149, 150, 152].The rate equations describe the behaviour of the semiconductor laser and help better understand the laser optical and electrical performance under DM in addition to the potential limitations [135]. The current I_s in (2.1) and (2.2) can be expressed as:

$$I_s = I_{dc} + I_{rf} \sin(\omega_m t), \tag{2.4}$$

where I_{rf} and ω_m is the amplitude and modulation frequency for the sinusoidal modulation current.

The VCSEL can be modelled by solving the equations (2.1) and (2.2). The RF carrier that was shown in (2.4) can be used to modulate the VCSEL directly, for which the

Table 2.2: Parameter values used in the VCSEL rate equations

Parameter	Parameter Symbols	Parameter Values
V_{act}	Active region volume	$4.8\text{x}10^{-18}$ m^3
e	Electronic charge	$1.6\text{x}10^{-19}$ C
τ_c	Carrier life time	5 ns
η	Coupling efficiency	0.6
g_o	Optical gain coefficient	$5.65\text{x}10^{-12}$ m^3/s
N_{tr}	Transparency carrier density	$3.25\text{x}10^{24}$ m^{-3}
ξ	Gain saturation coefficient	$1\text{x}10^{-17}$ m^{-3}
Γ	Lateral confinement factor	1
Γ_z	Longitudinal confinement factor	0.07
β	Fraction of spontaneous emission	$1\text{x}10^{-5}$
τ_p	Photon life time	6 ps
ω	Radius of mode distribution	3 μm
h	Planck's constant	$6.63\text{x}10^{-34}$
R_o	Reflectivity of m-type Bragg reflector	0.997
v_g	Group velocity	$8.1\text{x}10^{7}$ m/s

output power can be observed using (2.3). The first step for the rate equation resolution is to consider the case of the steady state, where in this state:

$$\frac{dN}{dt} = 0 . \tag{2.5}$$

$$\frac{dS}{dt} = 0 . \tag{2.6}$$

As illustrated in Figure 2.7, when $I<I_{th}$ the $S\approx 0$, which is the initial value of the photons number. While $N= N_i$, where N_i is the initial value of the carrier number below the threshold level, i.e, N_{th}. To observe the carrier density and photon density development numerically, the change rate for N and S can be represented in terms of the boundary condition t_B as in the following equations:

$$N\left(t+t_B\right) = \frac{dN}{dt}\left(t+1\right)\times t_B + N\left(t\right), \tag{2.7}$$

$$S\left(t+t_B\right) = \frac{dS}{dt}\left(t+1\right)\times t_B + S\left(t\right), \tag{2.8}$$

where t_B depends on the laser cavity distance L_{cavity} and can be estimated as:

$$t_B = \frac{L_{cavity}}{v_g}. \tag{2.9}$$

2.4.3 Optical Channel

The hybrid RoF-FSO system is proposed to enhance the 4G-LTE signal performance for the building networks. In this regard, the optical channel consists of the optical fibre and FSO channel, for which the optical fibre is used as a backbone cable for the inter-building structure connecting the indoor facilities. In contrast, the FSO channel is used as an infrastructure for the intra-building, which serve to connect multiple RoF links. In the following sections, both channels in addition to the impairments associated with them will be discussed in detail.

2.4.4 Optical Fibre

The RoF schemes can use the SMF, MMF or (POF) links depending on the length of the network and application [134]. In RoF links, a simultaneous operation of multiple systems can be considered as a significant advantage of the RoF technology, which has already been used by the SMF in many deployments [153]. The SMF is characterised by the high performance in terms of very low dispersion and attenuation, and ultra-high bandwidth-length product (BW.L), which is typically about 17 ps/km.nm, 0.2 dB/km, and 100 GHz. km, respectively [135]. However, the cost of using SMF for in-building networks may result in considerable delays in terms of installation, maintenance, and fibre itself, due to the relatively smaller SMF core size i.e., 5 µm to 10 µm [154], it requires higher precision equipment and the need for well-trained technicians [136]. Alternatively, MMF with its large core i.e., 50 µm to 62.5 µm [154] can be easier to install due to its low sensitivity with splicing process and connector misalignments [155]. In several instances, MMF according to its optical

mode (OM) properties have been utilized for short distance networks. The majority of the existing in-building fibre networks have deployed the MMF links, either OM1 and OM2, which may support 1 Gbps data rate or OM3 and OM4, which on the other hand may support 10 Gbps [41], and according to the projection made in [126], an estimated 17 million kilometres worldwide had already been installed with indoor links. On the other hand, the POF has the largest core size in comparison with the other fibre types i.e., 100 µm to 1880 µm [135], and it can be readily installed even by unskilled individuals, thus do-it-yourself (DIY) installation process can be implemented with low cost [136]. Figure 2.8 shows a comprehensive study of using different cable types (i.e., copper CAT-5E, POF, SMF, and MMF) for in-building networks in terms of its cost and power consumption for the required devices that can be connected with such links [127].

As it can be seen from Figure 2.8(a), the installation cost of POF is relatively lower than the CAT-5E because of the factor of sharing the ducts with the electrical power cables. Moreover, the differences observed in installation cost of POF with the SMF and MMF, particularly in terms of easy connectorizing of POF links are quite clear. On the other hand, the operation cost shown in Figure 2.8(b) explains the advantages of POF over the silica fibres. However, the power consumption of POF solutions is slightly more than that of CAT-5E, because of the consumption of media converters [127]. Another cost analysis by [156] supported using POF as building backbone network, for which three topologies are presented, namely single star, double, and ring. A study of cost evaluation for these topologies using the SMF, MMF, and POF was carried out. In this regard, the findings indicated that the devices that are used with POF links may involve relatively lower cost than those of SMF and MMF, in particular, the media converters, mounted connectors, WDM filters, add/drop

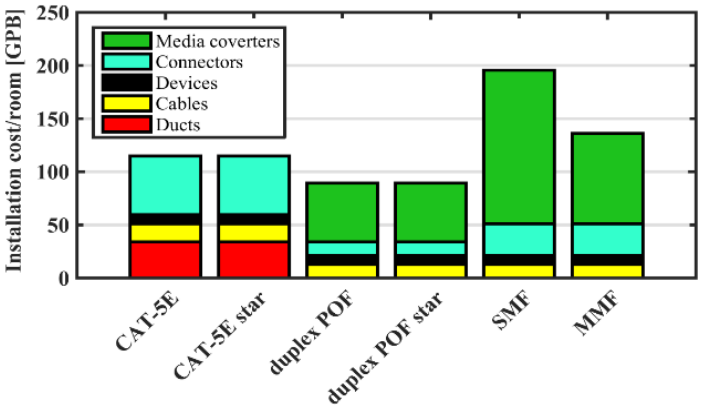

(a)

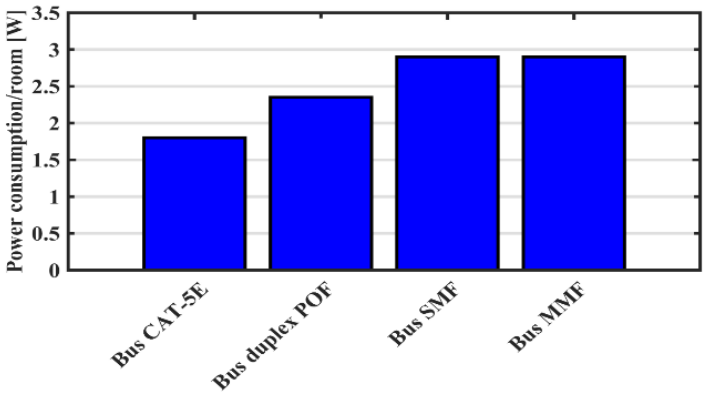

(b)

Figure 2.8: Comparison of different in-building channels in terms of: (a) Installation cost and (b) Power consumption per room [126]

multiplexer (ADM), in addition to the fibre cost. The POF represents the potentially lower cost solution for such networks in terms of devices and the possibility of sharing the existing ducts with the electrical cables [44].

In the present study, the MMF and POF are adopted as in-building networks for their attractive properties. However, different challenges may limit the RoF capacity, which are discussed in the following:

2.4.4.1 Optical Fibre Limitations

The optical fibre limitations are classified into linear and non-linear effects, which can be neglected in the POF channel owing to the short distance application for such

links in addition to the low input optical power, particularly for the POF [45]. The linear effects may include both the fibre attenuation and dispersion. The fibre attenuation effect may reduce the signal power reaching the receiver. The optical power of the light, which travels through the fibre may decay exponentially with distance L according to [134], as stated in the following:

$$P_o = P_i \exp(-\alpha L), \tag{2.10}$$

where P_o is the received power, P_i is the power launched into the fibre and α is the attenuation coefficient (dB/km).

The use of silica optical fibres (i.e., SMF and MMF) is considered more traditional in the optical communication system owing to the lower attenuation levels. However, the fibre loss is a sum of three major mechanisms, namely the intrinsic loss, bending and splicing losses. The intrinsic loss, which mainly consists of the absorption and Rayleigh scattering loss, depends on the wavelength of the transmitted optical signal. The silica fibres may exhibit lower intrinsic losses of about 0.3 and 0.15 dB/km in the wavelength regions of 1300 and 1550 nm, respectively [147]. On the other hand, the POF channel, which uses polymers instead of the silica material, exhibits much higher attenuation levels. The earlier POF type is polymethylmethacrylate (PMMA), where the smallest attenuation is approximately 100 dB/km at around 550 nm because of the strong absorption of carbon-hydrogen (C-H) bonds and Rayleigh scattering. In addition, there have also been some recent developments, which have led to reduce the fibre loss by replacing the hydrogen atoms (H) with heavier atoms like fluorine (F), which may create C-F bonds [157]. In [158, 159], a comparison of the different POF types was presented. It has been highlighted in recent studies that perfluorinated POF (PF-POF) represents a better choice among other POF types. In PF-POF, the low-

loss wavelength dependent characteristics are extended to more than 1350 nm, which may lead to use the same laser diodes and photodiodes that are already used for the silica fibre. The lower level attenuation reported for the PF-POF is around 60 and 20 dB/km at the 850 and 1300 nm regions, respectively [149]. However, these values are still considerably higher in comparison with the silica based fibres. The main causes for the POF fibre are the Rayleigh scattering, absorption, principally at the C-H bond, and losses through geometric imperfection at the core/cladding interface [45]. In contrast with silica fibres, the attenuation for the guided modes of the POF is not identical and the attenuation level for each mode may depend on the propagation angle. Thus, the average attenuation for all modes may significantly vary [157]. Other factors which may equally contribute to POF attenuation are, inter alia, the mode conversion and mode mixing at the fibre bends and the fibre links respectively, in addition to the unguided or leaky modes which may travel over the fibre [45, 135].

Apart from the fibre losses, the dispersion may severely degrade the system's performance due to the signal broadening, which may lead to the ISI. Figure 2.9 summarizes the dispersion types that appear in the optical fibres. The dispersion mechanism depends either on the optical signal wavelength and/or propagation paths. In the multimode fibres, the pulse broadening is produced by the modal dispersion and chromatic dispersion including the material and profile dispersion (i.e., in the graded index fibres). The waveguide and polarization mode dispersion are exhibited in SMF only [45]. Owing to the proposed work in this thesis zooms in on using multimode fibres i.e., either silica or polymer based, the author therefore discusses the modal dispersion, which is the most dominant type that may potentially limit the available fibre bandwidth [136].

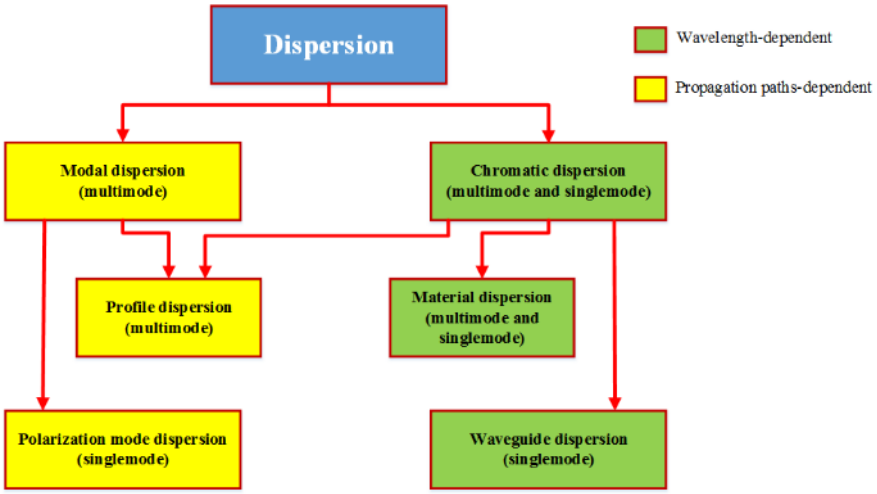

Figure 2.9: Dispersion mechanisms in the optical fibres

The light transmitting over step-index POF (SI-POF) is suffered massive number of modes, while this number reduced with the GI-POF. The number of propagated modes can be described using V_f parameter [45]:

$$V_f = \frac{2\pi a}{\lambda}.\, NA = \frac{2\pi a}{\lambda}.\, \sqrt{n_1^2 - n_2^2}\,, \tag{2.11}$$

where λ is the wavelength of the light, a is the core radius of the fibre, NA is the numerical aperture, n_1 and n_2 describe the refractive indices at the fibre core and fibre cladding, respectively.

The greater NA and a, the more modes can be seen guided through the fibre i.e., approximately proportional to ${V_f}^2$. The condition of single mode propagation is $V_f < 2.405$, which may require much smaller fibre core radius or reducing the relative refractive index difference. Both these procedures may generate more difficulties in terms of fibre jointing, launching light into the fibre, and fibre fabrication process [135].

The most important parameters that can affect the dispersion level in the multimode fibres are the wavelength, refractive index profile, light lunching condition, fibre laying condition, and the homogeneity of the fibre's characteristics [45].

The refractive index profile has a significant effect on the propagated light distribution, which is important to reduce the dispersion effect in multi-mode fibres. If we consider circular and symmetric GI-POF, the refractive index profile can be defined by the power law [151] as:

$$n(r,\lambda)=\begin{cases} n_1(\lambda)\left[1-2\Delta(\lambda)\left(\frac{r}{a}\right)^{g}\right]^{1/2} & r\le a \\ n_2(\lambda) & r>a \end{cases}, \tag{2.12}$$

where r is the distance from the core centre, g is the refractive index exponent and Δ is the refractive index contrast that is defined as:

$$\Delta(\lambda)=\frac{n_1^2-n_2^2}{2n_1^2}\cong\frac{n_1-n_2}{n_1}. \tag{2.13}$$

Moreover, the wavelength dependence of the refractive index is fit by a three-term Sellmeier dispersion relation[144]:

$$n(\lambda)=\left[1+\sum_{i=1}^{3}\frac{B_i\lambda^2}{\lambda^2-C_i^2}\right]^{1/2}, \tag{2.14}$$

where B_i (unit-less) and C_i (nm) indicate the oscillator strength and oscillator wavelength, respectively. Table 2.3 shows the coefficients used for (2.14) as indicated in [160], which is specified for the PMMA and fluorinated (PHFIP 2-FA) polymers.

The GI-POF fibre can be characterized by its transfer function considering the chromatic, which is known to be strong in the POF fibres, modal dispersion and

Table 2.3: Sellmeier coefficients for the PMMA and PF-POF [159]

Polymer	B_1	B_2	B_3	C_1	C_2	C_3
PMMA	0.4963	0.696	0.322	7180	1174	9237
PHFIP 2-FA	0.42	0.046	0.348	5874	8785	9271

differential mode attenuation (DMA), while the mode coupling can be neglected as indicated in [161, 162].

The transfer function of the GI-POF $H_{POF}(f)$ can be stated as:

$$H_{POF}(f) = H_{ch}(f) \cdot H_{\mathrm{mod}}(f) , \tag{2.15}$$

where $H_{ch}(f)$ and $H_{mod}(f)$ refer to the chromatic dispersion and modal dispersion, respectively. The transfer function in (2.15) describes two independent effects that can be assessed separately. The chromatic dispersion is generated since the delay time of each mode is considered as a function of the wavelength, which mainly depends on the laser linewidth as given by [163]:

$$H_{ch}(f) = \exp\left[-\frac{1}{2}(\omega_m DL\sigma_\lambda)^2\right], \tag{2.16}$$

where $\omega_m = 2\pi f$, f is the modulation frequency, D [ps/nm.km] is the material dispersion coefficient, L is the fibre length [km], σ_λ is the laser linewidth [nm]. The chromatic dispersion coefficient is obtained by [161]:

$$D = -\lambda \frac{n''}{c} . \tag{2.17}$$

The double prime indicates the second derivative of the n with respect to the wavelength, which can be derived from (2.14). The coefficient D of the PMMA and PF-POF can be estimated using (2.17), as it is shown in Figure 2.10. The value of D is ~ -60 and ~ -160 ps/km.nm for the PF-POF and PMMA, respectively, which are in agreement with the values reported in the literature and data sheets [161]. On the other

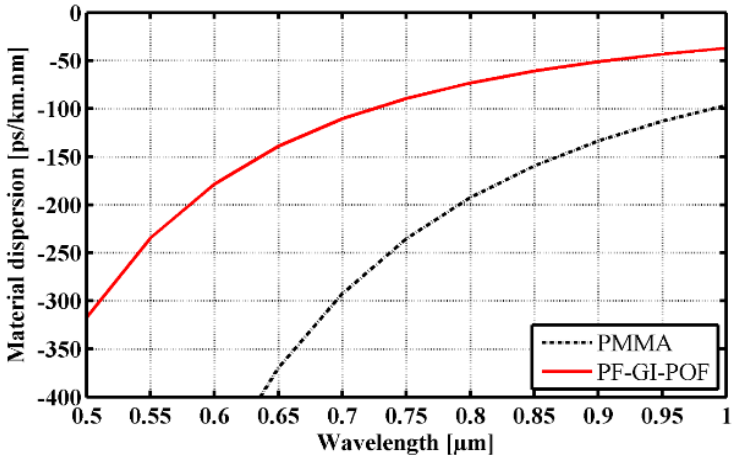

Figure 2.10: Material dispersion for the PMMA and PF-POF

hand, the modal dispersion is caused by different propagation velocity of the mode groups and can be described as:

$$H_{\mathrm{mod}}(f)=\sum_{k=1}^{K}P_k\exp(-j\omega_m\tau_k L)\cdot 10^{-\alpha_k L/10}, \tag{2.18}$$

where K is the total number of the mode groups, P_k represents the input power of the k^{th} mode group, τ_k , and α_k are the group delay and mode dependent attenuation coefficient of the k^{th} mode group, respectively, which can be determined by [161]:

$$K=2\pi a\frac{n_{eff}}{\lambda}\left(\frac{g\cdot\Delta}{g+2}\right)^{1/2}, \tag{2.19}$$

$$\tau_k=\frac{n_{eff}}{c}\left[1+\frac{g-2-\varepsilon}{g+2}\Delta\cdot\left(\frac{k}{K}\right)^{\frac{2g}{g+2}}+0.5\frac{3g-2-2\varepsilon}{g+2}\Delta^2\cdot\left(\frac{k}{K}\right)^{\frac{4g}{g+2}}\right], \tag{2.20}$$

$$\alpha_k=\alpha_0+\alpha_0 I_p\left[\eta_w\left(k-k_0\right)^{2g/g+2}\right], \tag{2.21}$$

where n_{eff} is the effective refractive index, ϵ is the profile dispersion parameter, α_0 is the attenuation of the fundamental mode, I_p is the p^{th}-order modified Bessel function, η_w and k_0 are the weighting and fitting constants, respectively. n_{eff} and ϵ are given by:

Table 2.4: Parameter values used in the PF-GI-POF model

Parameter	Parameter Symbols	Parameter values
n_{eff}	Group refractive index in the core	1.356
n_2	Cladding refractive index	1.342
Δ	Refractive index contrast	0.01
NA	Numerical aperture	0.19
$2a$	Core diameter	62.5 µm
λ	Wavelength	850 nm
σ_λ	Laser linewidth	0.65 nm
g	Refractive index exponent	2
ϵ	Profile dispersion parameter	0.6034
D	Chromatic dispersion parameter	60 ps/nm.km
η_w, k_0	Weighting and fitting constants	12.2, 9
K	Total number of mode groups	22

$$n_{eff} = n_1 - \lambda n_1'. \tag{2.22}$$

$$\varepsilon = -\frac{2n_1}{n_{eff}} \cdot \frac{\lambda \Delta'}{\Delta}. \tag{2.23}$$

Here the prime in n_1' and Δ' denotes for the first derivative with respect to the wavelength, which can be derived from (2.14) and (2.13), respectively.

As it can be seen from (2.18), the POF transfer function strongly depends on the P_k, which is an indication of the launching condition and power distribution across the fibre core. In general, there are two types of launching conditions, namely the overfilled launch (OFL) condition and restricted mode launch (RML). In OFL, all modes can be excited equally, while in RML only a restricted number of modes can be generated, which can be obtained using a laser-fibre interface such as the mode filtering techniques [165]. By compensating (2.16) and (2.18) in (2.15) using the parameters highlighted in Table 2.4, the $H_{POF}(f)$ is simulated in Figure 2.11 for 100 m of PF-GI-POF showing the channel frequency response, where the OFL condition is adopted. The fluctuations observed in the $H_{POF}(f)$ reveal that POF channel may suffer from a dramatic degradation due to the modal behaviour through the fibre,

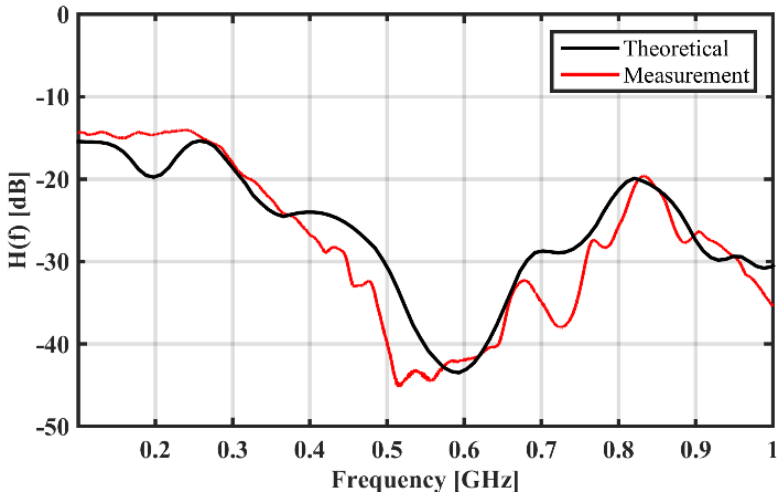

Figure 2.11: Frequency response for 100 m of PF-GI-POF

which may limit the BW.L significantly. The simulated $H_{POF}(f)$ indicates similar behaviour to that used in the experimental part. The experimental part will be explained in section 5.2.

2.4.5 Atmospheric Channel

The Earth's atmosphere is considered as a dynamic environment and therefore, it may not serve as an ideal medium for optical field propagation. It can affect the optical signal characteristics which may result in distortion in terms of several aspects such as diffraction, attenuation, turbulence-induced fluctuation in both amplitude and phase linearly [166]. As the channel properties are random in nature, their atmospheric effects can be characterized by means of the statistical approaches such as Kim theory, log-normal, Gamma-Gamma, and negative exponential model [53].

2.4.5.1 Atmospheric Channel Loss

The light intensity in the atmospheric channel may get degraded by the attenuation effect, which can be because of the interaction observed between the optical beam and aerosol particles present within the atmosphere. At dry air, it is composed of

permanent gases with a concentration of about 21% oxygen, 78% nitrogen, and 0.9% argon of total tropospheric gases. In addition to about 0.04% carbon dioxide, 4×10^{-6}% ozone , the water vapour (H_2O) is about 4% only, in addition to the particles of dust, combustion, and soil which make up 1×10^{-6} % [89]. Such a scenario may indicate that the FSO communications can be severely affected by the light absorption and scattering, which may have been resulted by gaseous molecules and aerosol particles in the atmosphere.

The absorption process is produced when a gaseous molecule, which can lead to quantum state excitation to a higher energy level and absorbs a radiation's photon. Hence, some photon energies can be converted into heat. Moreover, the atmospheric absorption is a function of wavelength and therefore it may characterize a selective behaviour, which may in turn lead to create preferable windows that have minimal absorption rate. The absorption rate is relatively smaller at the visible wavelengths, i.e., 400 to 700 nm, near IR at the wavelengths of 830, 940, and 1550 nm [85, 167]. On the contrary, the absorption may lead to eliminate the radiation propagation at wavelengths below 200 nm, where the absorption is dominated by the H_2O molecules [166]. On the other hand, the collisions observed between the photons and molecules may result in the scattering that may lead to deteriorate the performance of FSO drastically in the visible and IR wavelengths. It may induce noise into the receiver in addition to degrading the optical beam intensity [53]. In the scattering process, the photons' energy is redistributed with and without wavelength modification. The scattering phenomenon is affected by the size of particles with respect to the transmission wavelength. The scattering is specified into several regimes such as Rayleigh and Mie regimes. Rayleigh scattering is notably caused by the interaction observed between the propagated light with the atmospheric molecules that are smaller

in size compared to the radiation wavelength. It is applicable for the clear atmosphere and its dominant only at the wavelengths which are shorter than 1500 nm , owing partly to the scattering coefficient being proportional to $1/\lambda^4$, as indicated in the Rayleigh law [166]. Mie scattering may occur when the size of particles that scatter light is similar in scale to the wavelength. Hence, haze, aerosol, and fog molecules are the contributors to the Mie scattering. In particular, the latter effect is the major source of such type of scattering resulting in extreme loss of the light intensity [89].

The atmospheric loss can be considered as a time invariant parameter over multiple fading effects of the atmospheric channel and may have resulted from the combined deterministic factors of absorption and scattering. Therefore, for a terrestrial FSO network, transmitting an optical beam over the free space link distance d_i, the path loss component h_l can be defined using the exponential Beer-Lambert's law as [95]:

$$h_l = \exp(-\beta_l d_i), \tag{2.24}$$

where β_l denotes for the atmospheric attenuation coefficient i.e., wavelength and weather dependent parameter. Typical values of β_l are 0.43, 4.3 and 43 dB/km for clear, haze and fog weather, respectively [86].

2.4.5.2 Fog and Visibility

In terrestrial FSO, fog is among the atmospheric components that can potentially limit the link's length. The largest impact on the FSO performance is due to the size of fog droplets that may vary between 0.5 μm to 2 μm, which are in the same order of the typical FSO wavelengths where the Mie scattering may become dominant [167]. The loss in the receiver signal due to the fog effect is mainly because of the scattering rather than the absorption, particularly in the IR range [89]. The visibility-weather

Table 2.5: Attenuation coefficients based on link visibility [104]

Fog's type	Visibility V (m)	Attenuation β_l (dB/km)
Dense	40-70	143-250
Thick	70-200	40-143
Moderate	250-500	20-40
Light	500-1000	9-20

conditions such as fog may cause significant attenuation of the transmitted laser beam, which applies degradation in the channel range and availability. For example, dense fog may cause a severe intensity deterioration in the propagated signal owing to relatively higher attenuation on the order of hundreds of decibels per kilometre [168]. Practical measurements reported in [168] compared between two fog events: one was in Graz, Austria with continental (i.e., moderate) fog condition, and the second was in La Turbie, France with advection (i.e., dense) fog. The results indicated that the fog attenuation was 130 dB/km and 480 dB/km, respectively, which may cause significant restriction in relation to the availability of the FSO [109]. According to Kim's model, the fog attenuation is characterised based on the channel's visibility V, which is defined as the distance where the optical beam power may drop to a fraction of 5% or 2% of its original power [168]. As reported in [168], the attenuation for the FSO visibility below 100 m can reach up to 170 dB/km under the dense fog condition. Table 2.5 shows an empirical data for the attenuation β_l based on the link visibility [104].

2.4.5.3 Beam Divergence

One of the reasons to adopt the laser sources in the FSO networks is their capacity to transmit narrow optical beam, but due to the diffraction phenomenon, the travelling optical beam may experience spreading, which in turn may reduce the received optical

energy. The beam spreading that is caused by pure diffraction is related to the wavelength, size of emitting aperture, and shape of the wavefront, which can be assumed as a uniform plane wave. Therefore, part of transmitted beam may not be captured by the receiver, a loss which is known as geometric loss. It can however be increased with the FSO distance unless the size of the receiver is increased or receiver diversity technique is used [70]. Figure 2.12 demonstrates a typical FSO channel. The optical beam is transmitted from a LD with θ angle, and then launched to free space distance with d_i distance using optical lenses, which are positioned at the focal length L_{focal} to collimate and focusing the incoming optical beam into the PD. However, the optical beam is observed to spread constantly with the increase of d_i at a rate determined by the divergence angle θ_B. Hence, the beam diameter (i.e., spot size) $2W$ at the receiver can be defined by:

$$2W = 2W_B + \left(2 \times \tan\left(\theta_B\right) \times d_i\right). \tag{2.25}$$

Note that the θ_B is a function of transmitted beam waist radius (W_B) and it can be estimated by[166]:

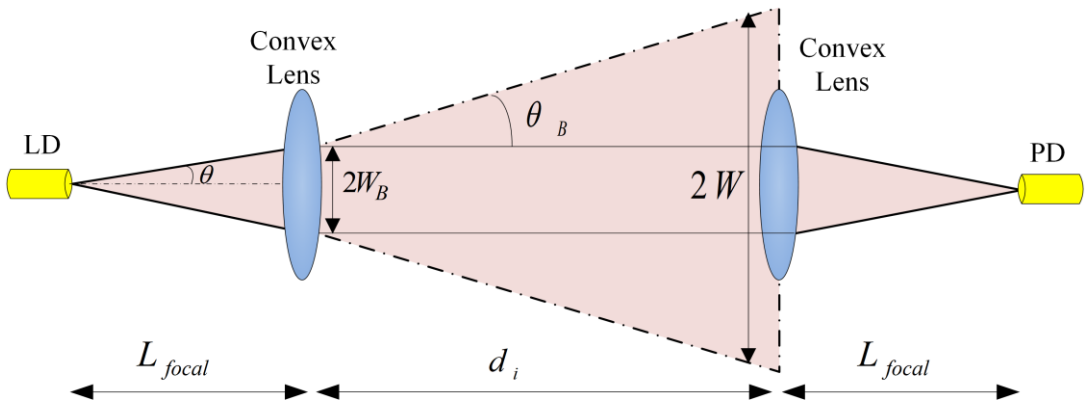

Figure 2.12: Typical atmospheric channel

$$\theta_B = \frac{\lambda}{\pi \cdot W_B} \ . \tag{2.26}$$

A theoretical model was proposed in [169] showing that the θ_B and W_B can be tuned to increase the average capacity for a given transmitted power. As the beam spreads through the FSO channel, geometric spreading loss (A_{geo}) is generated depending primarily on the divergence angle, receiver aperture and the free-space link and it can be defined by [140]:

$$A_{geo}[\mathrm{dB}] = 20 \log \left[\frac{d_{rx}}{d_{tx} + d_i . \theta_B} \right], \tag{2.27}$$

where d_{tx} and d_{rx} are the transmitter and receiver aperture diameter, respectively.

2.4.5.4 Atmospheric Turbulence

In the FSO channel with no fog, the atmospheric attenuation that is related to the visibility can be neglected [118]. However, the temperature inhomogeneity may cause a turbulence effect, which is associated with the variations in the refractive index of the FSO path. The channel fading because of the turbulence is known as scintillation, which refers to the random fluctuations in the amplitude and the phase of the received irradiance. Consequently, unstable air masses called as “eddies” are created with different sizes leading to deviations and fluctuations observed in the optical beam in comparison with its original state. Hence, a significant degradation in the FSO performance can be observed, especially in the long distance free-space propagation paths [118]. Numerous theoretical and practical investigations have demonstrated the effects of scintillation in relation to the FSO communication systems and have developed a variety of models to categorize its behaviour [139, 166, 168, 170]. Depending on the scintillation’s strength, the atmospheric turbulence is classified as

weak, moderate, strong and saturated [53]. In [166], a comprehensive study of turbulence models was presented to address the terrestrial FSO systems. In addition to the temperature, some other recent studies have also shown that the wind velocity, medium pressure and the altitude may affect the turbulence strength. The refractive index structure parameter C_n^2 [$m^{-2/3}$] is commonly adopted to describe the optical characteristics of the medium, which may depend on the altitude weather condition. Several theoretical and practical models were presented in [139, 171] to predict the C_n^2 for different weather conditions. The obtained results have shown that the scintillation, i.e., turbulence is strongly dependent on the wind velocity, pressure, altitude, relative humidity and aerosols size for both daytime and night-time conditions.

One of the most useful parameters is the scintillation index σ_I^2, which can be used to quantify the irradiance fluctuations effect and to characterize the strength of the optical turbulence. It is usually adopted to define the probability distribution function (PDF) of the irradiance fluctuations owing to the scintillation, as given by:

$$\sigma_I^2 = \frac{\left\langle I_{op}{}^2 \right\rangle}{\left\langle I_{op} \right\rangle^2} - 1, \tag{2.28}$$

where I_{op} denotes the received optical intensity and $\langle \cdot \rangle$ refers to the ensemble average.

In order to fully characterize the turbulence-induced scintillation fading effect, several statistical models were developed both theoretically and practically in order to predict and deduce the stochastic nature of the irradiance fluctuations under different atmospheric conditions. The random behaviour of the turbulent medium can be expressed as probabilistic terms rather than deterministic [139]. Therefore, the optical beam fluctuations resulting from the scintillation can be represented in terms of the

PDF [170].The most common models are the log-normal and Gamma-Gamma distribution models, which are widely used to describe the PDF under weak and weak to strong turbulence regimes, respectively [172]. Several schemes have been introduced to mitigate the optical turbulence effect such as the aperture averaging [173] and spatial diversity using multiple input multiple output (MIMO) systems [174]. More details about the atmospheric turbulence mathematical model are discussed in chapter 3 of this thesis.

2.4.6 Optical Receiver

In RoF-RoFSO system, the optical receiver is used to recover the electrical transmitted signal from the incident light. It has to be noted that it is composed of receiver optics, p-i-n (PIN) PD, trans-impedance amplifier (TIA), and the signal analyser. For the FSO part, the receiver telescope or lens focuses on the received optical beam towards the PD, which converts the optical energy into electrical energy prior to being amplified by the TIA. The signal analyser captures the amplified signal for off-line signal processing, equalization, demodulation and link performance assessment. The aperture of the telescope is usually large to help enable it collect as much of the uncorrelated propagation fields as possible, which is called as the aperture averaging technique. However, the background ambient light can be captured as well with a wide aperture area that may equally introduce additional noise at the receiver [53]. Hence, an optical band pass filter may need to be adopted to decrease the impact of the background noise.

There are two main detection schemes, namely IM-DD and coherent detection. The IM-DD is widely adopted in the optical communication systems because of its simplicity and cost-effective detection scheme, whereas the light intensity is used to

deliver the information data without considering the phase of the optical carrier. However, its performance is limited by the noise generated in the receiver amplifier and PD, which may degrade the receiver sensitivity [134].

On the other hand, the coherent detection pays attention to the light intensity, phase and the frequency. This technique adopts an optical local oscillator in the receiver, where its output combines with the received signal prior to being detected by the PD. It is worth highlighting that the use of coherent detection may enhance the spectral and signal-to-noise ratio (SNR) efficiency, and it has been examined as a method to extend the transmission span for long-haul networks before introducing EDFA as an effective device to increase the link span dramatically. Recently, it drew more attention for the higher data rate optical systems. In [175] and [176], an optimization for the coherent OFDM system was carried out. Additionally, an experimental transmission of the OFDM along 80 km SMF was reported in [177]. Nguyen *et al* [178] demonstrated theoretically a nonlinear equalizer in the coherent OFDM system for transmitting 40 Gbps over 400 km SMF link. However, the coherent detection involved relatively higher cost and architecture that is more complex. Hence, the IM-DD scheme is adopted in most of the RoF and RoFSO systems. In this study, as the RoF is adopted in the 4G-LTE architecture, there are some potential advantages of shifting the system complexity and signal processing to the CS rather than the multiple BSs. The use of coherent detection may increase the design complexity for the BS significantly, which is found contradicting to the main purpose of using RoF topology for the 4G-LTE systems. Consequently, the IM-DD is deployed in this thesis. The IM-DD scheme is introduced theoretically and practically for the RoF in the 4G-LTE in [22, 72]

Table 2.6: Accessible emission limits for 850 nm and 1550 nm wavelengths [53]

Type	Average optical power (mw)	
	λ = 850 nm	λ = 1550 nm
Class 1	< 0.22	< 10
Class 2	This category reserved for the range between 400-700 nm, same AEL for Class 1.	
Class 3R	0.22 - 2.2	10 - 50
Class 3B	2.2 - 500	50 - 500
Class 4	> 500	> 500

2.5 Eye Safety and Standards

Theoretically, high power optical beams may suppress some of the transmission limitations though compensating the high channel attenuation may lead to meeting the required data rate, achieve high SNR and improve the transmission path further [139]. However, the design of FSO system is always governed by the peak power constraints, which is related to the eye and skin safety standards that impose restrictions on the peak of the propagated optical power [118]. A number of international standards bodies provide guidelines on the safety of optical radiations, such as the European committee for electrotechnical standardization (CENELEC), American national standards institute (ANSI) and the international electrotechnical commission (IEC), in which the latter standard is widely adopted in FSO design regulations [139]. These standards classify the exposure limits of the laser sources. In general, the lasers are classified into four categories, namely Class 1 to Class 4. Class 1 represents the lower power while Class 4 being the most powerful laser group. Table 2.6 presents the accessible emission limits (AEL) for the wavelengths of 850 nm and 1550 nm, which are the widely adopted wavelengths in the FSO links [53].

As presented in Table 2.6, the Class 1 lasers that operate at 1550 nm wavelength are able to generate about 50 times more optical power in comparison with the 850 nm wavelength due to the fact that the light wavelengths beyond 1400 nm tend to be absorbed by the eye cornea, prior to be concentrated and focused on the retina[139]. Accordingly, longer FSO span and higher data rate can be supported. Nevertheless, it is noteworthy that the laser output power defines the laser classification and there is no inherent or eye safe wavelength.

2.6 Summary

In this chapter, the principles of both the RoF and RoFSO technologies are discussed, following which related studies of these two constructs are reviewed. The fundamental features of the RoF and RoFSO systems are presented in detail in addition to the applications of both technologies including the short and long range networks. The combination of hybrid RoF and RoFSO is presented as an appealing option for distributing radio signals and connecting multi-indoor RoF networks in places where the underground fibre may not be available. The basic hybrid RoF-FSO block diagram is presented to show the main system concepts, including the transmitter, channel and the optical receiver. On the other hand, the main challenges that may potentially affect the system performance are introduced. The MMF and POF impairments are explained in detail with the analytic model that can be used to simulate the channel in terms of the channel transfer function. The impact of the FSO channel is highlighted including the contribution of the atmospheric attenuation, turbulence and fog. The fog effect and the visibility range are discussed for different fog types. A background of the atmospheric turbulence is discussed with the aim of characterizing the turbulence effect. These effects are presented in a basic theoretical model and will be taken up

for discussion at length in the following chapters. Moreover, since the RoMMF-FSO system is presented in this thesis, the modal dispersion of the MMF represents the main challenge that may limit the system performance. Therefore, a mode filtering technique will be presented to mitigate the modal effects in the following chapter.

Chapter 3

Modal effects Mitigation of a novel Hybrid RoMMF/FSO system under turbulence effect

3.1 Introduction

In chapter 2, the overview of the hybrid radio over multi-mode fibre and free space optics (RoMMF-FSO) was introduced for transmitting the 4th generation-long term evolution (4G-LTE), where the main challenges were discussed in detail.

The integration of optical and radio frequency (RF) systems represents one of the most attractive solutions to deal with the growing traffic demands. The radio-over-fibre (RoF) technology has the ability to improve the coverage by means of adopting enhanced NodeB (eNB) and remote unit (RU) that deployed in the distributed antenna system (DAS) for the access and in-building networks. Traditionally, single-mode fibre (SMF) is employed for long distance applications owing to its low attenuation, whereas, the MMF is widely used for short distance applications [126]. In [179], the coverage of eNB was extended up to 2.1 km by means of using the RoF technology based on SMF. Commercial LTE-RoF solutions were demonstrated by CommScope for in-building applications by employing distributed antenna system to overcome the high RF signal penetration losses [180]. An experimental demonstration of transmitting LTE over 525 m MMF was reported in [41] at wavelength of 1310 nm with a ~3% error vector magnitude (EVM). At present, MMFs, identified by their

optical mode (OM), have different modal bandwidth as outlined in the ISO/IEC 11801 standard [181] and are considered for use as fibre backbone infrastructure in existing buildings. The types of MMF are defined by overfilled launch (OFL) bandwidth, which refers to a launching technique that employs a light source with a spot size larger than the fibre core diameter. The typical OFL bandwidth length products (BW.L) of OM1, OM2, OM3, and OM4 at 850 nm are 200, 500, 1500, and 3500 MHz·km, respectively [181]. A survey in [126] highlighted that ~17 million km of MMF are employed in in-building networks worldwide. Nonetheless, the modal dispersion in such fibres may induce the pulse broadening that limits the available bandwidth severely [126]. Correspondingly, several techniques were proposed in order to mitigate the impact of the number of co-propagating modal groups at the receiver, including the single-mode filtering technique (SMFT) [57] and the offset launch technique [58].

Apart from RoF, there is another complementary technology of FSO, which can be employed in the "last mile" of the access networks in urban/rural areas to deliver RF type signals. This particular technology is referred to as radio-over-FSO (RoFSO), which offers high bandwidth, immunity to the electromagnetic interference and free license fees in comparison to RF wireless communications. It is noteworthy that the link performance of FSO systems are affected by atmospheric channel conditions such as atmospheric absorption, scattering and scintillation, which affect the transmission quality, as well as the link availability [166, 172]. Scintillation is a random phenomenon initiated by small temperature variations along the optical path, i.e., optical turbulence, which in turn, resulted in the refractive index and irradiance fluctuations [170]. In [118], several schemes were introduced to combat turbulence induced fading effects. Apart from that, the impact of turbulence on the propagating

optical beam can be evaluated by means of employing several statistical models, which include log-normal and gamma-gamma distribution model adopted for weak and weak-strong turbulence regimes, respectively [172]. In this study, the author adopted log-normal model to theoretically assess the performance of the proposed system under weak turbulence.

It is noteworthy that the combination of RoF and RoFSO will be employed in both access and in-building networks in order to extend the transmission range of the wireless services [67]. RoFSO will be employed as a bridge between the multi-RoF systems, in which, no fibre optic infrastructure exists in the place, particularly in rural areas. In [125], an analytic model for transmission of an orthogonal frequency division multiplexing (OFDM) signal over a FSO link was reported, exhibiting that RoFSO is highly sensitive to the atmospheric turbulence, received optical power and modulation index. In [117], experimental investigation of the work in [125] was reported, whereby a digital TV-based RF signal was transmitted over a 1 km FSO link at λ of 1550 nm. Although a lot of research has widely considered the atmospheric effects on the FSO link when using short length SMFs, the perturbing effects generated by MMF have been not studied. In [172], experimental demonstration of the baseband signal transmission at 100 Mbps over a 1 m of MMF and a 2.5 m of a FSO link with weak turbulence was reported with a packet error rate (PER) of ~10^{-2} by means of using coding. Furthermore, an experimental RoF and RoFSO systems using the RF frequency ranges from 0.4 - 4 GHz and a 10 km of SMF were reported in [106].

In this chapter, a RoMMF-FSO system is proposed for the last metre (inter-room networks) and the last mile of the access networks as presented in Figure 3.1. The line of sight (LOS) FSO links are employed to inter-connect buildings with transmission

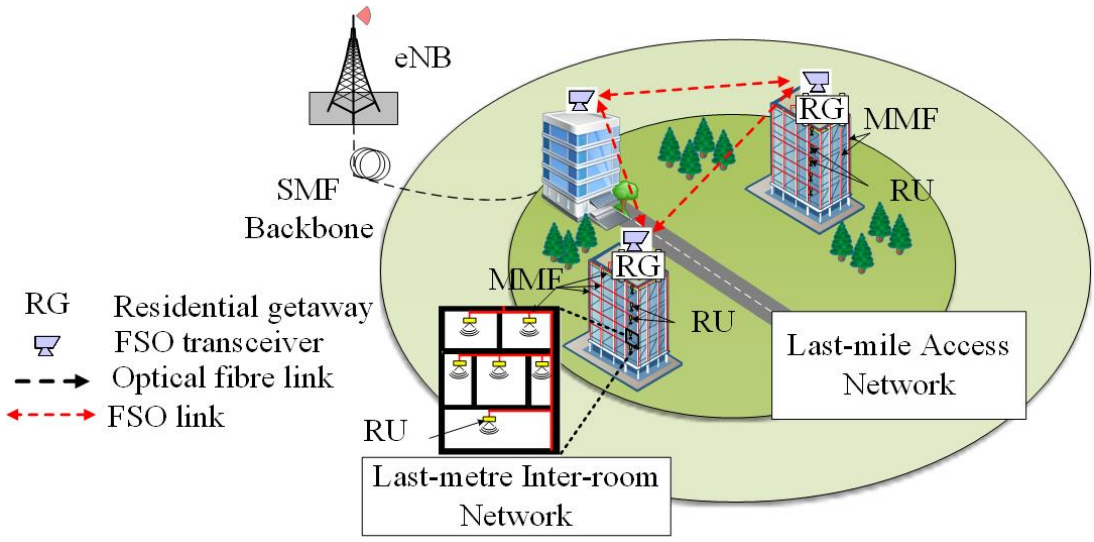

Figure 3.1: RoMMF-FSO scenario providing wireless services in the last-metre and last-mile access networks [121]

spans of a few kilometres [182]. Indoor RoF systems with MMF are deployed for connecting the residential gateway (RG) with the RU. A mode filtering technique is proposed and theoretical and experimental verifications are carried out in order to mitigate the modal effects with the aim of improving the system performance, in terms of the channel transfer function, optical beam profile and EVM for a range of signal-to-noise ratio (SNR). The author has published the resulting output of this chapter in [56, 120, 121].

3.1.1 Mode Filtering Techniques

It should be noted that the hybrid RoMMF-FSO link may provide an advantageous solution. Nevertheless, MMF may experience significantly higher distortion effects with regards to modal dispersion [183]. Different mode groups propagate at different velocities within MMF and thus, result in signal distortion at the photodetector (PD). In a hybrid system, different modal groups of the MMF to the free space are coupled with a different group delay, which in turn, may result in affecting the hybrid RoMMF-FSO link. Furthermore, different mode groups have different beam shapes as they are

affected differently by the channel condition they go through such as turbulence. This, in turn, may lead to additional distortions and fluctuations in the frequency response of the system. The reduction of the modal dependence is deemed to be very important owing to the fact that the modal dispersion has the strongest effect on the hybrid channel. Several methods were proposed to improve the modal behaviour of the fibre channel, and some of them will be adopted for the hybrid channel. The utmost imperative techniques are mode filtering [57] and offset launch techniques [58]. The latter requires precise positioning, hence the complicated practical applications. Nevertheless, it is reported that this technique is unable to solve the hybrid RoMMF-FSO system's beam profile problem. Consequently, the mode filtering technique is adopted for the proposed hybrid RoMMF-FSO system. It should be noted that there are a number of mode filtering schemes, which are used to reduce the number of mode groups. One of them is the SMF filter, which has the ability to filter all higher mode groups, except for the fundamental mode [57]. The SMF filter is installed between the MMF and the FSO part of the link to ensure that only the fundamental mode is transmitted over the free space channel. Hence, the author intends to investigate the development of the mode filtering for RoMMF-FSO system with SMF. Apart from that, the gradient index (GRIN) lenses are employed, through which the transmitted signal will be coupled to the free space. The GRIN lens is employed at the receiver side to project the light beam to be focused onto the PD. In addition, with the employment of GRIN lens, the FSO channel loss is reduced due to the beam focusing, which in turn, leads to further improvement in the performance of the system.

3.2 Theoretical Model

The proposed system presented in Figure 3.2 is modelled using MATLAB^{TM} with the following principal aspects:

3.2.1 Hybrid Linear Model

The hybrid RoMMF-FSO link can be separated into three different sections, namely transmitter, Tx (i.e., electrical-optical conversion), receiver, Rx (i.e., optical-electrical conversion) and optical channel, which includes the fibre to free space interface (see Figure 3.2). OFDM LTE signal is generated at the Tx and the baseband signal is composed of 16-quadrature amplitude modulation (16-QAM) at 20 MHz as a single carrier modulation (SCM), $\boldsymbol{X}(m)$, where m=0, 1, ……, N_s-1 is the subcarrier index, and N_s=2048 is the number of subcarriers. An N_s–point inverse fast Fourier transform (IFFT) is applied to generate the OFDM signal $\boldsymbol{S}(x)$, which is used to describe the LTE signal as:

$$\boldsymbol{S}(x) = \frac{1}{\sqrt{N_s}} \sum_{m=0}^{N_s-1} \boldsymbol{X}(m) e^{j2\pi mx / N_s}, \tag{3.1}$$

where x = 0, 1, ……, N_s-1 is the time domain index. The cyclic prefix (CP) is added at the rate of ¼ in order to generate $\boldsymbol{S}_{cp}(x)$ signal to avoid ISI, which is then passed through a parallel-to-serial converter (P/S) and a digital-to-analogue (DAC) converter. The continuous signal $\boldsymbol{S}_{cp}(t)$ is then converted into a passband OFDM signal $\boldsymbol{S}_{RF}(t)$ at f_{RF} of 2.6 GHz, which is the most common LTE band deployed in Europe [184], and is given by [72]:

$$\begin{aligned} \boldsymbol{S}_{RF}(t) = {} & \mathrm{Re}\{\boldsymbol{S}_{cp}(t) * \cos(\omega_{RF}(t))\} \\ & + \mathrm{Im}\{\boldsymbol{S}_{cp}(t) * \sin(\omega_{RF}(t))\}, \end{aligned} \tag{3.2}$$

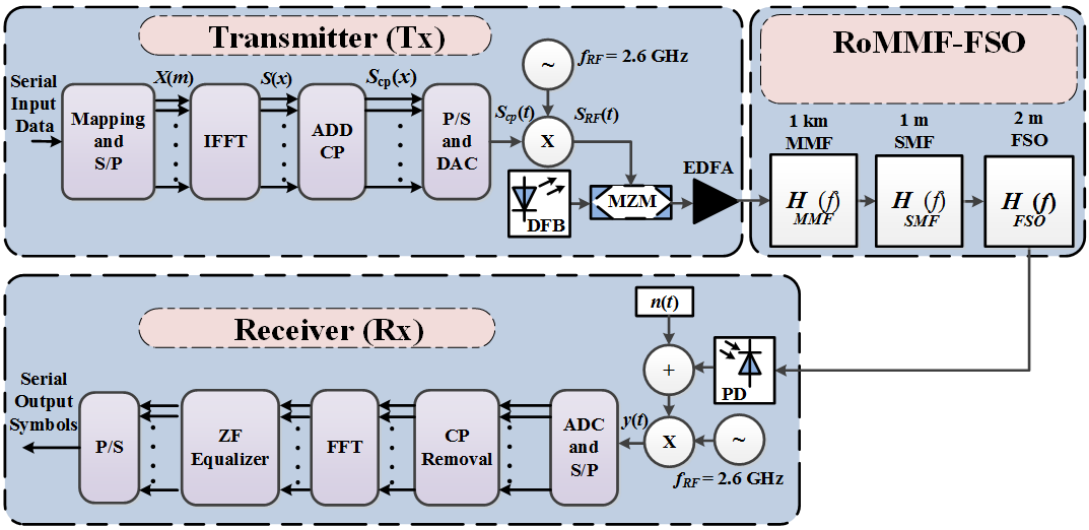

Figure 3.2: Theoretical model of the RoMMF-FSO system [121]

where $\omega_{RF} = 2\pi f_{RF}$.

The LTE signal $\boldsymbol{S}_{RF}(t)$ is employed to externally modulate the output of a distributed feedback laser (DFB) laser by means of using a Mach–Zehnder electro-optical modulator (MZM). In comparison, the MZM is recommended to be employed for high-frequency digital applications in order to decrease the signal distortion and noise than the direct modulation (DM). Moreover, MZM based transmitters are preferred to be operated at dense wavelength division multiplexing (DWDM), due to their wavelength range flexibility, which are able provide higher system capacity [130]. The transmitted optical field at the output of the MZM $E_o(t)$ and the power transfer function $P_{MZM}(t)$ are specified by [185]:

$$E_o(t) = E_i(t)\cos\left[\frac{\pi}{2}\frac{(\boldsymbol{S}_{RF}(t)+V_{bias})}{V_\pi}\right]e^{-j\left[\frac{\pi}{2}\frac{(\boldsymbol{S}_{RF}(t)+V_{bias})}{V_\pi}\right]}, \tag{3.3}$$

$$P_{MZM}(t) = \alpha_{MZM} P_i \cos^2\left[\frac{\pi(\boldsymbol{S}_{RF}(t)+V_{bias})}{V_\pi}\right], \tag{3.4}$$

where $E_i(t)$ is the input optical fields of the MZM, V_{bias} is the MZM biasing voltage, V_π is the driving voltage, which is required to create a π radian phase shift at the MZM output, and α_{MZM} is the MZM insertion loss.

The output of MZM is amplified by the erbium-doped fibre amplifier (EDFA) in order to compensate the link loss, as well as to ensure a sufficient link power budget, prior to the transmission over 1 km, 1 m and 2 m of MMF, SMF and FSO links, respectively. Apart from that, a patch cord SMF is employed as a mode filter between MMF and FSO.

At the Rx, following the optical to electrical conversion by means of using a PD, the modulated signal, which is down converted into 20 MHz using a local oscillator running at the same frequency of 2.6 GHz as in the Tx. The remaining parts of the Rx are exactly the same as the Tx, except for the frequency domain of zero forcing (ZF) equalizer, which is used to compensate for phase and amplitude distortions incurred by propagating signal.

In this work, a number of assumptions has postulated, which include: (i) a linear MZM (i.e., chirp free);(ii) no fibre nonlinearities since the optical power level is relatively low, i.e., not exceeding10 dBm [186]; and (iii) a non-selective frequency of FSO channel since the FSO link has a negligible delay spread [118]. It is noteworthy that the proposed link in clear channel is time invariant and therefore, it can be modelled as a linear time-invariant system. In addition, it can be defined in terms of the link transfer function, which depends strongly on the modal group delay and the modal power distribution induced by the link characteristics and launching conditions at the Tx/Rx ends and the intermediate MMF/SMF interface [187].

3.2.2 Fibre Channel

The modulated optical signal is launched to the free space via MMF and SMF as depicted in Figure 3.2. In the proposed model, SMF is employed as a mode filtering technique, in which dominant mode is allowed to be propagated. The total transfer function $H_{total}(f)$ is specified as:

$$H_{total}(f) = H_{MMF}(f) \cdot H_{SMF}(f) \cdot H_{FSO}(f), \tag{3.5}$$

where $H_{MMF}(f)$, $H_{SMF}(f)$ and $H_{FSO}(f)$ are the transfer functions for MMF, SMF and FSO channels, respectively. $H_{MMF}(f)$ is given as [188]:

$$H_{MMF}(f) = \overbrace{\exp\left[-\frac{(2\pi f D L \sigma_{\lambda})^2}{2}\right]}^{\text{First term}} \cdot \overbrace{\sum_{k=1}^{K} P_k \exp(-j2\pi f \tau_k L) \cdot 10^{-\alpha_k L/10}}^{\text{Second term}}, \tag{3.6}$$

where f is the modulating frequency, D [ps/nm.km] is the material dispersion coefficient, L is the fibre length [km], σ_{λ} is the laser linewidth [nm], K is the total number of the mode groups, P_k, τ_k , and α_k are the input power, group delay and mode dependent attenuation coefficient of the k^{th} mode group. It should be noted that, the first and second terms in (3.6) represent the chromatic and modal dispersions, respectively. Chromatic dispersion depends on the spectral extent of the light source, while modal dispersion is due to the different propagation velocity of the mode groups. For the refractive index with a parabolic profile in the fibre core, (2.19) can be used to describe the total number of mode groups in the MMF as [161]:

$$K = \frac{\pi d_{MMF} n_{eff}}{\lambda} \left(\frac{g \cdot \Delta}{g+2}\right)^{1/2}, \tag{3.7}$$

where d_{MMF} is the MMF core diameter, n_{eff} is the effective refractive index of the MMF core, g is the refractive index profile parameter and Δ is the refractive index contrast. For the fibre that adopted in the theoretical model, the parameters of d_{MMF}, n_{eff}, g and Δ are 50 μm, 1.45, 2 and 0.01 (please see Table 3.1) the number of propagating mode groups K is 10.

The linear $H_{SMF}(f)$ describes the effect of the chromatic dispersion in addition to the SMF attenuation. Nevertheless, these effects can be neglected due to the short length of SMF (i.e., 1 m). However, the insertion loss due to the coupling between MMF and SMF is considered in this work (see Table 3.1). As indicated in Figure 3.2, the output of MMF is applied to SMF as a modefilter in order to ensure the propagation of the fundamental mode in the free space channel. Accordingly, the transfer function of the filtered beam can be defined as:

$$H_{filtered}(f) = H_{MMF}(f) \cdot H_{SMF}(f), \tag{3.8}$$

which is approximated using (3.6) as:

$$H_{filtered}(f) = \exp\left[-\frac{(2\pi fDL\sigma_{\lambda})^2}{2}\right] \cdot P_{fund} \exp\left(-j2\pi f \tau_{fund} L\right) \cdot 10^{-\alpha_{fund} L/10}, \tag{3.9}$$

Where P_{fund}, τ_{fund} and α_{fund} are the power, group delay and the attenuation of the transmitted fundamental mode, respectively. It has to be noted that a uniform power distribution in the MMF core is considered to estimate P_{fund} in (3.9).

3.2.3 FSO Channel

In modelling a clear FSO channel, the simplest plane wave model is adopted, in which, the electrical field distribution can be modelled as the superposition of far field distributions of each mode groups. The far field delay different mode groups in

identical way and thus, a clear FSO channel can be modelled as a summative attenuation. A FSO channel state h_{FSO}, which represents the optical intensity fluctuations due to the atmospheric loss, and turbulence- and misalignment-induced fading is defined as [90]:

$$h_{FSO} = h_l \cdot h_s, \tag{3.10}$$

where h_l and h_s denote attenuations due to beam extinction arising from scattering, absorption and geometric spread and scintillation. Notably, the author assumed that there is no misalignment induced losses. h_l is a deterministic parameter and hence, is considered as a constant scaling factor over a long time scale, compared to the bit intervals of ~10^{-9} s [189], which is given by [90]:

$$h_l = \left[\frac{A_{rx}}{\pi \left(\frac{\theta_B}{2} d_i \right)^2} \right] \exp\left(-\beta_l d_i\right), \tag{3.11}$$

where $A_{rx} = \pi(d_{rx}/2)^2$ is the Rx aperture area, d_{rx} is the Rx aperture diameter, θ_B is the divergence angle, d_i is the FSO span, and β_l is the atmospheric attenuation coefficient, which is ~0.43 dB/km for clear channel condition [90]. h_s is time-variant factors, which exhibit variations in the fading channel in the order of milliseconds, in which their stochastic behaviour is described by their respective distributions [190]. The turbulence (i.e., scintillation) is caused by random variations in the refractive index of the medium, along the transmission path. The refractive index structure parameter C_n^2 [$m^{-2/3}$] is widely employed to measure the strength of the refractive index fluctuations, which is defined as [166]:

$$C_n^2 = \left(79 \times 10^{-6} \frac{P}{T^2} \right) \cdot C_T^2 , \tag{3.12}$$

where P is the atmospheric pressure in millibar, T represents the absolute temperature in Kelvin, C_T^2 stands for the temperature structure constant that describes the C_n^2 sensitivity to small-scale temperature variations, which can be obtained from the mean square temperature difference of two adjacent temperature points T_1 and T_2, separated by distance R_p as outlined by [170]:

$$C_T^2 = (T_1 - T_2)^2 / R_p^{2/3}, \qquad l_0 \ll R_p \ll L_0 \tag{3.13}$$

where l_0 and L_0 are the inner and outer scales of the temperature fluctuations.

Turbulence is classified as weak, moderate and strong, depending on the strength of scintillation and is defined using Rytov variance σ_R^2. The σ_R^2 is deduced based on the assumption that the laser beam propagates in a plane wave with homogeneous turbulence (i.e.,C_n^2 is constant along the horizontal path), which is given as [120]:

$$\sigma_R^2 = 1.23\, C_n^2 w^{7/6} d_i^{11/6} , \tag{3.14}$$

where $w = (2\pi / \lambda)$ is the optical wavenumber. Note that, $\sigma_R^2 < 1$, $\sigma_R^2 \sim 1$, and $\sigma_R^2 > 1$ corresponds to weak, moderate and strong turbulence regimes, respectively [166]. For weak turbulence, log-normal distribution model is widely used to describe the FSO channel statistically with the probability distribution function (PDF) of the irradiance fluctuation is given by [189]:

$$f_{h_s}(h_s) = \frac{1}{\sqrt{2\pi\sigma_X^2}} \frac{1}{h_s} \exp\left\{ - \frac{\left(\ln(h_s) + \sigma_X^2 / 2 \right)^2}{2\sigma_X^2} \right\}, \tag{3.15}$$

where $f_{h_s}(h_s)$ is the PDF of the atmospheric channel and σ_X^2 is $\sim\sigma_R^2/4$ for the case of plane wave propagation [189]. Figure 3.3 illustrates the variation in log-normal distribution against the turbulent channel state h_s for different values of σ_R^2 in the weak turbulence regime. It is evident that for σ_R^2 = 0.01 and less, the PDF distribution is nearly Gaussian. However, for $\sigma_R^2 \geqslant 0.1$ the PDF distributions are not Gaussian and are skewed to the right, which indicate the significant effect of the atmospheric turbulence on the intensity fluctuations of the optical signal.

The link total transfer function can be approximated by:

$$H_{total}(f) = \left|H_{filterred}(f)\right| \cdot 10^{-\alpha_{total} L_{total}}, \tag{3.16}$$

where α_{total} and L_{total} is the total system attenuation and total channel distance, respectively. Equation 3.16 includes the effects of both fibre and FSO channels, where the latter is represented in terms of link attenuation in clear weather condition.

The proposed system can be assessed by means of using. EVM that can be defined as [191, 192]:

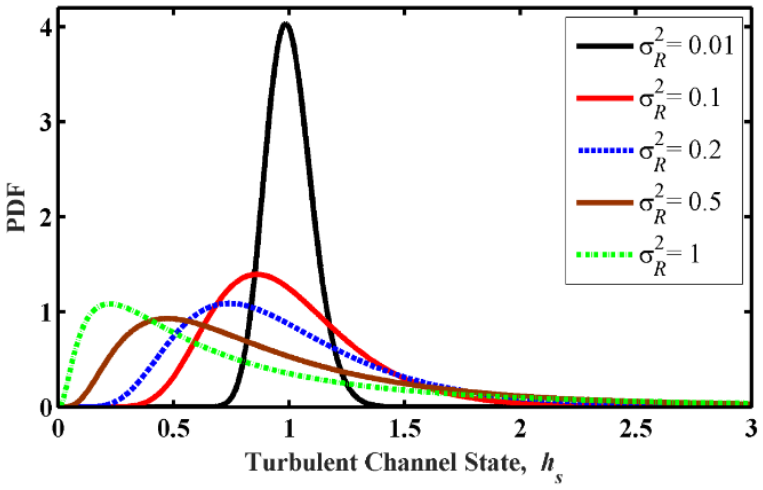

Figure 3.3: Log-normal PDF variations for different values of Rytov variance [120]

$$\mathrm{EVM} = \sqrt{\frac{\frac{1}{N_s}\sum_{x=1}^{N_s}\left|S_r(x_s) - S_t(x_s)\right|^2}{P_{\max}}}, \tag{3.17}$$

where N_s is the number of the symbols for the in phase- quadrature (I-Q) constellation, $S_r(x_s)$ and $S_t(x_s)$ are the received and transmitted baseband symbols. $P_{\max}$ is the maximum magnitude of the ideal transmitted symbol power, which is utilised for normalization.

Also, the system frequency response and laser beam profile are employed to evaluate the system performance under modal effects and turbulence fading.

3.3 Experimental Model

The schematic block diagram of the experimental set up for the proposed system is presented in Figure 3.4. All the key relevant system parameters are shown in Table 3.1. The LTE signal (i.e., 16-QAM with a passband frequency of 2.6 GHz and a bit rate of 67.2 Mbps) is generated at the Tx using a Rohde&Schwarz (R&S) vector signal generator (VSG), which is used to externally modulate a DFB laser at λ of 1550 nm

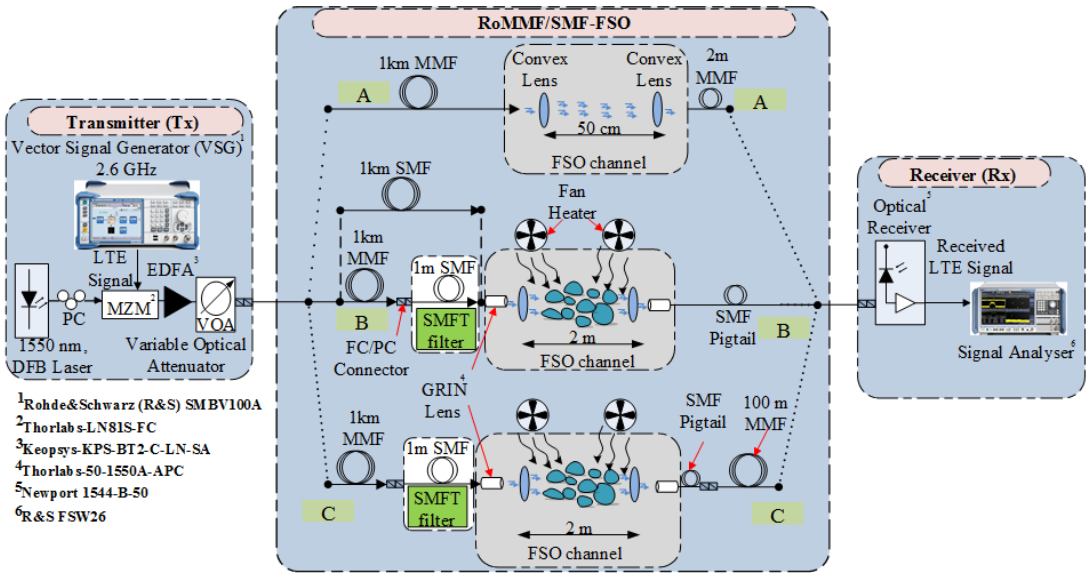

Figure 3.4: Experimental setup of RoMMF-FSO system with three practical scenarios [121]

Table 3.1: System parameters

Parameter	**Values**
Modulation scheme	16-QAM
Baseband multiplexing	OFDM
Carrier frequency	2.6 GHz
Signal bandwidth, bit rate	20 MHz, 67.2 Mbps
RF power	-10 dBm
DFB wavelength, power	1550 nm, 6 dBm
Relative intensity noise (RIN)	-145 dB/Hz
MZM insertion loss	6 dB
EDFA gain, noise figure	13.5 dB, 3 dB
MMF d_{MMF}, $n_{eff,}$ α_{fund}	50 µm, 1.45, 0.3 dB/km
MMF Δ, g	0.01, 2
SMF loss	0.15 dB/km
MMF/SMF coupling loss	1.7 dB
FSO total loss	15 dB
GRIN lens aperture	1.8 mm
Plano-convex lens diameter	25.4 mm
PIN PD responsivity	0.75 A/W
TIA 3dB bandwidth	DC to 12 GHz
VSA noise floor at 2.6 GHz	- 152 dbm

using MZM. Note that, a polarization controller (PC) is employed to control the polarization of the DFB laser. A low noise EDFA and a variable optical attenuator are used to optimize the transmitted optical power prior to being launched into a 1 km OM2 MMF. As for the channel, three setups are considered (see Figure 3.4), which depicts various inter-building network configurations. In all three setups, collimating optical lenses are used to launch light from fibre into a free space channel and capture light from the channel into a fibre. The output of the Tx (i.e., a downlink LTE signal) is transmitted via: (i) Setup A ;(ii) Setup B, which includes either a 1 km MMF or a 1 km SMF to validate the proposed technique; and (iii) Setup C, as presented in Table 3.2. Setups A & B are chosen to show the DL connection between in-building network to the UE, while setup C represents the FSO connection between multiple in-building networks as shown in Figure 3.1. It has to be noted that, a 100 m MMF in setup-C represents the fibre length used in an indoor environment. In Setups B and C, pigtailed GRIN lenses are used to align the optical beam propagating through the FSO

Table 3.2: Experimental setups with their applications

Setup	Details	Application
A	1 km MMF, 50 cm long free space channel and 2 m MMF	Building-to-UE (MMF-FSO) connection without SMFT
B	1 km MMF, 1 m SMF, 2 m FSO channel and 1 m SMF	Building-to-UE (MMF-FSO) connection with SMFT
C	1 km MMF, 1 m SMF, 2 m FSO channel, 1 m SMF and 100 m MMF	Inter-building network (MMF-FSO-MMF) with SMFT

channel. The GRIN lens can correct the monochromatic aberrations, as well as enhance the alignment tolerance and the coupling efficiency (i.e., fibre to free space and free space to fibre) [193].

At the Rx, a combination of p-i-n (PIN) PD and a trans-impedance amplifier (TIA) are employed to regenerate the electrical LTE signal, which is captured by means of using a real-time signal analyser for off-line signal pocessing, equalization [194], demodulation and link performance assessment.

In order to validate the proposed system's performance under atmospheric turbulence, a dedicated indoor FSO chamber is added to mimic the outdoor environment. To generate turbulence, two fans were used to blow hot and cold air into the chamber, perpendicularly to the propagating optical beam. Twenty temperature sensors with a spacing of 10 cm were deployed along the chamber to monitor and measure the temperature profile. In order to create different scintillation effects, two levels of thermal gradient, i.e., 6° C and 31° C were introduced to the chamber. Subsequently, these values are used to determine the turbulence strength in terms of C_n^2, followed by σ_R^2 using (3.12) and (3.14), respectively. The weak turbulence calculated values of C_n^2 are 5.37×10^{-13} $m^{-2/3}$ and 4.09×10^{-10} $m^{-2/3}$ and for d_i= 2 m, while the values of σ_R^2 are 1.2×10^{-4} and 0.1, respectively. The experimental implementation of the proposed system is illustrated in Figure 3.5, which demonstrates the setup of

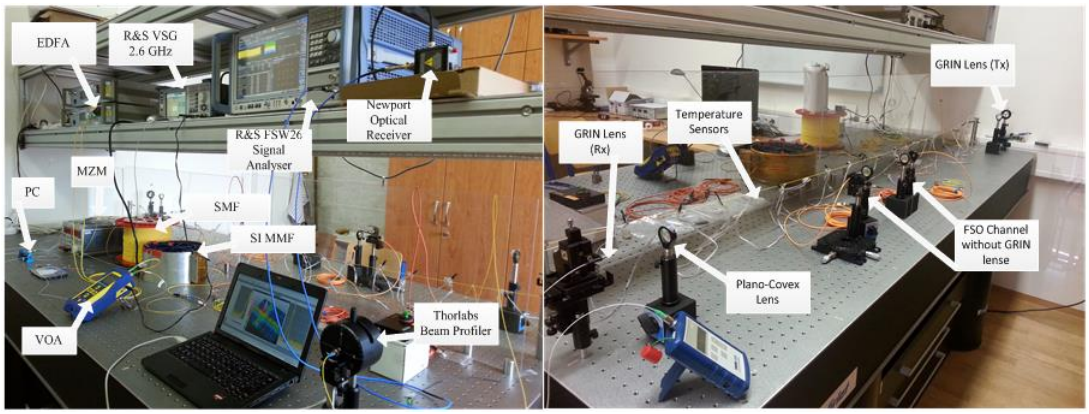

Figure 3.5: Laboratory setup showing the RoMMF-FSO system [56]

RoMMF channel, including the beam profile measurement and the two FSO channels for RoFSO network. The beam profile is captured using a BP104-IR beam scanning profiler from Thorlabs.

3.4 Results and Discussions

In this section, the performance of SMFT is evaluated, in terms of the measured system transfer function and the laser beam profile. Also, the influence of atmospheric turbulence on LTE signals transmitted over RoMMF-FSO links is investigated theoretically and practically. The measured system performance is validated in terms of EVM by using MATLAB^{TM} simulations.

3.4.1 Transfer Function

The transfer function of the overall system is measured using the Agilent E5071C network analyser. The system transfer function describes the perturbing effects on the propagating optical beams along with the MMF and FSO channels, due to the multi-mode propagation within MMF as described in (3.6). Figure 3.6 illustrates the transfer function of the RoMMF-FSO system for setups A, B and C. At lower frequencies, the transfer function for setup A, with no SMFT showed degrading in the system gain due

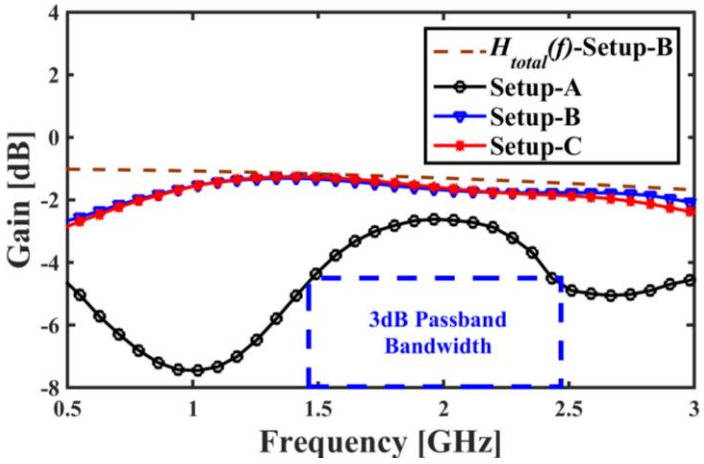

Figure 3.6: Transfer function of the RoMMF-FSO system [121]

to the high attenuation and dispersion with a maximum drop at 1 GHz. The results revealed that the system performance fluctuates beyond the baseband showing highly sensitive performance to frequency changes. Furthermore, this shows a limited pass band bandwidth to ~1 GHz (by considering ~1.45 GHz and ~2.45 GHz as the lower and upper cut-off frequencies, respectively). This indicates that LTE based OFDM signal at a 2.6 GHz carrier frequency will experience frequency selective fading, which in turn, resulted in corrupted orthogonality that leads to channel induced ISI [195].

In comparison to Setup A, the transfer functions for setups B and C depict a significant enhancement in the frequency dependent stability when SMFT is adopted. Notably, the SMFT interface can filter out higher order modes, which makes the system transfer function much flatter. This is established through minimizing the number of modal groups as evident by a significant reduction in the ripple level from ~5 dB to < 1 dB and hence, enhancing the channel bandwidth effectively for a wider range up to 3 GHz. Furthermore, Figure 3.6 compares the experimental results with the predicted transfer function model $H_{total}(f)$ of the Setup B in clear weather FSO link using (3.16). The difference lies on the low frequencies (i.e., f < 1 GHz) owing to the

no consideration of the transfer function of the optoelectronic devices (i.e., MZM and PD) in the theoretical model.

3.4.2 Optical Beam Profile

The beam profile was captured in real-time by means of using a BP104-IR beam scanning profiler from Thorlabs. Figure 3.7 illustrates the measured laser beam profiles for setups A and B for three different turbulence strengths (i.e., σ_R^2), in addition to the clear FSO channel. Table 3.3 depicted a summary of the obtained results. The beam profile showed the optical power distribution at a plane transverse to the beam

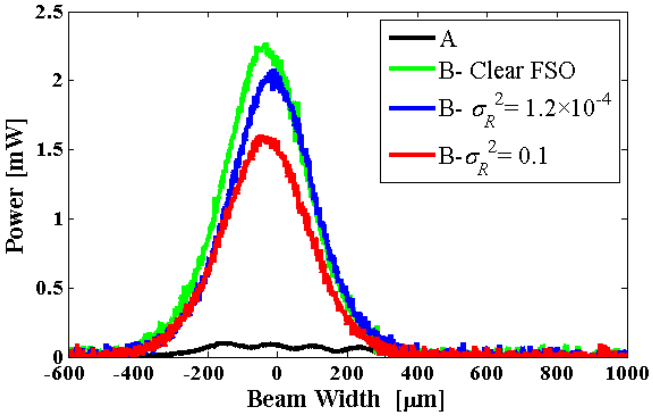

(a)

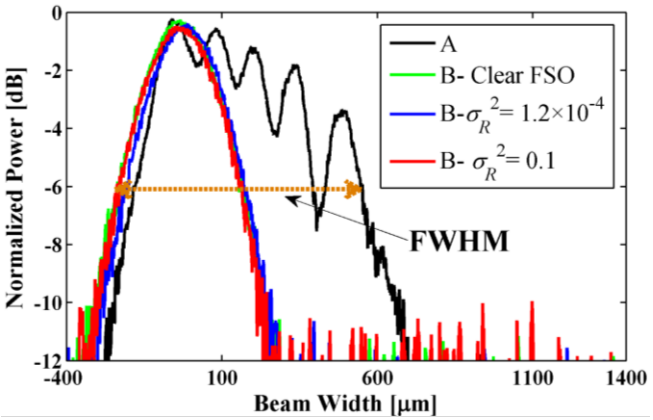

(b)

Figure 3.7: Beam profile of the RoMMF-FSO shown turbulence effects on: (a) Amplitude, and (b) FWHM [121]

Table 3.3: Beam profile characteristics

Setup	Peak Power (mW)	Coupling Efficiency (dB)	FWHM (μm)
A	0.1	--	374
B- clear FSO	2.3	13.6	258
B- σ_R^2=1.2×10^{-4}	2.1	13.22	267
B- σ_R^2=0.1	1.6	12	281

propagation path. Figure 3.7 (a) shows the peak power of the received beam for the two setups. As regards setup A with no filtering, the received signal was attenuated severely due to several reasons such as the lack of alignment, a large divergence angle and modal effects. Interestingly, the employment of SMFT (setup B) overcomes these effects significantly. Table 3.3 illustrates the enhancement of the peak received optical power, showing significant improvement in the coupling efficiency by 13.6 dB, which was determined with respect to setup A. Figure 3.7(b) displays the normalized power of the beam profile in order to illustrate beam width in terms of the full width at half maximum (FWHM). The optical beam is subjected to the shape deformations, which is mainly due to the diffraction and deflection that caused variations in the power levels of the received signal. As regards the received beam in setup-A, the measured beam profile has several peaks and the beam profile is relatively wide. In contrast, the received beam in setup B, the measured beam profile show an improvement in the FWHM by ~ 100 μm.

Even though MMF can support propagation of a large number of modes, a finite number of modes clustered in groups with nearly the same propagation characteristics are considered [161]. For the fibre with the parabolic refractive index profile (i.e., g=2) the number of propagating mode groups K estimated using (3.7) is 10. On the contrary, the beam shape is close to the Gaussian distribution with the dominant mode propagation when SMFT is adopted in the setup B as observed in Figure 3.8, which

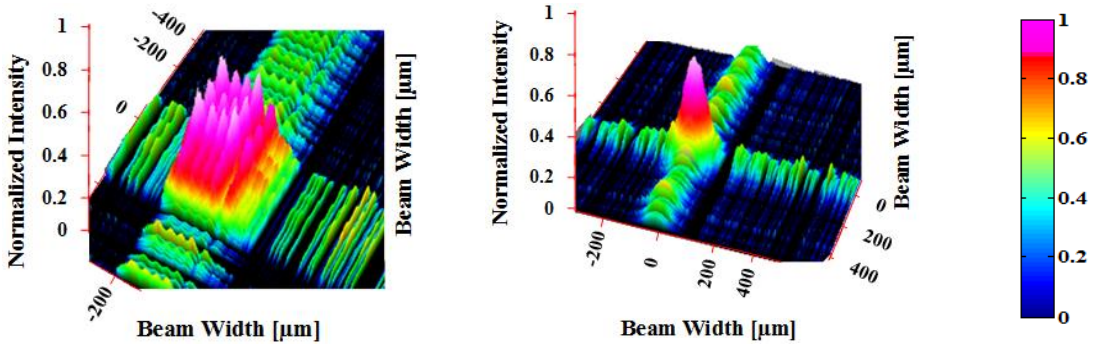

Figure 3.8: 3D illustration of the beam profile: (a) with no SMFT, and (b) with SMFT [121]

indicates three-dimension (3D) illustration of the captured beam profile. It can be observed in Figure 3.8(a) that the modal distribution at the receiver is distorted due to the optical propagation with no SMFT (setup A), while Figure 3.8(b) illustrates the Gaussian distribution of the received optical beam following SMFT, which has eliminated high order modes.

3.4.3 EVM Results

The EVM parameter demonstrates the impact of distortion induced in the system. The proposed system is designed to achieve ≤12.5% EVM as a figure of merit, which is required by the 3rd generation partnership project (3GPP) LTE for 16-QAM modulation [196].In the simulation model, the LTE signal was used to modulate the DFB laser externally by means of using MZM. The MMF/SMF interface is modelled using (3.16), while the log-normal distribution model is used to simulate the FSO channel under weak turbulence regime. Predicted EVM results are determined using (3.17), while the measured values are captured using the signal analyser, which is equipped with built-in vector signal analyser (VSA) software. Firstly, the influence of SMFT is investigated with no turbulence induced fading effect.

Figure 3.9 demonstrates the measured EVM against the SNR for the three setups in comparison to the back-to-back (B2B) setup. The EVM-SNR performance can be used to estimate the minimum SNR that should be consider to achieve the 3GPP LTE EVM requirement. On the other hand, the noise floor of the VSA at 2.6 GHz is -152 dBm [194], which indicates a negligible noise induced by the measurement equipment. In setup A, EVM values are high and not stable due to the irradiance fluctuation, which is caused by the modal effects. The system performance is enhanced by using SMFT in setups B and C. At a SNR of 20 dB, EVM is reduced from ~11% to ~7% (i.e., 4% enhancement) when using a filter, which is identified as the setup-B-MMF in Figure 3.9. Additionally, a 1 km SMF was used in the setup B instead of a 1 km MMF and a 1 m SMF to validate the obtained results. The EVM value decreased from ~7% to ~6.6% (i.e., 0.4% difference only) for the same SNR value (i.e., 20 dB) compared to a 1 km MMF. The EVM values were measured via the VSA with a precision of ±0.2% [194]. Note that, the EVM results are based on the average of three sets of measurements under identical conditions. The required additional power of the input signal to achieve the EVM limit is referred to as the power penalty (PP).

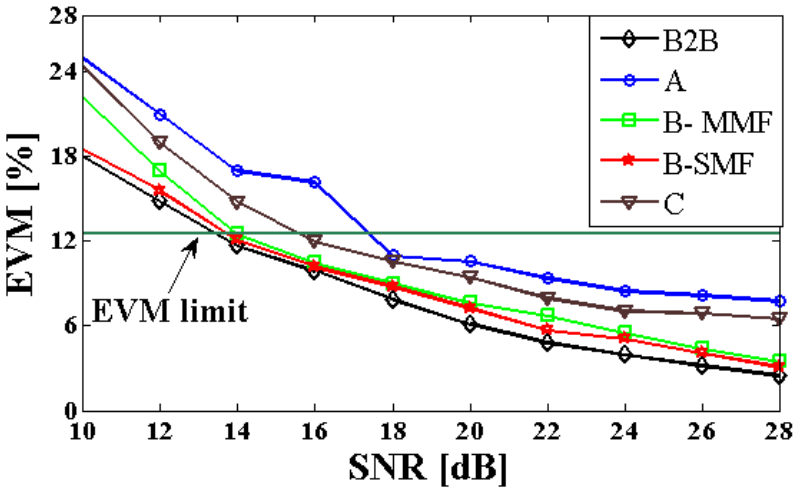

Figure 3.9: Measured EMM performance of the RoMMF-FSO system in clear channel [121]

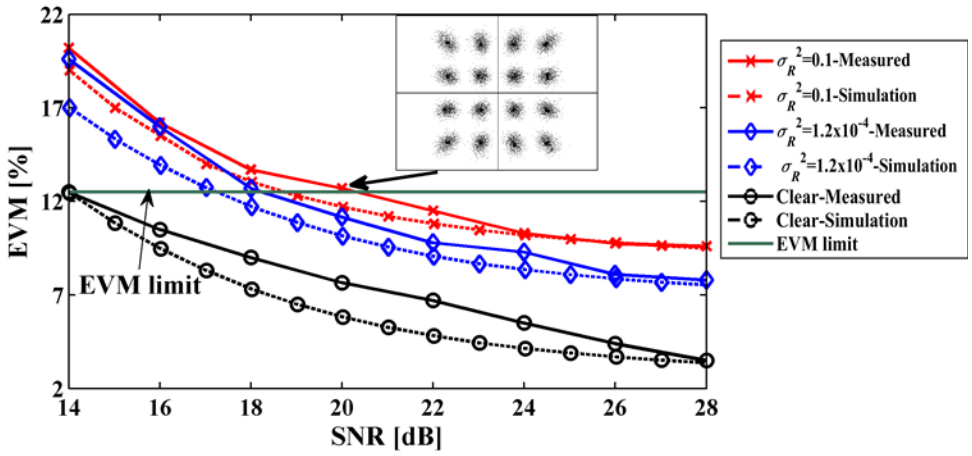

Figure 3.10: Measured and theoretical EVM performance of setup B under clear air condition and two weak turbulence levels [121]

PPs, with respect to the B2B link are 3.9 dB, 0.5 dB, 0.3 dB, and 2.3 dB for setups A, B-MMF, B-SMF, and C, respectively. The PP difference between the setup-B-SMF and the setup-B-MMF is 0.2 dB.

The turbulence effect is investigated theoretically and practically using setups B and C, in terms of EVM measurements as illustrated in Figure 3.10 and Figure 3.11. The inset figures show the measured constellation diagrams for the received LTE signal for the turbulence channel with turbulence i.e., σ_R^2 of 0.1. It should be noted that all constellation diagrams in this study have been captured for a 20 dB of SNR. Figure 3.10 depicts the theoretical and measured EVM values for the two levels of turbulence strength for the FSO channel as in setup B.

The simulation results show a good agreement compared to the measured SNR values at the EVM limit with < 1 dB difference at σ_R^2 of 0.1. The summary of the measured EVM and PPs are presented in Table 3.4 for a clear FSO channel and two turbulence strengths. The results demonstrate that, for increased turbulence strength, EVM levels will deteriorate due to the optical intensity fluctuations and fading, which is caused by the random variation of air refractive index. Notably, the turbulence

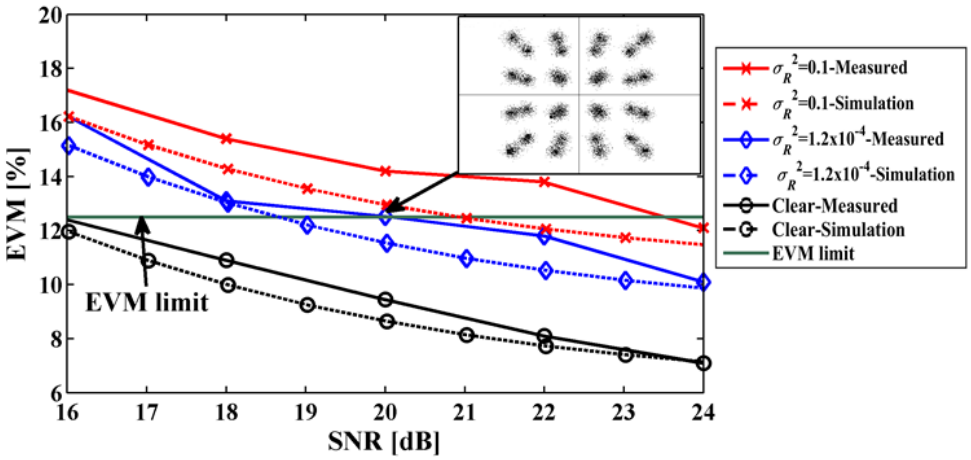

Figure 3.11: Measured and theoretical EVM performance of setup C under clear air condition and two weak turbulence levels [121]

strength (i.e., σ_R^2) depends on the temperature gradient along the propagation channel [120]. Consequently, a further spreading of PDF of the received signal can be induced as a result of signal fading [170]. The PPs, with respect to a clear channel shown in Table 3.4 indicates that at higher turbulence levels (i.e., σ_R^2 of 0.1 experienced in case of C_n^2 of 4.09×10^{-10} $m^{-2/3}$) the PP increased by ~2 dB. In order to compare setups B and C, the turbulence levels is kept identical. Figure 3.11 depicts the predicted and measured EVM values for setup C, while the obtained results are outlined in Table 3.4, which shows an increase of the required SNR values to achieve the EVM limit due to the additive loss and dispersion. In addition, the end-to-end simulation shows similar trend for measured SNR values. However, the measured SNR values show an increase by ~2 dB at the EVM limit for σ_R^2 of 0.1 compared to the simulation due to the intensity fluctuation of ±0.3% of the experimental EVM results. This intensity fluctuation is magnified by the modal effects generated by the additional MMF following the FSO. Furthermore, the EDFA amplified spontaneous noise (ASE) does

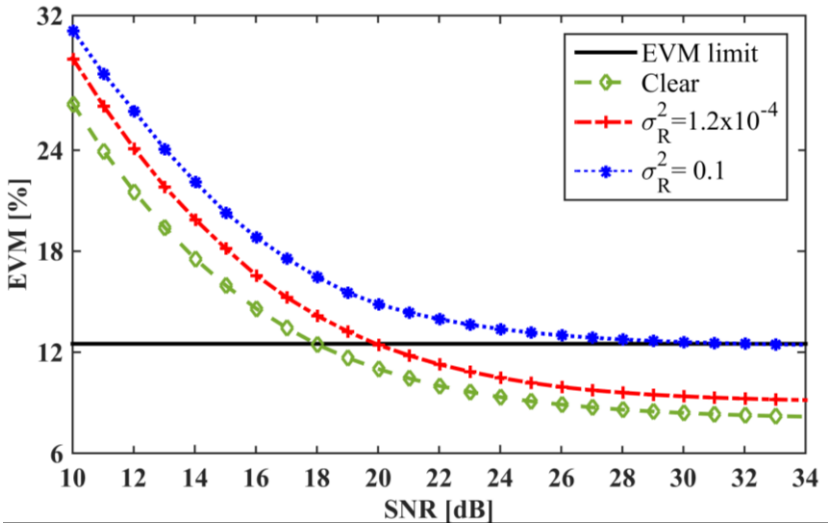

Figure 3.12: Analysed EVM performance for FSO span of 500 m [121]

affect the system performance and is not taken into consideration in this work and it will be studied in the future.

Finally, further analyses were carried out for the FSO path of 500 m long, which is the typical range for the last-mile access network in the urban areas [53, 197]. Figure 3.12 illustrates the predicted EVM as a function of SNR with weak turbulence (i.e., σ_R^2 = 1.2×10^{-4} and 0.1) and no turbulence. The results show that in order to achieve the 3GPP LTE EVM target of 12.5% the SNR power penalties are ~2 dB and ~11 dB for σ_R^2 of 1.2×10^{-4} and 0.1, respectively compared with no turbulence.

3.5 Summary

In this chapter, the hybrid RoMMF-FSO scheme was demonstrated in order to enhance the performance of the 4G-LTE signal for radio-over indoor MMF system as

Table 3.4: Measured SNR and PP at the EVM limit for setups B and C

	Setup B		**Setup C**	
Turbulence Strength	**SNR (dB)**	**PP (dB)**	**SNR (dB)**	**PP (dB)**
Clear FSO	14.1	--	15.8	--
σ_R^2=1.2×10^{-4}	18.25	4.15	20	4.2
σ_R^2=0.1	20.33	6.23	23.55	7.75

part of the last mile access networks. It is found that adopting SMFT may reduce the EVM level, apart from mitigating the modal effects within the MMF-FSO interface. This has resulted in a negligible difference compared to SMF-FSO in terms of EVM and PPs. Additionally, the proposed system was found to improve the available channel bandwidth by at least 2 GHz due to the reduced level of ripple fluctuation in the system transfer function by 4 dB. Moreover, the laser beam profile measurements indicated that the use of SMFT may significantly enhance the received power and FWHM. Also, the author has experimentally and theoretically validated the performance of the proposed system under turbulence by transmitting the LTE signal over the MMF and FSO channels. Furthermore, theoretical analysis for a longer FSO channel was carried out. The obtained results showed that for the FSO link span of 500 m to meet the EVM target of 12.5% the SNR power penalties were ~2 dB and ~11 dB for σ_R^2 of 1.2×10^{-4} and 0.1, respectively compared with no turbulence case. The results confirm that the proposed technique can be used successfully in the real practical environment for the last-mile access networks, achieving the 3GPP LTE target of 12.5% EVM. In the next chapter, further experimental investigation of the hybrid RoF-FSO system will be presented to examine the system performance under foggy weather condition.

Chapter 4

Transmitting LTE Signals over a Hybrid RoF-FSO system under Fog Atmospheric channel

4.1 Introduction

The previous chapter introduced a mode filtering technique to mitigate the modal dispersion in the hybrid radio over multi-mode and free space optics (RoMMF-FSO) system, which is validated under a real weak turbulence channel. In this chapter, a thick fog effect is exposed to the proposed hybrid RoMMF-FSO system, where the system performance will be characterized for transmitting different data rates of the 4^{th} generation-long term evolution (4G-LTE) signal.

4G-LTE technology was introduced to meet the rapid increase in the number of users and broadband applications [18]. Currently, most mobile operators worldwide have adopted the 4G-LTE mobile technology [16]. It should be noted that the architectural features of 4G-LTE were developed to meet the continuing growth of data traffic and coverage issues. Moreover, the 4G-LTE technology adopts small cell scenarios in enhancing the wireless coverage and as a result, pico- and femto-cellular networks were adopted. A promising solution for transporting 4G-LTE signals within small-cellular systems is the optical network. This concept is known as the radio-over-fibre (RoF), in which, the radio frequency (RF) broadband signals will be transported via optical fibre to outdoor/indoor cellular networks in order to extend the multi

wireless services for access and in-building networks. In this regard, the optical fibre access technology such as fibre-to-the-home (FTTH) has been employed as the bridge between broadband network distributer and building devices. Apart from that, the single-mode fibre (SMF) has been used for the broadband backbone network due to its low attenuation and huge bandwidth [71]. However, as regards the indoor networks, lower deployment costs must be observed in order to fulfil the low-cost requirements. This can be achieved by adopting the distributed antenna systems (DAS) and employing MMF to carry the 4G-LTE signals over the indoor connections since it is mainly adopted for short communication networks.

Visani *et.al.*,[41] demonstrated theoretically and practically an optimised version of the RoMMF by means of using the fabry-perot (FP) laser and central launch technique for the 4G-LTE wireless service for the indoor applications achieving ~3% error vector magnitude (EVM) at 1950 MHz band. It should be noted that the polymer optical fibre (POF) is preferable to be employed in in-building networks due to the fact that it is less brittle and more flexible compared to the silica based fibres. Moreover, due to its large core diameter, this type of fibre is generally associated with the ease of installation as well as low maintenance cost [49]. In [136], a novel radio-over-POF (RoPOF) system was proposed by means of using vertical cavity surface emitting laser (VCSEL) and light injection-locking technique for the intra-building networks with < 4% EVM for 50 m graded-index POF (GI-POF) channel distance. Since capacity and coverage have been the key concerns for the recent mobile communications, a relay node (RN) will be employed for further coverage extension. It was proposed that the RN to be positioned in the RF cell edge and linked the user equipment (UE) with the enhanced NodeB (eNB) base stations via SMF based

network [72] for outdoor applications, while home remote unit (RU) was proposed for indoor wireless applications [17, 36].

Nevertheless, the cost of deploying RoF for long haul applications may arise as an issue particularly in the rural areas where the cost will be even higher because of some regulations and environmental considerations, which may affect the fibre length employed and access to it. The combination of buried fibre and aerial deployment based on the RoF and the FSO technologies, which is also known as radio-over-FSO (RoFSO), may effectively offer a much better solution for both rural and urban environments with the FSO links, which offer the line of sight (LOS) path. It is noteworthy that in typical office and industrial environments, the combination of hybrid RoF and/or RoFSO can be a better option for distributing radio signals and connecting multi-indoor RoF networks, in which, the underground fibre may not be available at all places, particularly in the rural and sparsely populated areas. The latter option is even more appealing, since no digging is required between two buildings and consequently, the cost of installation will be lower. A theoretical study in [67] highlighted that the most efficient technology that will be employed to better enhance the wireless last-mile access links is by adopting the optical fibre, in addition to the FSO as complementary technologies for the RF based technology.

The integration between the RoF and RoFSO systems has been demonstrated theoretically in [125] and by means of experiment in [117] to demonstrate a transmission of orthogonal frequency division multiplexing (OFDM) signal between two RoF links using 1 km FSO under turbulence effect. However, these studies were carried out with the sole focus on the FSO channel effects without due consideration for the aspects of optical fibre type and distance. Further research by [198],were carried out on a dual transmission link, which operates at 1550 and 850 nm

wavelengths over an SMF link, followed by the wavelength division multiplexing (WDM) to guide both optical waves into one POF channel. A collimator lens was utilised at the end of the POF in order to propagate the beams over the FSO link. Furthermore, a heterogeneous optical access system was proposed in [199], which include POF, FSO and indoor infrared (IR) links with the ability of delivering 40 Gbps by means of using adaptive coded OFDM scheme. In this chapter, the hybrid RoF-RoFSO system and its characteristics are investigated experimentally under fog weather fading effect by employing simple and easy setup without adopting any coding technique. The MMF is employed as it has been widely adopted in the in-building networks.

Apart from that, POF is used not only to minimise the installation cost, but also due to the fact that it has high attenuation levels that may lead to severly limited transmission distance. By comparison, the MMF has relatively higher linear distortion and lower bandwidth than the SMF due to their modal dispersion. Therefore, in order to limit the effect of modal dispersion, a filtering technique, which is simple and cost effective, has been used for filtering the higher order modes, which in turn has resulted in improving the bandwidth of the RoF system. Although there are different types of mode filters, employing a short SMF patchcord as a mode filter has reportedly to have better performance compared to other solutions such as air gap filter. Notably, it is the cheapest and easiest method to mitigate the effect of modal dispersion [200].The RoFSO and RoF are employed in the proposed system to connect mobile phone users to the backbone network and hence, increasing the efficiency of coverage and

bandwidth in sparsely populated regions with low cost solutions in comparison to the existing coaxial copper cables.

The proposed solution is presented in Figure 4.1, in which, the FSO transceivers are placed on top of the buildings to ensure a LOS path as part of the "last mile" connectivity [182]. The MMF or the POF is used to connect the RUs and FSO transceiver modules to the eNB [41, 126]. Correspondingly, the current chapter proposed that the mode filtering technique be investigated experimentally under the atmospheric channel fading due to fog effect. The system performance will be assessed in terms of the link power budget and EVM for a range of signal-to-noise ratio (SNR) values under the effect of thick fog. The author has published the findings of this chapter in [119, 201].

4.2 Fog Atmospheric Channel

As discussed in Chapter 2, the performance of FSO networks is mainly affected by the large optical signal attenuation, which is due to the presence of air particles that produce scattering and absorption of the propagated beam. It should be noted that this fog effect will be dominant particularly when the water droplets dimensions are close to the optical signal wavelengths [89]. With regard the FSO links, the fog attenuation

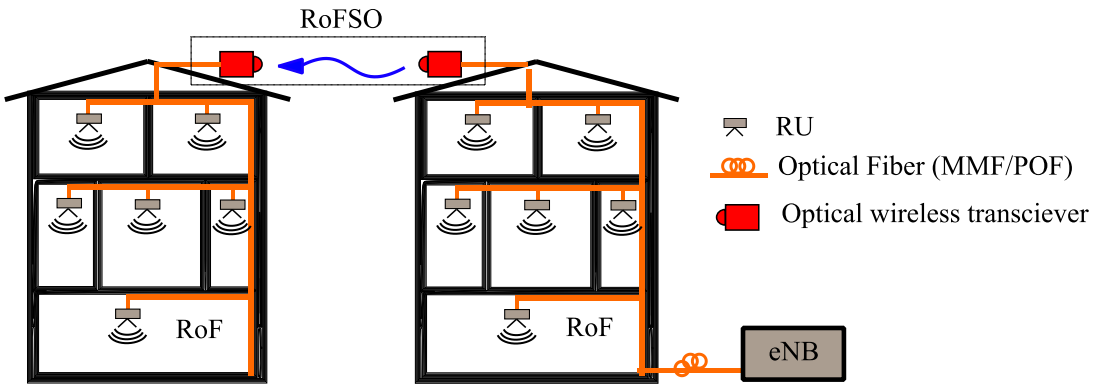

Figure 4.1: Hybrid RoF-FSO system structure [201]

is considered as the most challenging factor [139]. As reported in [109], due to moderate fog, the channel attenuation can reach up to 130 dB/km, while for dense fog weather condition, it may reach up to 480 dB/km. In addition, practical investigation was reported in [139] showing that the moderate fog attenuation level is stable over the event time. In contrast, the observation of the dense fog demonstrates major fluctuations of the attenuation over the same time scale with a variation rate of more than 45% of the average attenuation value per second. Several empirical models that predict the fog attenuation behaviour based on experimental data [202] or theoretical considerations [203] were reported in the literature. Generally, fog-induced attenuation is characterized by means of different parameters such as the visibility V, the transmittance threshold T_{th} and λ. The channel visibility is defined as the distance to object, where the optical beam power (i.e., T_{th}) drops to a fraction of 2% or 5% of its original power [204]. As regards the dense fog, the aerosol size is supposed to be larger than the propagating optical wavelength and thus, it can be concluded that there is no wavelength dependency of the fog attenuation as indicated in the measurements stated in [139]. Nonetheless, Kruse model predicts that the fog-induced attenuation may drop with the higher wavelength levels. Therefore, the atmospheric V can be expressed in terms of the attenuation coefficient β_l (dB/km), T_{th} and λ (nm) as [53]:

$$V(km) = \frac{10\log_{10} T_{th}}{\beta_l}\left(\frac{\lambda}{\lambda_o}\right)^{-q}, \tag{4.1}$$

where λ_o refers to the maximum sensitive wavelength for human eye, which is typically set at 550 nm, q is coefficient depending on the particle size distribution and the visibility, which is defined by Kim theoretical model in [203] as:

$$q = \begin{cases} 1.6 & V > 50 \text{ km} \\ 1.3 & 6 \text{ km} < V > 50 \text{ km} \\ 0.16V + 0.34 & 1 \text{ km} < V > 6 \text{ km} \\ V - 0.5 & 0.5 \text{ km} < V > 1 \text{ km} \\ 0 & V < 0.5 \text{ km} \end{cases}. \quad (4.2)$$

The visibility range indicates the weather condition. For example, the visibility range of 500 m < V < 1 km, V <500 m, V < 200 m and V < 50 m refers to light, moderate, thick and dense fog weather, respectively [97, 104, 198]. Kim *et.al.*, proposed a theoretical model indicating the wavelength independency for visibilities less than 500 m in [203]. However, an experimental evidence in [167] revealed that the optimum wavelength windows of 0.83, 0.94, and 1.55 μm are most suitable for fog conditions to ensure the link availability. Therefore, β_l can be defined by knowing the transmittance T of the optical signal and propagating distance d_i (in km) using Beer-Lambert law as [205]:

$$\beta_l \text{ (dB/km)} = -\frac{10\log_{10}(T)}{4.343\, d_i}, \quad (4.3)$$

which can be written as:

$$\beta_l \text{ (dB/km)} = -\frac{\text{Loss}}{4.343\, d_i}. \quad (4.4)$$

It is noteworthy that in the current chapter, the real-time measurements for the fog-induced attenuation using 1550 nm laser spectrum are reported to be in line with the measured visibility.

4.3 Atmospheric Visibility Measurement

Figure 4.2 illustrates an artificial atmospheric chamber, which is used to mimic the real outdoor atmospheric weather. The chamber has a dimension of 550×30×30 cm^3, consisting of seven sections; each one has a built-in fan and thermometer, in addition to air outlet for air circulation. The intensity of the hot air inside the chamber is controlled by aluminium-based plates. Therefore, the temperature, as well as the wind inside the chamber can be controlled to mimic, as close as possible the outdoor atmospheric conditions. The fog is generated by fog machine from ProSound (model: NB88GB), where it is pumped inside the closed chamber and its amount is controlled by the ventilation process. Accordingly, the transmittance of the FSO path can be controlled, as long as the aerosols inside the chamber are settled down homogeneously. An emprical approach utilising the wavelength of 550 nm to measure the visibility, along with the length of the outdoor FSO link was adopted in [167, 206] to estimate the closest value of the fog-induced attenuation corresponding to the measured link visibility. Figure 4.3 illustrates the block diagram of this approach. An optical source, which operates at 550 nm wavelength (i.e., green laser source) is adopted to characterize the fog. The visibility is measured at a distance, in which,

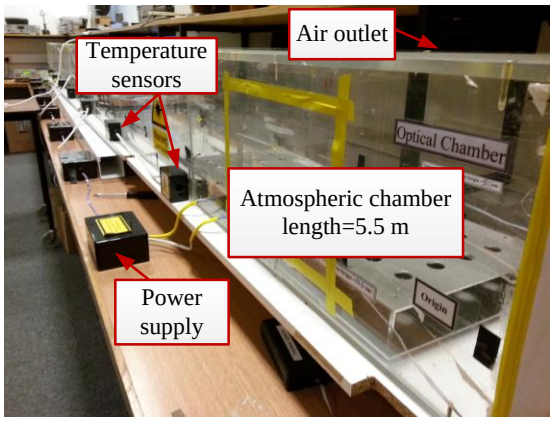

Figure 4.2: The laboratory controlled atmospheric chamber

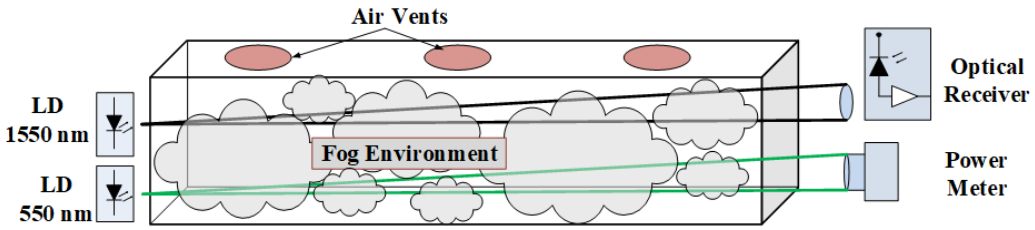

Figure 4.3: Fog attenuation and visibility experimental set up

parallel beams travel through the atmospheric chamber until the visual contrast drops to 2% (i.e., T_{th} = 2%) of its original contrast. Accordingly, the attenuation coefficient β_l can be calculated in terms of the measured V using (4.1), which can be employed to calculate the FSO attenuation in (dB) using (4.4).

4.4 Hybrid RoMMF-FSO under Fog Atmospheric Effect

As regards this work, the combination of radio over multimode fibre and radio over free space optical systems is experimentally investigated. In such hybrid systems, a mode filtering technique is adopted in dealing with the modal effects. Considering the mode filtering effect, a link budget analysis is performed as an addition to the measurement of EVM in order to verify the efficiency of the proposed systems in dealing with the modal effect. The results obtained were below 12.5% 3rd generation partnership project (3GPP) LTE EVM requirement, which is defined for 16-quadrature amplitude modulation (16-QAM).

4.4.1 Proposed Experimental Setup

Figure 4.4 demonstrates the outline of the proposed hybrid RoMMF-RoFSO system and the system parameters are presented in Table 4.1. The LTE signal is generated at the transmitter using Agilent signal studio N7624B, which configure the vector signal generator (VSG) in OFDM at 800 MHz band. This is the typical downlink (DL) carrier frequency adopted in LTE for Europe, particularly in the rural areas [5]. The baseband signal is composed of 16-QAM at 20 MHz and a bit rate of 67.2 Mbps.

The most widely used modulation format in wireless communication systems is adopted i.e., 16-QAM modulation format. Moreover, the LTE RF signal is employed for intensity modulation (IM) of a distributed feedback (DFB) laser at the wavelength of 1550 nm. The laser source output is passed through a variable optical attenuator (VOA) and the erbium-doped fibre amplifier (EDFA), which are used to optimise the transmitted power prior to being launched into 1 km of MMF. The single-mode filtering technique (SMFT) is employed as a filter technique to eliminate the modal effect at the end of MMF. Subsequently, the output is fed into an optical collimator for propagation over the free space channel of 11 m length, in which, a flat mirror is utilised to double the free space channel distance. Indoor atmospheric

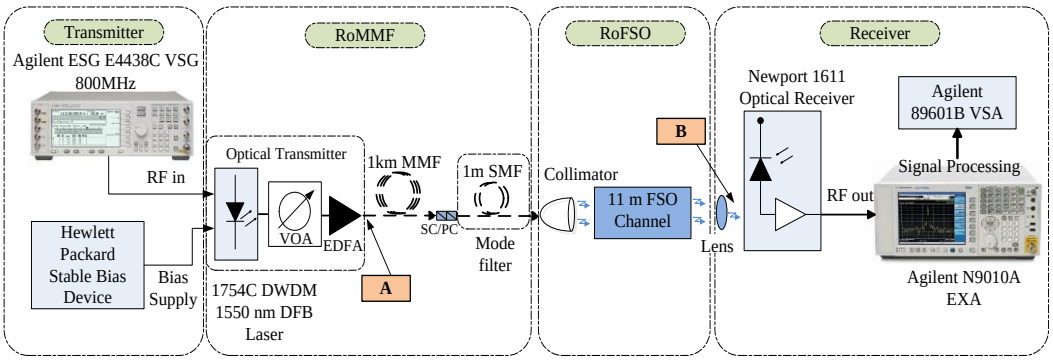

Figure 4.4: Block diagram of the experimental setup [201]

Table 4.1: RoMMF-FSO System parameters

Parameter	Values
Modulation scheme	16-QAM
Baseband multiplexing	OFDM
Carrier frequency	800 MHz
Signal bandwidth	20 MHz
Bit rate	67 Mbps
RF power	0 dBm
DFB wavelength	1550 nm
DFB power	6 dBm
EDFA gain, noise figure	7 dB, 3.5 dB
MMF core size, loss, NA	62.5 μm, 0.15 dB/km, 0.275
Newport PD responsivity	1 A/W
Collimator divergence angle	0.022 degree
Collimator aperture diameter	7 mm
Receiver lens diameter	60 mm

chamber was used in order to assess the impact of fog and turbulence on the proposed system. A lens is used to focus the incident light signal onto the photodetector (PD) at the receiver side. The output of the PD is amplified using a trans-impedance amplifier (TIA), which afterwards was captured by means of vector signal analyser for further EVM analysis.

4.4.2 Link Budget Analysis

The experimental link budget analysis is carried out in order to investigate the performance of the SMF mode filtering system from the power loss perspective. The available link margin L_M can be calculated by [87]:

$$P_R = P_i - L_{fibre} - L_{coupling} - L_{FSO} - L_M \,, \tag{4.5}$$

where P_R is the receiver sensitivity referring to the minimum received power required to achieve the level of 12.5% EVM, which is the 3GPP LTE requirement for the 16-QAM. P_i is the transmitted optical power including the amplification generated by the EDFA. L_{fibre} , $L_{coupling}$ and L_{FSO} are fibre, MMF-to-SMF coupling and FSO link losses, respectively.

For the negligible pointing errors, the major losses that are contributed in L_{FSO} are the atmospheric and geometric losses. Therefore, equation (4.5) can be written as:

$$P_R = P_i - L_{fibre} - L_{coupling} - 4.343 d_i \beta_l - A_{geo} - L_M , \quad (4.6)$$

where A_{geo} is the geometric loss defined in (2.27). Based on the results shown in Table 4.2, the mode filter is observed to be dominant in the total optical loss. Apart from that, the link margin was at 24 dB in the clear channel, which will be utilised to extrapolate the FSO channel distance up to ~2.5 km using (2.27) and (4.6). On the other hand, the FSO loss was observed to increase by 4.43 dB in the thick fog atmospheric channel. Nevertheless, the link margin will be added to the proposed system in order to increase the FSO length under thick fog effect up to ~133 m.

Table 4.2: RoMMF-FSO link budget for the clear and fog atmospheric channel

	Weather condition	
Parameter	**Clear**	**Thick Fog**
DFB output power (dBm)	6	6
VOA value (dB)	2	2
EDFA gain (dB)	7	7
P_i (dBm) (point A in Figure 4.4)	**11**	**10**
L_{fibre} (dB) 1 km MMF and connectors loss	**0.8**	**0.8**
MMF/SMF coupling loss	3.2	3.2
Insertion loss of collimator (dB)	0.4	0.4
$L_{coupling}$ (dB)	**3.6**	**3.6**
β_l dB/km	0.43	43
d_i (m)	11	11
FSO loss (dB)=$4.343 d_i \beta_l + A_{geo}$ (atmospheric and geometric attenuation)	**0.6**	**5.03**
Total loss (dB)	**5**	**9.43**
P_R (dBm)	-18	-18
L_M (dB)	24	19.57
Maximum FSO span	~2.5 km	~133 m

4.4.3 EVM Performance Analysis

The impact of different modes of propagation may not only cause modal dispersion in fibre, but may also affect the characteristics of beam propagation in the FSO channel. Thus, the proposed system performance is investigated in terms of the RF domain. In doing so, the EVM of the link is measured with the modulated RF signal at the carrier frequency of 800 MHz under fog channel condition as illustrated in Figure 4.5. The method to generate fog inside the indoor atmospheric chamber is described in section 4.3. The link visibility is estimated by measuring the attenuation of a green laser (i.e., 550 nm wavelength) in fog channel consistent with the clear channel as reference. In the experimental setup, the visibility was set to 100 m with 4.43 dB attenuation.

The EVM performance is investigated for typical LTE bandwidth of 5 MHz, 10 MHz, 15 MHz and 20 MHz. The results comprised of the RoFSO in clear condition, Hybrid RoMMF-FSO for clear and fog channel effects are shown in Figure 4.5. At low bandwidth, the EVM values are relatively small (i.e., not higher than 4%), but increasing the signal bandwidth resulted in higher EVM due to the reduced SNR.

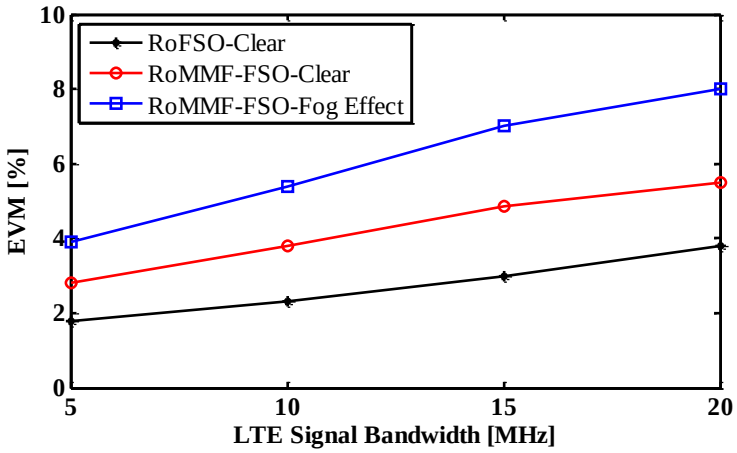

Figure 4.5: EVM performance for the RoMMF-FSO for clear and fog atmospheric channel [201]

Expectedly, the EVM increases after the signal was propagated through the 1 km MMF link. Due to the additional losses that degraded the received signal, the impacts of atmospheric conditions on the FSO link increased the EVM level. Notably, the EVM results are relatively low for all types of the hybrid RoMMF-FSO links. The worst case for the present proposed hybrid link is when EVM is only ~8%, which is smaller than the critical 12.5%, defined by the 3GPP for 4G-LTE systems, hence, showing the error-free capability of the proposed system [196].

4.5 Hybrid RoPOF-FSO System

In this section, a design of residential gateway (RG) for the perfluorinated GI-POF (PF-GI-POF) in-building network is presented. The proposed scheme addresses the integration between the outdoor and indoor 4G-LTE networks by means of employing the RoFSO technology for rural environments in order to enhance the wireless performance with low deployment cost as demonstrated in Figure 4.6. The system performance is characterized under thick fog atmospheric fading effect, with due consideration of 17.5%, 12.5% and 8% for EVM as the figure of merit for quadrature phase shift keying (QPSK),16-QAM and 64-QAM, respectively [196].

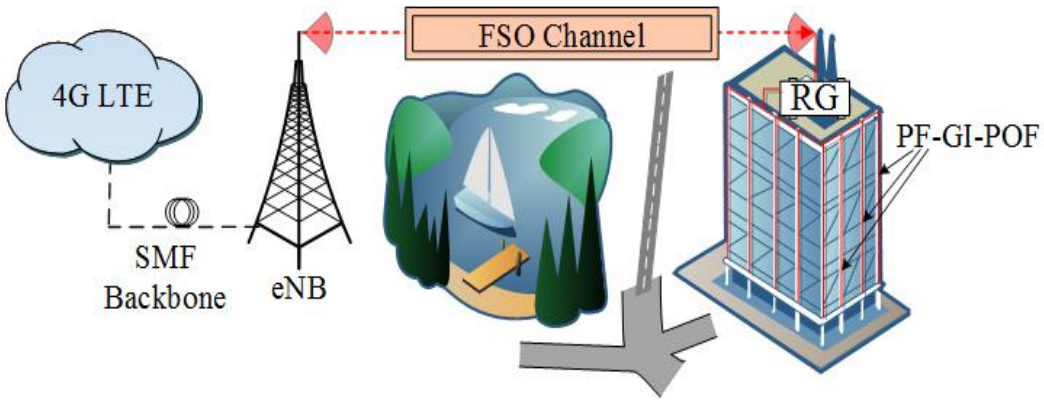

Figure 4.6: 4G-LTE access network in rural environments [119]

4.5.1 Proposed Experimental Setup

The overall experimental setup for the DL LTE-over-RoFSO channel is indicated in Figure 4.7 and the system parameters are presented in Table 4.4 The transmitter, which was described in section 4.4.1, represents the outdoor SMF system backbone link and the LTE base station (i.e, eNB) in optical domain. Here, the LTE signals are generated in the OFDM format with QPSK, 16-QAM and 64-QAM in the baseband by means of using Agilent ESG E4438C. It should be noted that the LTE signals at 800 MHz have analogue radio bandwidth of 5 MHz, 10 MHz, 15 MHz and 20 MHz, which are the standard values for the LTE technology [18]. The standard transmitted data rate associated with the LTE signal bandwidth is presented in Table 4.3 [207,

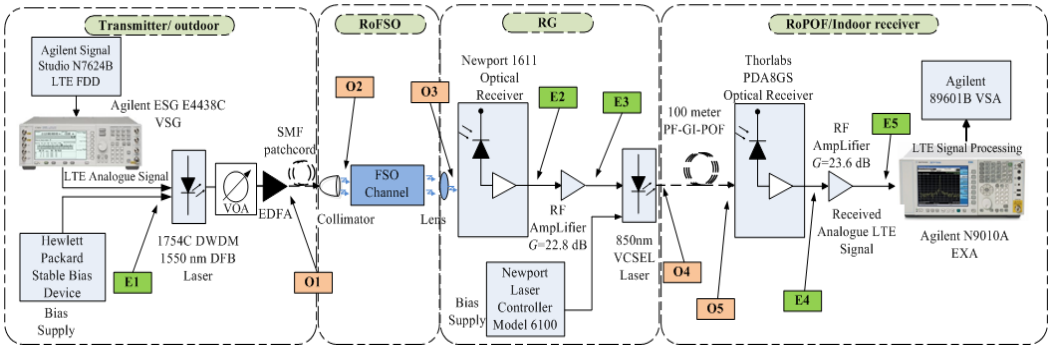

(a)

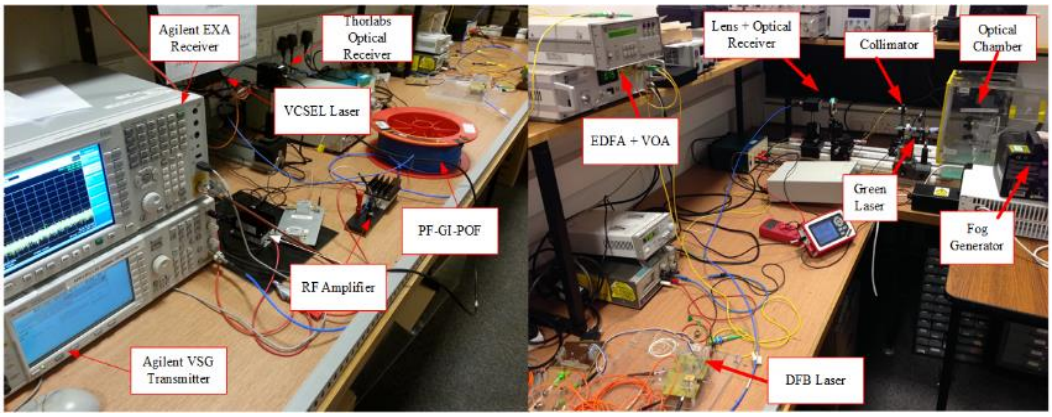

(b)

Figure 4.7: (a) Block diagram of the experimental hybrid system, and (b) Laboratory setup showing the RoPOF and FSO networks [119]

Table 4.4: System parameters

Parameter	Value
Modulation scheme	QPSK, 16-QAM, 64-QAM
Baseband multiplexing	OFDM
Carrier frequency	800 MHz
Signal bandwidth	5, 10, 15, 20 MHz
RF power	-8 dBm
DFB wavelength	1550 nm
DFB power	3 dBm
VCSEL wavelength	850 nm
VCSEL power	- 3 dBm
EDFA gain, noise figure	20 dB, 3.5 dB
FSO channel distance, d_i	11 m
PF-GI-POF core size, loss, NA	62.5 μm, 60 dB/km, 0.19
Newport PD responsivity	1 A/W
Thorlabs PD responsivity	0.525 A/W
Collimator divergence angle	0.022 degree
Collimator aperture diameter	7 mm
Receiver lens diameter	60 mm

208]. The real-time LTE signal is applied directly to intensity modulated DFB laser source operating at 1550 nm wavelength. This is followed by the optimisation of optical launch power level by means of using VOA and fixed gain EDFA.

At the RoFSO part, the output of EDFA is coupled by 1 m SMF patchcord to the collimator in order to adjust the divergence angle of the FSO beam, which is transmitted over a free space channel of 11 m long. At the input stage of the RG, the optical beam is passed through an aperture (i.e., lens) and is captured using optical receiver from Newport. The RG employs a wavelength conversion between the RoFSO link, which operates at 1550 nm, and the RoPOF link operating at the commonly employed wavelength of 850 nm.

Table 4.3: LTE bit rate throughputs

Bandwidth	5 MHz	10 MHz	15 MHz	20 MHz
QPSK bit rate (Mbps)	8.4	16.8	25.2	33.6
16-QAM bit rate (Mbps)	16.8	33.6	50.4	67.2
64-QAM bit rate (Mbps)	25.2	50.4	75.6	100.8

The output of Newport optical receiver is then converted into an electrical signal by means of a TIA amplifier, in which the output is further amplified using an RF amplifier prior to the IM of 850 nm VCSEL source. A Newport laser controller is used to provide 5 mA, as a bias current for the laser operating in the linear region. At the RoPOF network, the output of the VCSEL is coupled to 100m of PF-GI-POF, which is a typical distance employed for residential buildings [49]. Note that, this output is detected by means of an optical receiver. The RF amplifier output is captured and analysed using Agilent N9010 EXA Signal Analyser. The EVM measurement is employed for the investigation and analysis process.

4.5.2 Link Budget Analysis

With regard to the Hybrid RoPOF-FSO system, the main losses are primarily due to the high POF attenuation and the atmospheric induced attenuation in the FSO channel. In the clear hybrid channel, the attenuation in the link is due to electrical-optical (E/O) and optical-electrical (O/E) conversions, fibre to FSO coupling and POF. Table 4.5 presents the summary of the measured power, while the measurement points are labelled in Figure 4.7. In subcarrier modulated intensity-modulation/direct-detection optical systems, the power of the input electrical signal is limited owing to the threshold current of the DFB laser. In order to obtain the best slope efficiency of the DFB laser, the biasing level is set to 34 mA to ensure both maximum input RF power of -8 dBm and RF linear modulation. The RF attenuation after RoFSO link is 13 dB, which is caused by the 0.07mW/mA slope efficiency of the DFB laser, in addition to the propagation loss of FSO channel. After the RG, the losses are due to the 0.15 mW/mA slope efficiency of the VCSEL and the POF loss. Hence, the optical losses resulted in double attenuation in the electrical domain and thus, 8 dB optical loss of the total channel is equivalent to 16 dB loss in the electrical domain. Electrical

gain for the RoFSO and RoPOF links are 9.8 dB and 7.1 dB, respectively, coming from the RF amplification at the RG and the indoor receiver.

On the other hand, the attenuations due to the E/O and O/E for the RoFSO and RoPOF networks are 9.2 dB and 4.5 dB, respectively, which indicates the high POF attenuation in the RoPOF link. It should be noted that the optical link budget is investigated under clear and fog channel conditions in order to extrapolate the FSO channel distance up to ~755 m and ~80 m, respectively.

Table 4.5: RoPOF-FSO link budget for the outdoor and indoor links

Electrical			**Optical**		**weather condition**	
Description	**Point**	**Electrical power**	**Description**	**Point**	**Clear**	**Thick Fog**
Outoor RoFSO link						
RF input power (dBm)	E1	-8	P_i **(dBm)**	O1	-2.7	-2.7
Received power at the RG (dBm)	E2	-21	$L_{coupling}$ **(dB)** (Insertion loss of collimator)	--	1	1
RF amplifier gain	--	22.8	FSO input power (dBm)	O2	-3.7	-3.7
Amplified power at the RG (dB)	E3	1.8	β_l dB/km	--	0.43	43
RF Gain (dB)	--	9.8	**FSO loss (dB)=4.343$d_l\beta_l$+A_{geo}** (clear atmospheric and geometric attenuation)	--	0.9	6.33
Power margin (dB) [RF amplification - RF gain]	--	13	Received power at the RG (dBm)	O3	-4.6	-10.03
Attenuation due to E/O and O/E conversion [Required power- (2×optical loss)	--	9.2	**Total loss (dB) of RoFSO link**	--	1.9	7.33
Indoor POF link						
RF loss of the RoPOF link (dB)	--	20.1	P_i **(dBm)**	O4	-3	-3
Received power at the indoor link (dBm)	E4	-18.3	L_{fibre} **(dB)** 100 m POF and connectors loss	--	6	6
RF amplifier gain (dB)	--	23.6	Received power at the indoor link (dBm)	O5	-9	-9
Amplified power at the indoor link (dB)	E5	5.3	**Total loss (dB) of RoPOF link**	--	6	6
RF Gain (dB)	--	7.1	P_R (dBm)		-18	-18
Power margin (dB) [RF amplification - RF gain]	--	16.5	L_M (dB)		13.4	8.97
Attenuation due to E/O and O/E conversion [Required power- (2×optical loss)	--	4.5	Maximum FSO span		~755 m	~80 m

4.5.3 EVM Results Analysis

Figure 4.8 depicts the EVM versus the LTE signal bandwidth for QPSK, 16-QAM and 64-QAM modulation schemes for 100 m of PF-GI-POF to perform the RoPOF only, RoPOF-FSO link with and without fog, as well as the B2B link, which describes the direct transmitter to receiver link. The results are shown in Figure 4.8, which

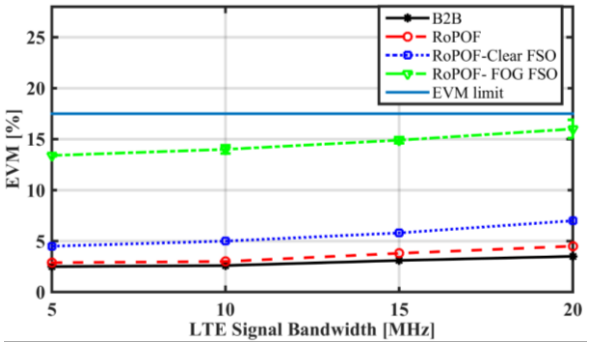

(a)

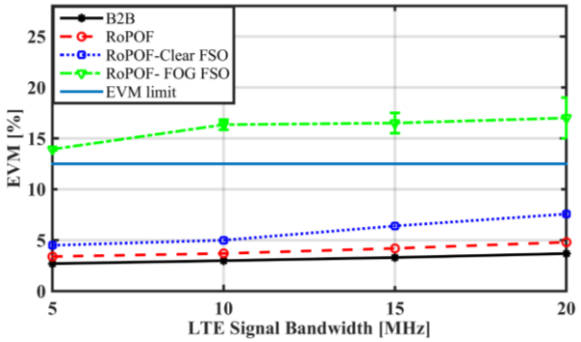

(b)

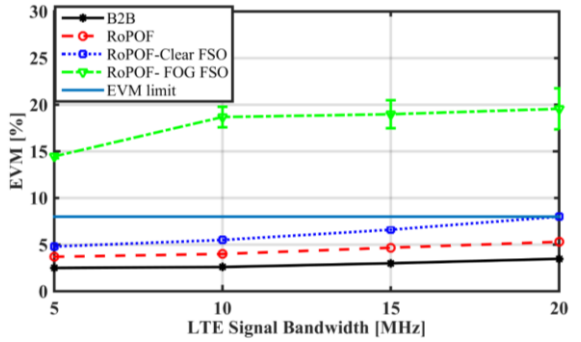

(c)

Figure 4.8: EVM performance for the proposed hybrid system using :(a) QPSK, (b) 16-QAM, and (c) 64-QAM

represent the average of four sets of measurements under identical conditions. Moreover, the 3GPP EVM requirement for 4G-LTE is highlighted in Figure 4.8 as 17.5%, 12.5% and 8% for the QPSK, 16-QAM and 64-QAM, respectively [196]. For the LTE QPSK, the EVM values for employing the PF-GI-POF only, without the FSO channel is close to the level of the B2B with the increase rate of ~1% due to short fibre distance and high optical power (-2.7 dBm) that are launched to the RG. On the other hand, the EVM is doubled when the FSO channel is added for the setup, which highlighted the effect of additional losses generated by the fibre/FSO coupling and the geometric losses. Furthermore, the EVM increased from ~3.5% to ~16% for the 20 MHz bandwidth due to fog-induced attenuation in 100 m visibility, which can be classified as thick fog [97, 104, 198].

Nevertheless, these results indicate an error-free transmission with the QPSK scheme up to 33.6 Mbps, which is achieved with EVM values less that the LTE EVM limit. Figure 4.8(b) and (c) illustrate the results of the 16-QAM and 64-QAM LTE transmissions, respectively. The transmitted data rate for the 16-QAM increased to 67.2 Mbps and up to 100.8 Mbps for 64-QAM. Notably, both modulations indicate a successful transmission for the clear FSO channel. However, the performance of the proposed hybrid system is degraded with high EVM values for the FSO link with fog, which displays the EVM value of ~17% and > 19.5% for 16-QAM and 64-QAM at 20 MHz bandwidth, respectively. As predicted, QPSK displays lower EVM in comparison to the 16-QAM and 64-QAM, because of the decreasing SNR for higher modulation order, which leads to the increased symbol error probability [192]. Accordingly, the SNR power penalty for both 16-QAM and 64-QAM can be determined with respect to the EVM limit.

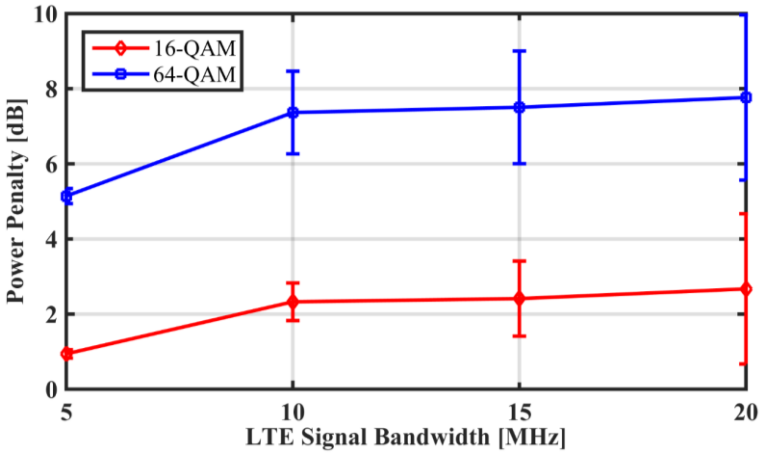

Figure 4.9: Power penalty vs LTE signal bandwidth for the 16-QAM and 64-QAM modulation schemes [119]

Figure 4.9 demonstrates the measured PP against the signal bandwidth with respect to the required SNR at the EVM limit, which are 18 dB and 22 dB for the 16-QAM and 64-QAM, respectively. The PP increases in linear with the LTE signal bandwidth due to the drop in the SNR value, which reaches a maximum value of ~3 dB and ~8 dB at 20 MHz bandwidth for 16-QAM and 64-QAM modulation schemes, respectively. This indicates the required additional power to compensate the thick fog-induced attenuation.

4.6 Summary

To sum up, a hybrid RoF-FSO was experimentally investigated under atmospheric fog effect. This chapter was divided into two main sections, the first section outlines the adoption of SMFT to address to the modal dispersion effect created in MMF link and hence, improving the overall hybrid network performance. The effectiveness of the mode filtering technique was verified by means of using power budget and EVM analysis. An error-free transmission was demonstrated at up to 20 MHz signal bandwidth for 1 km MMF and 11 m FSO under thick fog effect with the EVM of ~8 %, which is less than the 3GPP LTE requirement, i.e. 12.5% for 16-QAM . On the other hand, the second section

of this chapter demonstrated the use of 100 m PF-GI-POF as indoor optical network proposing a practical design of the RG to extend the LTE signal coverage in rural areas. In thick fog effect, a successful transmission of the 4G-LTE signal with QPSK and up to 33.6 Mbps was demonstrated while observing ~3 dB and ~8 dB of power penalty under the same fog condition at the LTE bandwidth of 20 MHz for 16-QAM and 64-QAM, respectively. To conclude, the measurement results have verified the capabilities of the proposed hybrid radio over FSO and radio over POF system under fog condition.

Chapter 5

Optimising the 4G-LTE indoor coverage using PF-GI-POF

5.1 Introduction

In chapters 3 and 4, a design of the hybrid system was proposed for the last mile access networks under the impact of the outdoor weather conditions. This chapter is dedicated to an efficient design for the indoor coverage of the 4th generation-long term evolution (4G-LTE) signals in urban environments.

For the last few years, the rapid development of mobile communications has evidently become one of the most important issues to mobile operators in meeting up the tremendous demand with regard to coverage and data services. A massive growth and considerable deployment of optical systems have offered foreseen solutions in coping with the wireless traffic bottleneck [69]. A recent survey in [209] showed that the total mobile subscriptions up to the year of 2014 were about 6.7 billion and the number is expected to reach around 9.3 billion by the end of 2019. Furthermore, it is predicted that the explosion of bandwidth demands may increase rapidly over the next few years. The traffic reached up to 15 gigabyte per capita in the year of 2016, which is more than 4 gigabyte per capita reported in the year of 2011 [28]. It should be noted that, [28] and [26] posited that between 80% to 90% of data services and 2/3 of mobile calls take place inside buildings, while a poor indoor coverage experienced by households and businesses are 45% and 30%, respectively. The typical approaches

being adopted for improving the coverage are based on the 'outside in'[1] and high power antennas. However, these solutions have a number of drawbacks such as high cost of base stations implementation, as well as low 4G-LTE penetration level and beyond network operating at 2 GHz [26]. Consequently, the sizes of wireless cells at these frequencies tend to be small. In general, the wireless cells sizes are > 1 km, ~500 m, ~100 m, <30 m for the macrocell, microcell, picocell and femtocell, respectively. It is noteworthy that 4G-LTE provides a framework that has the ability to enhance the coverage and capacity in indoor wireless applications by means of using home eNB (HeNB) based on small cell scenarios [5, 17]. The integration of optical and wireless networks is one of the most promising wireless access technology in congested urban areas, especially in terms of increased capacity, coverage and energy consumption [69].

The radio-over-fibre (RoF) technology has attracted significant interest for in-building applications due to its advantages, such as enhancing the coverage by means of low power distributed antenna system (DAS) and utilizing the wide bandwidth of optical fibre. Hence, RoF is deemed to have the potential to be a 'green' alternative to the conventional approaches to wireless access. In [210], it has been reported that in the dual transmission of a baseband signal based on electrical multiplexing at ~10 Gbps and a 60 GHz wireless, radio frequency (RF) is capable of offering the data rate of 155 Mbps. As regards the optical transmission part, a dispersion shifted single-mode fibre (SMF) at a wavelength of 1550 nm together with an external modulation (EM) has been employed. Simultaneous baseband, non-return to zero data format at 2.5 Gbps, and RF sub-carrier multiplexed based cable television transmission over a 5 km of standard multimode fibre was demonstrated in [211]. In comparison to the

[1]This term is used in [24] to describe using outdoor macrocells to enhance the indoor coverage.

glass optical fibres, plastic optical fibre such as is polymethylmethacrylate (PMMA) and perfluorinated graded-index polymer-optical fibre (PF-GI-POF) are deemed to be more compatible to be employed in high-speed/medium-range home/office based networks owing to the fact that they are less brittle and more flexible. Furthermore, PF-GI-POF offers higher bandwidth in the infrared (IR) spectra, particularly both at 1st and 2nd optical transmission windows of 850 and 1300 nm, respectively [212]. Figure 5.1 illustrates a typical PF-GI-POF based network for wireless services. The RF signal captured either by a directional donor antenna, which is carried via a coaxial cable to the residential gateway (RG), or by the outdoor optical channel. The RG is an interface between the outdoor and indoor optical networks. Following the electro-optical conversion at RG, the optical signals are distributed within buildings through POFs to the remote unit (RU). The converted RF signal is broadcasted by means of low power antenna modules with a typical coverage area in the range of tens of metres (i.e., femtocell size).

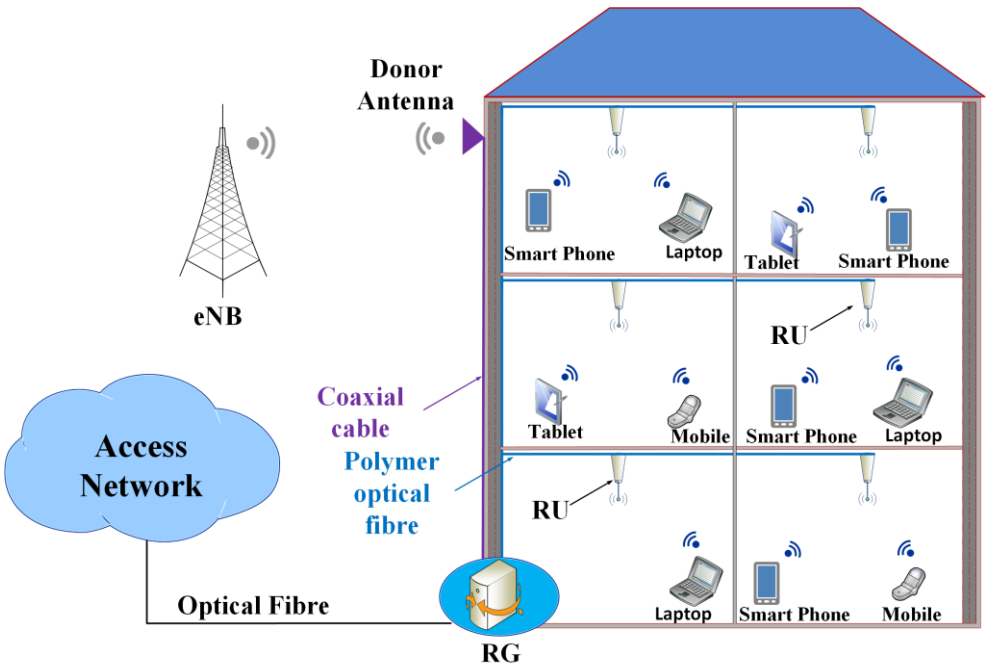

Figure 5.1: In-building PF-GI-POF network for indoor LTE coverage [191]

Notably, the utilisation of DAS and femtocell is the most promising scenario in improving the indoor coverage and the quality of service (QoS) [36]. It is worth highlighting that the key advantage of the proposed system is the employment of PF-GI-POF, which offers ease of installation and low maintenance cost devices, as well as the possibility of sharing the existing ducts with electrical cables [44]. In [127], POF channel was deemed to be a cost competitive medium compared to SMF, silica based multi-mode fibre (MMF) and copper CAT-5E channel types for in-building network applications. However, higher fibre loss is the most significant factor that may affect the system performance and limit the coverage span. Consequently, it was reported that the typical distance for residential buildings are about 100 m [49] and less than 300 m [48]. In [212], an extension of the classical baseband existing network using PF-GI-POF bandwidth with the purpose of adding further services in a home/office network was proposed to offer indoor coverage of wireless signals using the RoF technology. The system uses 100 m of PF-GI-POF, which offers simultaneous transmission of 10 Gbs at 850 nm and 1300 nm. Additionally, a system based on 62.5 µm diameter of PF-GI-POF utilising the ultra-wideband (UWB) signal at a data rate of 53.3 Mbps over 200 m is demonstrated in [46].

This chapter demonstrates a successful transmission by means of employing 300 m of PF-GI-POF in RoF based network using single carrier frequency of quadrature phase shift keying (QPSK), 16-quadrature amplitude modulation (16-QAM) and 64-QAM modulation, which are used for the wireless transmission in 4G-LTE standard [22]. Notably, an error vector magnitude (EVM) of ~3.5% is achieved for 300 m channel distance and transmitting data rate of up to 60 Mbps in 2.6 GHz band. The system performance is evaluated by means of capturing the eye and constellation diagrams in order to estimate the bit error rate (BER) and the EVM

values, in addition to determining the required power penalty to achieve the LTE EVM limit for each modulation scheme. The author has published the findings of in-building radio-over-POF (RoPOF) system in [191].

5.2 POF Transfer Function

Polymer optical fibre has in the last decade, attracted considerable attention especially in short and medium optical communication network applications. POF channel model is typically related to the channel transfer function either in time domain [162] or frequency domain [161], which may describe the linear distortion in the POF channel as regards its attenuation and dispersion. The transfer function analysis provides an indication of the overall system frequency response in terms of transmission parameter S_{21} over the frequency range. An Agilent E5071C ENA network analyser is employed to measure the end-to-end system transfer function, including the vertical cavity surface emitting laser (VCSEL) and photodetector (PD) as depicted in Figure 5.2. The network analyser RF output is set for a range of frequencies up 3 GHz and -10 dBm for all measurements. RF signal is used to modulate the VCSEL intensively via the Bias-T at the transmitter, which is used to

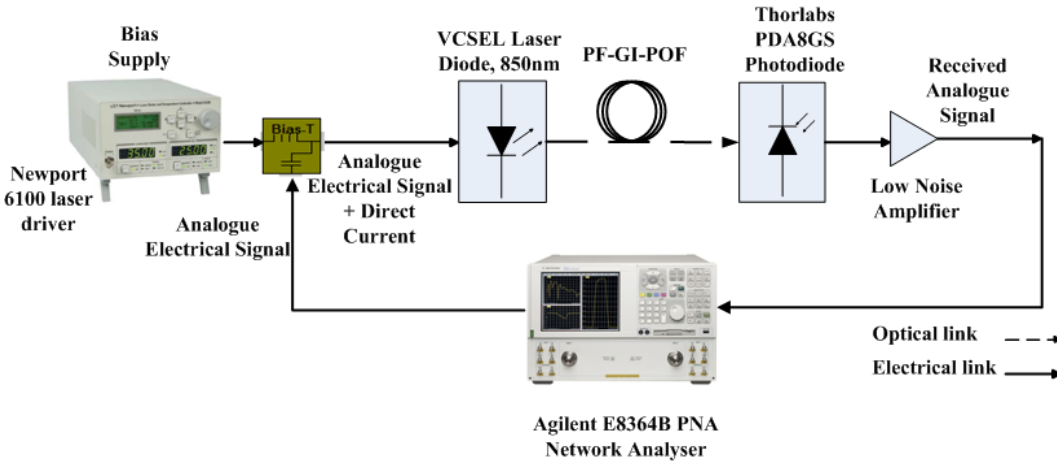

Figure 5.2: End-to-end system transfer function measurement setup

shift the analogue RF signal from bipolar to unipolar in order to drive the VCSEL. The VCSEL bias is set to be at 7 mA, which is in the linear characteristic region. Moving on, the optical signal is then applied to the PF-GI-POF channel with a distance of 100, 200 and 300 m to measure the transfer function for the system without the PF-GI-POF by means of connecting the VCSEL to the PD via 1 m MMF patchcord. On the other hand, the received signal at the receiver side is identified using the PD and followed by the low noise amplifier, the output of which is captured using the network analyser for further analysis.

The system transfer function of GI-POF is considered as quasi-static as illustrated in [161, 213, 214]. Consequently, its investigation will be employed to predict the fading effects of the optical signal travelling along the POF link and subsequently to perform the system performance analysis. Figure 5.3 depicted the different lengths of transfer function of the POF channel, which is up to 300 m, as well as the transfer function for the system without including the POF (i.e., VCSEL only). It should be noted that the same parameters were used for all the measurements including biasing, RF power and launching condition. At low frequency levels, the transfer function for

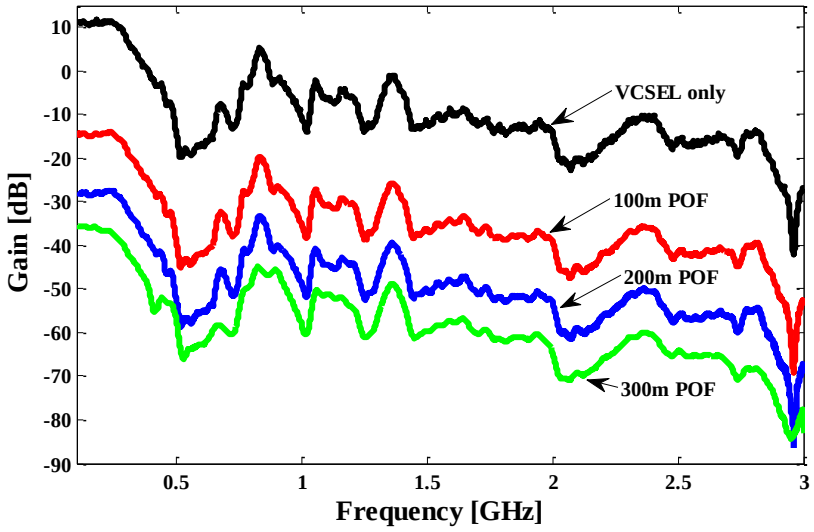

Figure 5.3: Measured transfer function for the PF-GI-POF up to 300 m

all the setups were degraded due to high attenuation with maximum drop at ~500 MHz.

Notably, the system performance fluctuated beyond the baseband, showing high level of frequency sensitivity, which is one of the MMF characteristics observed in [215] owing to the variations of the mode group powers. The gain is observed to significantly decrease with the longer POF channel, which is caused by high attenuation levels. Apart from that, the POF transfer function incorporates different perturbing effects such as the modal delay and mode dependent attenuation. All these effects are the products of the multi-mode propagation inside the POF. Nevertheless, this investigation illustrated the linear behaviour of the POF channel. Notably, the system transfer function for the VCSEL has almost the same performance for all the setups except for the gain degradation with the additional link distance up to 300 m.

5.3 Proposed System and Theoretical Model

The proposed practical setup for RoF over the PF-GI-POF channel is shown in Figure 5.4 constructed on single carrier modulation (SCM) and the key system

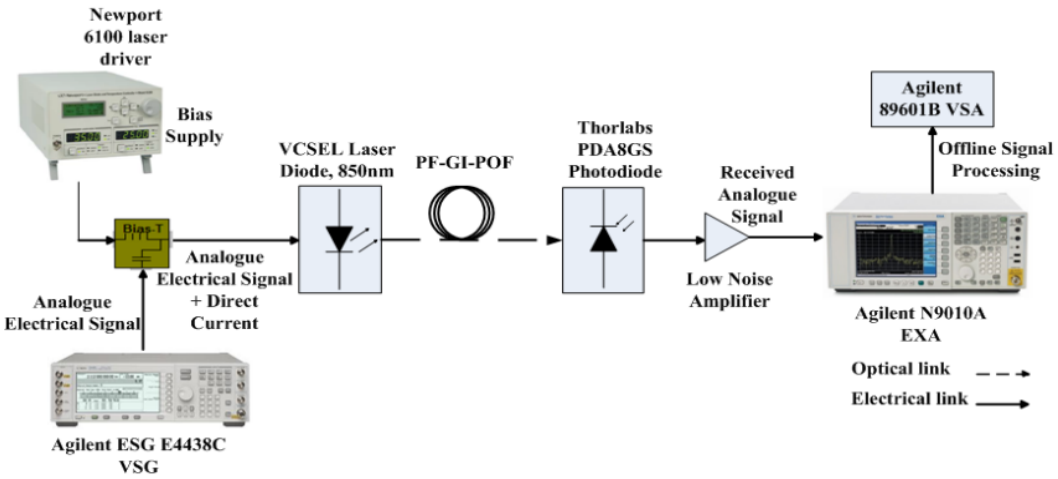

Figure 5.4: Experimental setup of the radio over PF-GI-POF channel

Table 5.1: System parameters

Parameter	Values
SCM modulation	QPSK, 16-QAM
Bit rate	QPSK=20 Mb/s, 16-QAM= 40 Mb/s 64-QAM= 60 Mb/s
Carrier frequency	2.6 GHz
Signal bandwidth	10 MHz
VCSEL bias	7 mA
Optical launch power	-14 dBm to 3 dBm
Wavelength	850 nm
Linewidth	3 nm
POF core size	62.5 µm
POF NA	0.19
POF loss	60 dB/km
POF length	100 m, 200 m, 300 m
PIN PD responsivity	0.525 A/W
LNA-gain, NF	25 dB, 2.5 dB

parameters are presented in Table 5.1. The RF signal is generated by means of Agilent ESG E4438C vector signal generator (VSG) with three modulation schemes of QPSK, 16-QAM and 64-QAM. The VSG produces RF signal in real-time passband frequency of 2.6 GHz with 10 MHz bandwidth, the standard LTE signal frequency used in the urban areas of Europe [72]. The VSG output is applied for direct modulation (DM) of the VCSEL diode (PD-LD Inc.) at a wavelength of 850 nm. The operation of the VCSEL can be defined by means of laser differential rate equations that elucidate the interaction between carrier density and photon density in active region, in terms of rate of change with time evolution using (2.1) and (2.2).

Figure 5.5 illustrated the characteristics of the VCSEL, which can be divided into three regions, i.e., A, B and C. The laser is off the threshold point at ~ 1.7 mA in region A, while region B is the most linear part of the light current (LI) curve and VCSEL is biased at 7 mA in order to ensure maximum amplitude swing (i.e., higher signal-to-noise ratio (SNR)). Region C displays the saturation characteristics of laser beyond the biasing current of 12 mA. The VCSEL diode is deemed as a suitable candidate for

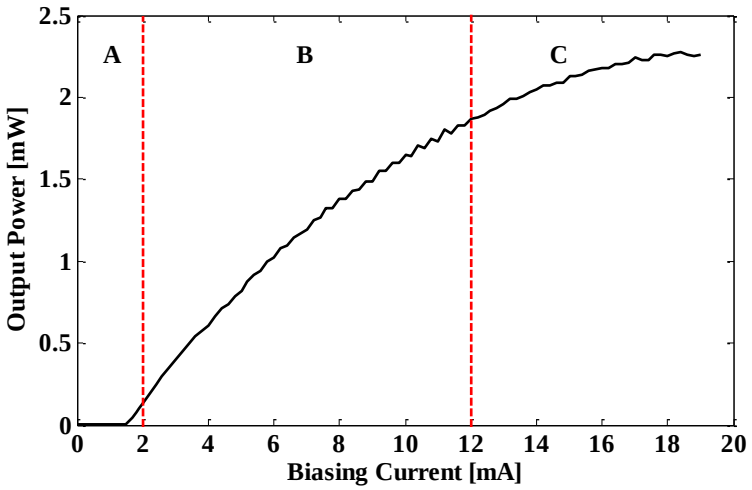

Figure 5.5: LI curve of the VCSEL showing the operating regions [191]

short distance transmissions due to its fair trade off between the cost and device characteristics (i.e., linewidth, power, and low threshold current). For biasing VCSEL and controlling its temperature, a combined device from Newport is used.

The transfer function of PF-GI-POF has been discussed in chapter 2, in which, it is defined by compensating (2.16) and (2.18) in (2.15). Depending on the wavelength, core diameter, and the numerical aperture, the propagation of light is driven by a number of mode groups, which can be estimated as 22 using (2.19). Each guided mode group has a particular propagation velocity that is able to produce a modal delay and mode-dependent attenuation. Apart from the mode dependent attenuation, the transfer function model of the PF-GI-POF also depicts the effect of intramodal (chromatic) and intermodal dispersion, while the mode coupling effect can be disregarded for the GI-POF [161]. Following the measuring of end-to-end system transfer function, the practical transfer function is employed in the simulation model to predict the system performance. Also, the system using 62.5 µm PF-GI-POF (Chromis Fiberoptics) of 100, 200, and 300 m length, which is optimised to operate at 850 nm are tested . Figure 5.6 depicted the linear increment of the fibre loss with the distance and the fibre attenuation coefficient is ~0.06 dB/m.

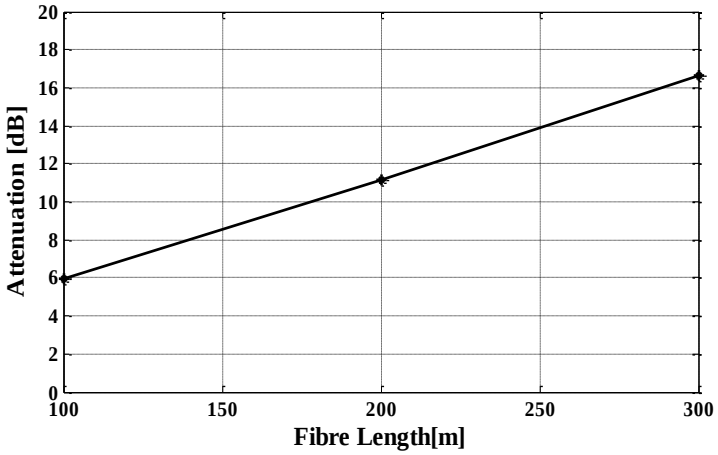

Figure 5.6: Practical measurements of the PF-GI-POF attenuation up to 300 m [191]

The RF signal at the receiver is extracted using a Thorlabs PD and a low noise trans-impedance amplifier (TIA) prior to being processed by Agilent MXA signal analyser, together with the Agilent 89601B vector signal analyser (VSA). The VSA software is used to analyse the detected symbols, i.e., the estimate of EVM and BER.

The EVM describes the receiver performance in the presence of channel impairments and noise. The detected symbol $S_r(x_s)$ is represented by:

$$S_r\left(x_s\right) = g\left(x_s\right) \cdot S_t\left(x_s\right) \cdot \eta\left(x_s\right), \tag{5.1}$$

where $g(x_s)$ is the multiplicative channel impairment which is due to the multipath fading and dispersion that may lead to ISI. $S_t(x_s)$ is the transmitted value of the x_s^{th} symbol and $\eta(x_s)$ is the additive white Gaussian noise (AWGN) with a power spectral density of $N_0/2$ [53]. In an AWGN channel, with $g(x_s) \approx 1$ and a large number of symbols, the ideal EVM is expressed using (3.17) as [192]:

$$\text{EVM} \approx \sqrt{\frac{N_0}{P_{\max}}} = \sqrt{\frac{1}{\text{SNR}}}\,. \tag{5.2}$$

However, as regards SNRs and considering the channel impairments, the measured EVM is expected to be less than the ideal values [192].

BER is the popular criterion for assessing the performance of communication systems, while EVM metric has the advantage upon BER due to the fact that it provides the desired measure of performance prior to the demodulation process [216]. In the course of comprehending the deviation of EVM values with respect to its ideal level, the BER will be evaluated and linked to the EVM performance. BER is estimated using the eye diagram by means of the Q-factor for each value of SNR. The Q-factor represents the ratio of eye opening to the total noise, which is determined by using the following equation [53, 146]:

$$Q = \frac{\left|\mu_1 - \mu_0\right|}{\sigma_1 + \sigma_0}, \tag{5.3}$$

where μ_0, μ_1 are the mean values of low and high levels, respectively. σ_0, σ_1 are the standard deviation of the low and high signals. Consequently, a higher eye opening is indicated by lower BER, which is estimated using [146]:

$$\mathrm{BER} = \frac{1}{2} erfc\left(\frac{Q}{\sqrt{2}}\right). \tag{5.4}$$

Additionally, the BER is the approximation of the EVM value as [217, 218]:

$$\mathrm{BER} = \frac{1 - M^{-1/2}}{\frac{1}{2}\log_2 M} erfc\left[\frac{3/2}{(M-1)\cdot(k_m \cdot \mathrm{EVM})^2}\right], \tag{5.5}$$

where M is the constellation size, k_m is the modulation format-dependent factor, which is specified in [218] as 1, 9/5 and 7/3 for the QPSK, 16-QAM and 64-QAM, respectively.

Hence, the EVM value can be derived as:

$$\mathrm{EVM} = \frac{1}{k_m}\sqrt{\frac{3}{2}\cdot\frac{1}{M-1}}\cdot\frac{1}{erfcinv\left[\frac{0.5\log_2 M}{1-M^{-0.5}}\cdot \mathrm{BER}\right]}. \tag{5.6}$$

In (5.5) and (5.6), the BER-EVM performance is dependent on the modulation format even with the normalisation process in (3.17) with due consideration for the nonlinear effects and electronic noise especially at lower SNR, where the k_m parameter is a dominant effect on the error estimation process.

It should be noted that the required value of BER for an un-coded wireless communications is 3.8×10^{-3} [199], while the required EVM for the 3rd generation partnership project (3GPP) in 4G-LTE systems are 17.5 % , 12.5%, and 8% for the QPSK, 16-QAM, and 64-QAM, respectively as outlined in [196]. Hence, in this analysis, the relationship between EVM and BER is deduced and the results are compared with the predicted data extended from the simulation model that uses the system transfer function to estimate the EVM values. The simulation model is employed to estimate the true EVM values at low SNR due to the fact that errors in estimation process performed by the VSA software are caused by high symbol error probability on this range of SNR.

5.4 Results and Discussions

Figure 5.7 illustrates the EVM plots captured by VSA against the optical launch power (OLP) for QPSK, 16-QAM, and 64-QAM. The OLP is controlled by changing the bias current from 2 mA up to 12 mA. For the back-to-back (B2B) system, the RF signal and the input electrical power used were 2.6 GHz and -30 dBm, respectively. Apart from that, the regions are defined in accordance with the VCSEL characteristics (see Figure 5.5). In region A with low OLP values and DM effect, the positive frequency chirp (PFC) was stimulated by signal distortions, which increased the EVM

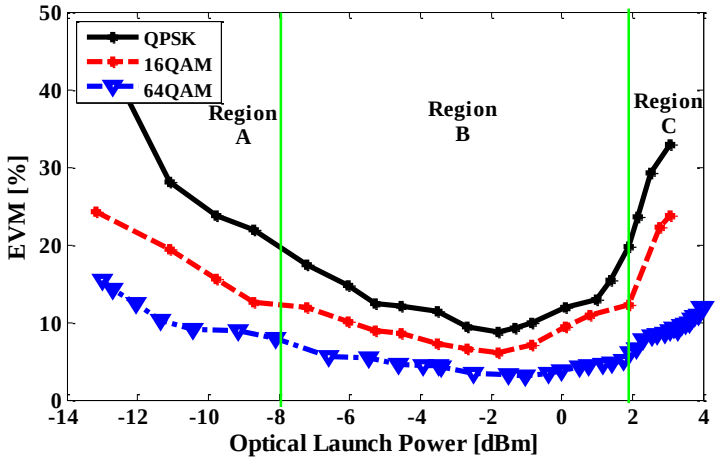

Figure 5.7: The EVM against OLP performance of B2B QPSK, 16-QAM and 64-QAM [191]

values for the three modulation schemes [219]. Moreover, this particular performance is dependent on the dynamic range characteristics of the VCSEL as depicted in Figure 5.5, in which, low modulation index leads to a decline in SNR, which in turn, leading to an increase in EVM. With regards to region B, the high dynamic range of the VCSEL L-I curve shown in Figure 5.5 can increase the output OLP that leads to a high SNR, which was shown by lower EVMs for the three modulations. At -2 dBm, EVM values of ~8.5%, ~6 %, and ~ 2.5% were observed for QPSK, 16-QAM, and 64-QAM, respectively. Finally, the difference of EVM between the three modulations was observed to increase with OLP owing to the nonlinear behaviour of VCSEL that were exhibited at high bias currents [220].

In addition to determining the OLP, the EVM performance against the SNR values has been determined, which is presented in Figure 5.8 for transmitting 20 Mbps, 40 Mbps and 60 Mbps using QPSK, 16-QAM and 64-QAM modulation formats, respectively, up to 300 metres of PF-GI-POF. The EVM value was estimated using VSA software, which analyses the constellation diagram of received signal. On the other hand, SNR was measured using VSA by means of calculating the ratio between the measured signal power to measured noise power over the signal bandwidth.

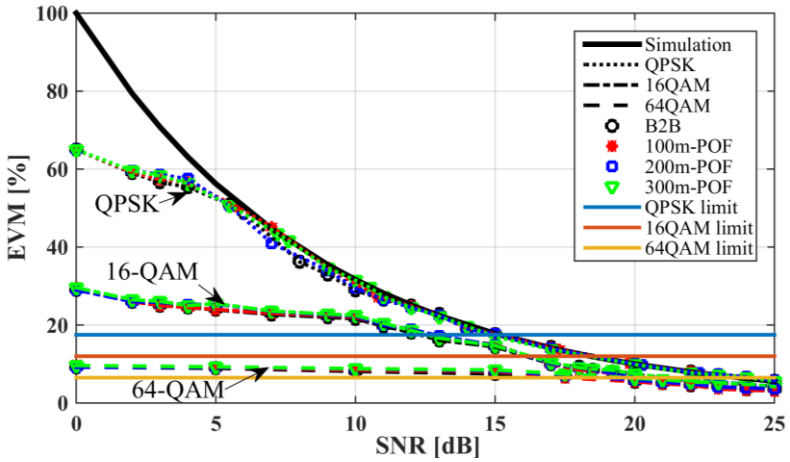

Figure 5.8: Practical EVM performance of the RoPOF using QPSK, 16-QAM and 64-QAM modulation schemes [191]

Figure 5.8 depicts the plots for B2B links and the predicted data obtained by employing the MATLAB^{TM} simulation model, where the SCM signal is generated at the transmitter in baseband either in QPSK, 16-QAM or 64-QAM at 10 MHz bandwidth. The baseband signal is then converted into a passband signal at 2.6 GHz, which is used to direct modulate the VCSEL that is modelled by (2.1), (2.2) and (2.3). The optical signal is then transmitted over the PF-GI-POF channel, which adopts the measured transfer function explained in section (5.2). Hence, the effect of modulation order on the EVM for the same SNR can be observed. The EVM difference of its estimated value increased for the large modulation order due to high symbol error probability, as highlighted in [192]. It should be noted that at lower values of SNR, the measured values were less than the predicted data particularly for 16-QAM and 64-QAM. This is due to the error in the estimation process of the constellation point. Accordingly, a theoretical model will be used to estimate the true EVM values at the low SNR values. However, higher values of SNR demonstrated that the measured plots are much closer to the predicted results as the ISI started to be mitigated. The maximum acceptable EVMs for QPSK, 16-QAM, and 64-QAM are 17.5%, 12.5%, and 8% at SNR of at ~15 dB, ~16.2 dB, and ~17.5 dB, respectively, which were in

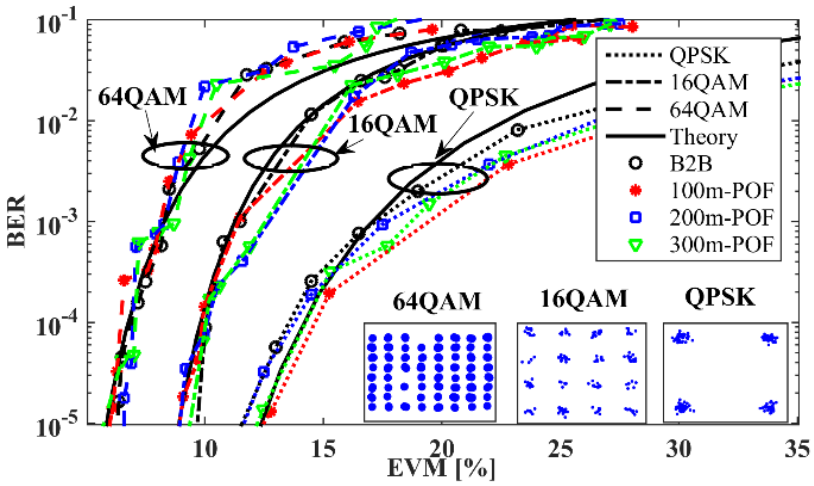

Figure 5.9: The EVM against BER performance of the RoPOF using QPSK, 16-QAM and 64-QAM modulation schemes [191]

the error-free levels outlined in [221]. These values were achieved up to 300 metres transmission span for the QPSK, 16-QAM and 64-QAM. Furthermore, the EVM-BER performance was scrutinized for the three modulation formats, B2B and a range of PF-GI-POF length as shown in Figure 5.9. First, the received data were captured using the signal analyser, which was followed by the estimation of BER estimated using (5.3) and (5.4). Subsequently, the EVM value will be estimated using (5.6) in comparison to measured values for QPSK, 16-QAM and 64-QAM. Also, the constellation diagrams and plots for B2B links at BERs of 10^{-5} for the three modulation formats were displayed, which is lower than the forward error correction (FEC) limit of 10^{-3} [199]. This figure complements Figure 5.8, in which the maximum acceptable EVM corresponded with the targeted BER, depending on the modulation type since the EVM standard for 64-QAM should be less than what of QPSK and 16-QAM due to the high noise sensitivity of the high order modulation schemes compared to the low modulation order.

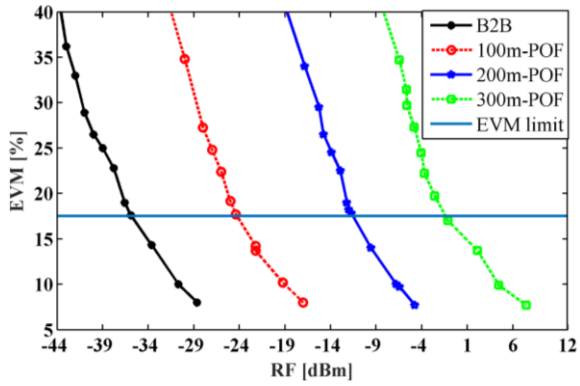

(a)

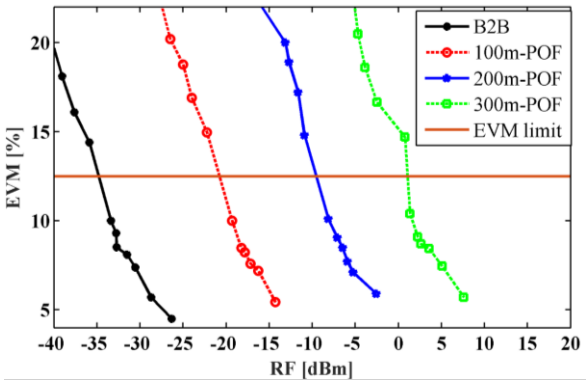

(b)

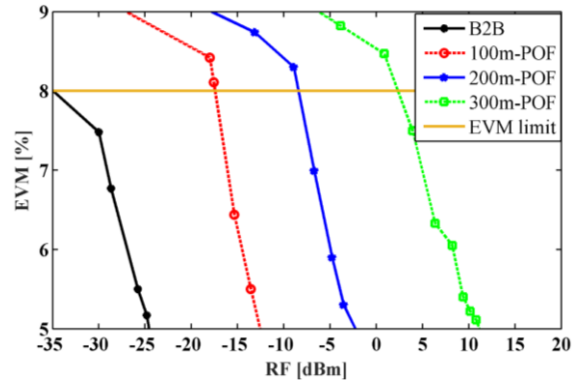

(c)

Figure 5.10: The EVM against input RF power performance of the RoPOF using (a) QPSK, (b) 16-QAM and (c) 64-QAM modulation schemes

Furthermore, the system performance was degraded for longer POF distance owing to the high attenuation levels. Figure 5.10 indicates the EVM performance for a range of the RF input power for the three modulation formats up to 300 m of PF-GI-POF channel using the experimental setup shown in Figure 5.4. To compensate the

channel losses, either optical or electrical power should be increased. In this investigation, the RF power was optimised while the VCSEL biased with 7 mA for the all measurements. At this juncture, the effect of POF losses on the RF power is investigated in order to achieve the required 4G-LTE EVM for each modulation type. This exploration may lead to the estimation of the increased necessary in input signal power to offset the EVM degradation, which is referred to as the power penalty.

Figure 5.11 illustrates the input power penalty against the PF-GI-POF length for the specified EVM limit of 17.5%, 12.5% and 8% for the QPSK, 16-QAM and 64-QAM modulation schemes, respectively. Notably, the electrical power penalty values were related with the optical loss of PF-GI-POF (see Figure 5.6). It should be noted that for such transmission spans, the most dominant effect is the channel attenuation. Power penalty depends primarily on the channel attenuation since a low OLP is applied, and thus, channel nonlinear effects do not influence the system performance. Moreover, the increment of power penalty was not dependent on the modulation order and the transmitted data rate, which shows the low levels of modal dispersion up to 300 metres of PF-GI-POF.

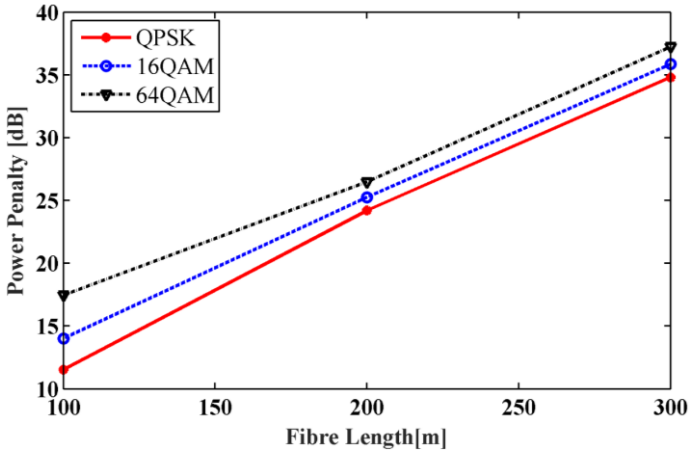

Figure 5.11: Power penalty vs POF length for the QPSK, 16-QAM and 64-QAM modulation schemes [191]

5.5 Summary

To sum up, the implementation of RoF by means of employing PF-GI-POF for QPSK, 16-QAM, and 64-QAM was validated both theoretically and experimentally in this chapter. The scenario of adopting DAS for short-distance communication systems was also demonstrated by providing the RF signals. The end-to-end system transfer function was practically investigated to be employed in the simulation model with the aim of accurately estimating the system performance at low SNR values. Apart from that, the advantage of using a VCSEL laser was illustrated by employing low biasing current and obtaining lower values of EVM at OLP of about -2 dBm for the three modulation types. The relationship among EVM, BER and SNR were investigated both practically and theoretically, in order to show that the system can operate within the specified EVM limits of 17.5%, 12.5% and 8% for QPSK, 16-QAM and 64-QAM, respectively up to 300 metres transmission span. An EVM of ~3.5% and BER of 10^{-5} was achieved in transmitting 60 Mbps over 300 metres PF-GI-POF length. Finally, an investigation was carried out of the input signal power penalty for the three modulation schemes and a range of PF-GI-POF length followed by the linear behaviour of the PF-GI-POF channel being outlined and showed that the fibre attenuation was the most significant factor of such networks in this range of POF distance.

Chapter 6

Conclusions and Future Work

6.1 Conclusions

The drastic development along with the explosive growth observed in the telecommunication systems are reflected in the recent steady rise of the number of subscribers and high data traffic. Such a development necessitates a mobile technology, which can efficiently cope with the bandwidth-hungry and delay-sensitive applications. It is worth highlighting that the 3rd generation partnership project (3GPP) adopted the 4th generation- long term evolution (4G-LTE) as a framework to meet both the rapid recent and future growth in relation to data traffic requirements. The 4G-LTE and the next generation mobile technologies have adopted higher frequency bands in order to address the significant data evolution. However, as it was discussed earlier in chapter 2, the radio frequency (RF) signals that are transmitted over frequencies relatively higher than 2 GHz may experience a severe path loss. Such a loss may exceed 100 dB at 2.6 GHz band along with the multipath fading in urban environments. Consequently, rather lower penetration levels to the walls and buildings may result in poor indoor coverage.

Therefore, this thesis proposed an integration between the radio-over-fibre (RoF) and radio-over-free space optics (RoFSO) technologies in terms of a hybrid RoF-FSO system in order to extend the wireless services for the access and in-building networks for both rural and urban areas. The thesis began with an overview of the evolution of the mobile communication technologies, which was delved deeper in Chapter 1. An

overview of the hybrid RoF-FSO including the related optoelectronic devices was outlined in Chapter 2. More specifically, the significant features of the RoF and RoFSO technologies along with the main applications were demonstrated. In addition, a detailed account of the hybrid RoF-FSO system model was provided in terms of the transmitter, channel and the receiver. Different modulation schemes, namely intensity modulation (IM) and external modulation (EM) that are adopted in the hybrid RoF-FSO system were described to capture their advantages and capabilities in supporting relatively higher data rate and the transmission length. Furthermore, a fair comparison between different light sources, which can possibly be adopted in the hybrid RoF-FSO, was drawn. It was discovered that the IM method with the vertical cavity surface emitting laser (VCSEL) and EM with Distributed feedback (DFB) laser offered the best characteristics for the indoor and outdoor network applications, respectively. Therefore, both lasers were studied in terms of their structures and the mathematical models, which can be used to model the laser diode for the indoor networks. Three channels were introduced in this research, namely the multi-mode fibre (MMF), polymer optical fibre (POF) and FSO, for which the impairments of each channel were discussed in detail along with the associated mathematical expressions.

In Chapter 3, the hybrid radio over MMF and FSO channels (RoMMF-FSO) was proposed to improve the 4G-LTE indoor performance for the application of connecting multiple in-building RoMMF networks using FSO link in the last-mile access network. Besides, the modal dispersion that was induced in the MMF channels was demonstrated. In addition, the single-mode filtering technique (SMFT) as a cost-effective and simple design technique, which can be used to mitigate the modal behaviour, was also focused. The system performance was evaluated theoretically and practically in terms of the total system transfer function, optical beam profile and the

error vector magnitude (EVM) vs signal-to-noise ratio (SNR) performance. The obtained results revealed the modal behaviour of the MMF in terms of random variations of the transfer function beyond the baseband with high sensitivity to the frequency changes. Moreover, the pass band bandwidth was limited to ~1 GHz, which may potentially cause a significant degradation for the LTE signals operating at 2.6 GHz. On the contrary, the adoption of the SMFT may filter off the propagated mode groups except for the fundamental mode. As a result, SMFT was found to have enhanced the transfer function in terms of a dramatic decrease in the fluctuations and increased the channel bandwidth by 2 GHz at least owing to diminishing the modal behaviour of the MMF channel.

Furthermore, the experimental results of the received beam profile indicated that the adoption of the SMFT along with the gradient index (GRIN) lens helped improve the coupling efficiency and the full width at half maximum (FWHM) by 13.6 dB and ~100 µm. Additionally, the proposed technique also enhanced the EVM performance by 4% for the clear atmospheric channel. As it was highlighted earlier, the system performance was also validated under real outdoor environment by two turbulence levels on the FSO channel, which were under weak turbulence regime. The experimental EVM results under turbulence showed the ability of transmitting 67.2 Mbps over 1 km MMF, 2 m FSO and 100 m MMF by retaining the error free EVM requirements for the 3GPP LTE, which was 12.5 % for 16-quadrature amplitude modulation (16-QAM). On the other hand, the theoretical analysis of the EVM performance pointed to the ability of extending the FSO channel of up to 500 m achieving the EVM < 12.5%, which indicated that the proposed technique can be adopted successfully in the real environment for the last-mile access networks.

Further research on the RoMMF-FSO was outlined in chapter 4. The SMFT was tested in the atmospheric fog channel, which may potentially cause a sever degradation in the SNR value. A 1 km MMF and 11 m FSO link were used to design the hybrid RoMMF-FSO for transmitting the 4G-LTE signal at 16-QAM baseband modulation of 5, 10, 15 and 20 MHz. The pass band frequency was observed at 800 MHz, which is notably the typical wireless band for the rural areas. The hybrid system was proposed to extend the 4G-LTE indoor coverage in the sparsely populated areas where the infrastructure for the fibre optical networks was rather scarce and scattered. The system performance was investigated in terms of power link budget and EVM performance. The obtained results revealed a successful transmission of the 4G-LTE signal of up to 20 MHz signal bandwidth at 67.2 Mbps bit rate with the EVM of ~8 %, which is less than the 3GPP LTE requirements. In addition, the link budget analysis confirmed that the proposed hybrid system was able to operate even with longer FSO channel, but only up to 3 km and ~140 m for the clear and thick fog atmospheric weather, respectively.

On the other hand, the use of the POF instead of the MMF was investigated in chapter 4. A hybrid radio-over-POF and radio-over-FSO (RoPOF-FSO) was demonstrated experimentally with the use of 11 m of FSO channel and 100 m of perfluorinated graded-index POF (PF-GI-POF) as in-building network. In this regard, the FSO channel was used to transmit the downlink (DL) 4G-LTE signals from the enhanced NodeB (eNB) to the residential gateway (RG). It has to be noted that the 4G-LTE signal was generated for the single carrier modulation (SCM) quadrature phase shift keying (QPSK), 16-QAM and 64-QAM in order to transmit bit rates of up to 33.6, 67.2 and 100.8 Mbps, respectively. In this study, a design for the RG was introduced, which can be used as the interface between the access and indoor

networks. The link assessment was achieved for the link budget and EVM performance under the effect of clear and thick fog atmospheric channel. In the clear channel, the obtained EVM results indicated a successful transmission of the 4G-LTE signals of up to 100.8 Mbps fulfilling the 3GPP LTE EVM requirements for the three modulation schemes. In thick fog fading effect, however, maximum successful transmission was observed only up to 33.6 Mbps, where the higher bit rate signals required a power penalty (PP) up to ~8 dB for transmitting the 100.8 Mbps signal.

Focusing on the RoF network, chapter 5 demonstrated theoretical and experimental investigations of the in-building RoF using PF-GI-POF links up to 300 m. The RoF links transmitted the three SCM modulation signals, namely QPSK, 16-QAM and 64-QAM at 2.6 GHz band. The DAS scenario was presented by providing the home RU with the RF signal through the optical fibres. The features of the PF-GI-POF were introduced for the in-building networks and to use the VCSEL as a good balance solution between the cost and the quality. The VCSEL characteristics were investigated in relation to the light current (LI) curve and the EVM vs optical launch power (OLP), which revealed the low VCSEL biasing current and the minimum EVM value at ~ -2 dBm for the three modulation formats. The system performance was evaluated theoretically and practically in terms of the total transfer function, EVM, bit error rate (BER) and OLP. The obtained results indicated that the capacity of the proposed system to may help operate successfully within the 3GPP LTE EVM limits of up to 300 m of PF-GI-POF. An average EVM of 3.5% and BER 10^{-5} was reported for transmitting 60 Mbps over the system that can operate within the specified EVM limits of 17.5%, 12.5% and ~8% for QPSK, 16-QAM and 64-QAM, respectively up to 300 metres transmission distance. A successful transmission of 60 Mbps was achieved with EVM of ~ 3.5% and BER of 10^{-5}. Finally, the PP for the input signal

was investigated by relying on three modulation formats. The PP results showed the linear behaviour of the PF-GI-POF and the results outlined that the fibre attenuation was the most significant factor of such networks within such a range of POF distance.

To conclude, a hybrid RoF-FSO system was introduced to improve the performance of 4G-LTE signal for the radio over indoor MMF system in the last mile bottleneck access networks. Moreover, the SMFT technique was adopted to mitigate the modal effects and deliver 67 Mbps under weak turbulence effect within the 12.5% LTE EVM requirements. The SMFT was tested under thick fog effect with 100 visibility range to deliver 67 Mbps with the EVM of ~8%. Furthermore, Hybrid RoPOF-FSO was presented with a design of the RG. The proposed system was verified by transmitting LTE signal with different data rate up to 100 Mbps. Finally, Indoor RoF was investigated using different lengths of PF-GI-POF up to 300 m. Successful Transmitting of 60 Mbps was achieved with ~3.5% EVM and 10^{-5} BER.

6.2 Future Works

It is noteworthy that within the given time frame, the present study has contributed to the design and development of the hybrid RoF-FSO and in-building RoF networks. In this section, the author recommends further research, which will be carried out in the future to extend the research reported in the present thesis.

In this research, the proposed hybrid RoF-FSO system was investigated using downlink (DL) LTE signal. In order to further emphasize on the LTE technology, uplink (UL) LTE signal can be used in the hybrid RoMMF-FSO for further investigation on using the SMFT technique.

In hybrid RoMMF-FSO system, the investigation will be verified practically by means of using longer FSO channel to connect multiple buildings. Additionally, it is

deemed that further investigations can cover multiple effects that may impact on the system performance, such as the amplified spontaneous noise (ASE) produced by the erbium-doped fibre amplifier (EDFA).

Apart from that, the theoretical and experimental investigation for the present study focused on the SMFT as simple, cost-effective and powerful technique to mitigate the modal behaviour of the MMF links in comparison to the typical signal processing tools such as the digital equalizers. However, the indoor networks beyond 300 metres of PF-GI-POF channel may lead to a strong effect of the fibre attenuation and modal dispersion. This, in turn may degrade the SNR and significantly increase the pulse broadening. It should be noted that an equaliser in the receiver is required to compensate the amplitude and phase distortions induced by the optical propagations. Therefore, further research looking into the design of less complexity equalizers that may be used at the receiver side to extend the transmission distance is of utmost importance. On comparison, the non-linear equalizers are considered as attractive candidates owing to their better performance than the linear types.

On the other hand, the POF attenuation is the most dominant distortion factor because of its operation within the 850 nm. An amplification solution is highly recommended in order to compensate the high level of loss. Currently, the tapered semiconductor optical amplifier has drawn the attention of many as an optical amplifier in the 850 nm wavelength. Furthermore, the employment of such amplifiers may extend the POF channel for longer than 500 m.

The present study proposes the utilization of VCSEL due to some reasons, namely its low cost, low threshold point and narrow circular beam, which improve the fibre coupling. However, its low output power has the tendency to be adopted in short-

distance networks. Notably, the nonlinear of VCSEL is a limiting factor in the analogue optical communications. Hence, an intensive investigation is recommended in order to enhance the in-building optical networks that and the adoption of the VCSEL as a light source.

In the last few years, mobile and wireless networks have made remarkable growth. In this regard, the 4G-LTE technology has now been used by the most mobile operators worldwide. Meanwhile, the dramatic development of the mobile data services driven by the smart devices and broadband applications has triggered the investigation of the fifth generation (5G) for the next generation of the mobile communications. Hence, further study on the hybrid RoF-FSO system using 5G mobile technology is highly recommended to cope with the future data traffic requirements.

Finally, the present study investigates the hybrid RoMMF-FSO, hybrid RoPOF-FSO and RoPOF mainly to enhance the indoor coverage for wireless communications. In this regard, the MMF and POF were proposed as an optical channel for short-distance indoor data applications. Recently, tremendous interest is evident in the integration of various data transmission and optical sensing applications. The low cost of POF may be employed as temperature and strain sensors for in-building environments based on several techniques, such as multimode interference, brillouin-based distributed sensors and intensity macrobend sensors.

References

[1] S. Deronne, V. Moeyaert, and S. Bette, "WiFi transmission in radio-over-fiber systems: Performance of the IEEE 802.11n aggregation mechanism," in *17th International Conference on Optical Network Design and Modeling (ONDM)*, , 2013, pp. 167-172.

[2] S. Carson and P. Jonsson, "Ericsson mobility report: On the pulse of the networked society," June 2016.

[3] OECD, *OECD Science, Technology and Innovation Outlook*. OECD Publishing, 2016.

[4] CISCO, "Cisco visual networking index: Global mobile data traffic forecast update, 2016–2021," *Cisco White Paper*, 2017.

[5] E. Dahlman, S. Parkvall, and J. Sköld, *4G LTE/LTE-advanced for mobile broadband*, Second edition. ed., 2014.

[6] J. Bergman, M. Ericson, D. Gerstenberger, B. Göransson, J. Peisa, and S. Wager, "HSPA Evolution–Boosting the performance of mobile broadband access," *Ericsson Review*, vol. 85, pp. 32-37, 2008.

[7] R. Kreher and K. Gaenger, *LTE Signaling: Troubleshooting and Performance Measurement*: Wiley, 2016.

[8] A. R. Mishra, *Cellular Technologies for Emerging Markets: 2G, 3G and Beyond*: Wiley, 2010.

[9] S. Shukla, V. Khare, S. Garg, and P. Sharma, "Comparative study of 1G, 2G, 3G and 4G," *Journal of Engineering, Computers & Applied Sciences*, vol. 2, pp. 55-63, 2013.

[10] 3GPP. (2016, 19/07/2016). *Releases*. Available: http://www.3gpp.org/specifications/67-releases

[11] N. Tripathi and J. H. Reed, *Cellular Communications: A Comprehensive and Practical Guide*: Wiley, 2014.

[12] Keysight Technologies, "3GPP long term evolution: System overview, product development, and test challenges," 2014.

[13] S. Jones, R. J. Kovac, and F. M. Groom, *Introduction to Communications Technologies: A Guide for Non-Engineers, Third Edition*: CRC Press, 2015.

[14] Y. Niu, Y. Li, D. Jin, L. Su, and A. V. Vasilakos, "A survey of millimeter wave communications (mmWave) for 5G: opportunities and challenges," *Wireless Networks*, vol. 21, pp. 2657-2676, 2015.

[15] T. Halonen, J. Romero, and J. Melero, *GSM, GPRS and EDGE Performance: Evolution Towards 3G/UMTS*: Wiley, 2004.

[16] A. Urie, A. N. Rudrapatna, C. Raman, and J. M. Hanriot, "Evolved multimedia broadcast multicast service in LTE: An assessment of system performance under realistic radio network engineering conditions," *Bell Labs Technical Journal*, vol. 18, pp. 57-76, 2013.

[17] S. S. Arunachalam, S. Kishore Kumar, V. Manickam, and S. S. Murugan, "Performance analysis of spatial channel separation for interference mitigation in femtocellular systems," in *International Conference onCommunications and Signal Processing (ICCSP)*, , 2012, pp. 62-65.

[18] A. Elnashar and M. A. El-Saidny, "Looking at LTE in Practice: A Performance Analysis of the LTE System Based on Field Test Results," *Vehicular Technology Magazine, IEEE*, vol. 8, pp. 81-92, 2013.

[19] H. Holma, A. Toskala, and J. Reunanen, *LTE Small Cell Optimization: 3GPP Evolution to Release 13*: Wiley, 2016.
[20] J. G. Rémy and C. Letamendia, *LTE Standards*: Wiley, 2014.
[21] A. Paradisi, M. D. Yacoub, F. L. Figueiredo, and T. R. Tronco, *Long Term Evolution: 4G and Beyond*: Springer International Publishing, 2016.
[22] T. Kanesan, N. Wai Pang, Z. Ghassemlooy, and L. Chao, "Experimental full duplex simultaneous transmission of LTE over a DWDM directly modulated RoF system," *Optical Communications and Networking, IEEE/OSA Journal of*, vol. 6, pp. 8-17, 2014.
[23] http://www.4g.co.uk/4g-frequencies-uk-need-know/. (03/02/2017).
[24] G. Yuan, X. Zhang, W. Wang, and Y. Yang, "Carrier aggregation for LTE-advanced mobile communication systems," *IEEE Communications Magazine*, vol. 48, pp. 88-93, 2010.
[25] H. Kim, J. H. Cho, S. Kim, K. U. Song, H. Lee, J. Lee, B. Kim, Y. Oh, and S. Hwang, "Radio-Over-Fiber System for TDD-Based OFDMA Wireless Communication Systems," *Journal of Lightwave Technology*, vol. 25, pp. 3419-3427, 2007.
[26] J. Zhang and G. De la Roche, *Femtocells : technologies and deployment*. Chichester, West Susssex, U.K. ; Hoboken, NJ: Wiley, 2010.
[27] A. Bezzina, M. Ayari, R. Langar, and L. A. Saidane, "A fair cluster-based resource and power allocation scheme for two-tier LTE femtocell networks," in *2016 Global Information Infrastructure and Networking Symposium (GIIS)*, 2016, pp. 1-6.
[28] T. Connectivity. (2014, 18/02/2014). *Fiber connectivity*. Available: http://www.te.com/
[29] A. E. Aighobahi and N. J. Gomes, "Capacity and Error Performance Verification of Multi-Antenna Schemes in Radio-Over-Fiber Distributed Antenna System," *Journal of Lightwave Technology*, vol. 34, pp. 4779-4785, 2016.
[30] H. Claussen, L. T. W. Ho, and F. Pivit, "Effects of joint macrocell and residential picocell deployment on the network energy efficiency," in *2008 IEEE 19th International Symposium on Personal, Indoor and Mobile Radio Communications*, 2008, pp. 1-6.
[31] K. Nakajima and K. Iwashita, "Electrical Equalization of Multipath Interferences Using Subcarrier Multiplexing of a Single Frequency Light Source," in *LEOS 2006 - 19th Annual Meeting of the IEEE Lasers and Electro-Optics Society*, 2006, pp. 410-411.
[32] N. J. Gomes, M. Morant, A. Alphones, B. Cabon, J. E. Mitchell, C. Lethien, M. Csörnyei, A. Stöhr, and S. Iezekiel, "Radio-over-fiber transport for the support of wireless broadband services [Invited]," *Journal of Optical Networking*, vol. 8, pp. 156-178, 2009.
[33] M. Tolstrup, *Indoor Radio Planning: A Practical Guide for GSM, DCS, UMTS, HSPA and LTE*: Wiley, 2011.
[34] B. Mitchell. (2016, 07/02/2017). *DSL speed: How fast is DSL internet service?* Available: https://www.lifewire.com/speed-of-dsl-internet-service-817523
[35] T. Guo, A. ul Quddus, N. Wang, and R. Tafazolli, "Local mobility management for networked femtocells based on X2 traffic forwarding," *IEEE Transactions on Vehicular Technology*, vol. 62, pp. 326-340, 2013.

[36] J. Hamalainen. (2011, 08/02/2017). *Femtocells: Technology and developments*. Available: http://www.cwc.oulu.fi/summerschool2011/Femtocells_Hamalainen2011.pdf
[37] M. Fabbri and P. Faccin, "Radio over Fiber Technologies and Systems: New Opportunities," in *2007 9th International Conference on Transparent Optical Networks*, 2007, pp. 230-233.
[38] R. Ramaswami, K. N. Sivarajan, and G. H. Sasaki, *Optical networks : a practical perspective*, 3rd ed. Amsterdam ; Boston: Elsevier/Morgan Kaufmann, 2010.
[39] K. S. Thyagarajan and A. Ghatak, *Fiber Optic Essentials*: Wiley, 2007.
[40] C. Industries. (2015, 21/12/2016). *What is the difference between OM1, OM2, OM3, OM4*. Available: http://www.cablek.com/technical-reference/fiber-optic-cable-types
[41] D. Visani, M. N. Petersen, F. Sorci, L. Tarlazzi, P. Faccin, and G. Tartarini, "In-building wireless distribution in legacy multimode fiber with an improved RoMMF system," *Microwave and Wireless Components Letters, IEEE*, vol. 22, pp. 598-600, 2012.
[42] A. Flatman. (2007). *In-Premises optical fibre installed base analysis to 2007*. Available: http://www.ieee802.org/3/10GMMFSG/public/mar04/flatman_1_0304.pdf
[43] S. Yan, C. Okonkwo, D. Visani, E. Tangdiongga, and T. Koonen, "Distribution of Broadband Services Over 1-mm Core Diameter Plastic Optical Fiber for Point-to-Multipoint In-Home Networks," *Journal of Lightwave Technology*, vol. 31, pp. 874-881, 2013.
[44] D. Visani, Y. Shi, C. M. Okonkwo, H. Yang, H. P. A. van den Boom, G. Tartarini, E. Tangdiongga, and A. M. J. Koonen, "Wired and wireless multi-service transmission over 1mm-core GI-POF for in-home networks," *Electronics Letters*, vol. 47, pp. 203-205, 2011.
[45] O. Ziemann, *POF handbook : optical short range transmission systems*, 2nd ed. Berlin: Springer, 2008.
[46] J. M. B. Oliveira, S. Silva, L. M. Pessoa, D. Coelho, H. M. Salgado, and J. C. S. Castro, "UWB radio over perfluorinated GI-POF for low-cost in-building networks," in *2010 IEEE Topical Meeting on Microwave Photonics (MWP)* 2010, pp. 317-320.
[47] G. P. Agrawal, *Fiber-optic communication systems*, 4th ed. New York: Wiley, 2010.
[48] C. Lethien, C. Loyez, J. P. Vilcot, L. Clavier, M. Bocquet, and P. A. Rolland, "Indoor coverage improvement of MB-OFDM UWB signals with radio over POF system," *Optics Communications*, vol. 282, pp. 4706-4715, Dec 15 2009.
[49] A. J. Koonen, H. P. A. Van den Boom, E. Tangdiongga, H. D. Jung, and P. Guignard, "Designing in-building optical fiber networks," in *Conference on (OFC/NFOEC) Optical Fiber Communication (OFC), collocated National Fiber Optic Engineers Conference, ,* 2010, pp. 1-3.
[50] E. Leitgeb and T. Plank, "Combination of Free Space Optics (FSO) and RF for different wireless application scenarios," in *2015 9th European Conference on Antennas and Propagation (EuCAP)*, 2015, pp. 1-4.
[51] J. A. Zhang, I. B. Collings, C. S. Chen, L. Roullet, L. Luo, S. W. Ho, and J. Yuan, "Evolving small-cell communications towards mobile-over-FTTx networks," *IEEE Communications Magazine*, vol. 51, pp. 92-101, 2013.

[52] H. D. Jung, K. W. Lee, J. H. Kim, Y. H. Kwon, and J. H. Park, "Performance Comparison of Analog and Digitized RoF Systems With Nonlinear Channel Condition," *IEEE Photonics Technology Letters*, vol. 28, pp. 661-664, 2016.
[53] Z. Ghassemlooy, W. Popoola, and S. Rajbhandari, *Optical wireless communications : system and channel modelling with MATLAB*. Boca Raton, FL: Taylor & Francis, 2012.
[54] H. Chen, H. P. A. v. d. Boom, E. Tangdiongga, and T. Koonen, "30-Gb/s Bidirectional Transparent Optical Transmission With an MMF Access and an Indoor Optical Wireless Link," *IEEE Photonics Technology Letters*, vol. 24, pp. 572-574, 2012.
[55] M. Atef, R. Swoboda, and H. Zimmermann, "1.25 Gbit/s Over 50 m Step-Index Plastic Optical Fiber Using a Fully Integrated Optical Receiver With an Integrated Equalizer," *Journal of Lightwave Technology*, vol. 30, pp. 118-122, 2012.
[56] H. K. Al-Musawi, T. Cseh, J. Bohata, P. Pesek, W. P. Ng, Z. Ghassemlooy, E. Udvary, T. Berceli, and S. Zvanovec, "Experimental optimization of the hybrid RoMMF-FSO system using mode filtering techniques," in *2016 IEEE International Conference on Communications Workshops (ICC)*, 2016, pp. 405-410.
[57] T. Cseh and T. Berceli, "Dispersion compensation in millimeter wave radio over fiber systems," *Microwave and Optical Tech. Letters*, vol. 57, pp. 204-207, 2015.
[58] K. Appaiah, R. Salas, S. Vishwanath, and S. R. Bank, "Offset coupling, feedback, and spatial multiplexing in 4,x,4 incoherent-MIMO multimode fiber links," *Journal of Lightwave Technology*, vol. 31, pp. 2926-2939, 2013.
[59] J. Bohata, S. Zvanovec, T. Korinek, M. Mansour Abadi, and Z. Ghassemlooy, "Characterization of dual-polarization LTE radio over a free-space optical turbulence channel," *Applied Optics*, vol. 54, pp. 7082-7087, 2015.
[60] K. S. Sanila and K. Appaiah, "Low Complexity Equalization Using Mode-Subset Selection in MIMO Multimode Fiber Links," in *2015 IEEE Global Communications Conference (GLOBECOM)*, 2015, pp. 1-6.
[61] E. Mammei, F. Loi, F. Radice, A. Dati, M. Bruccoleri, M. Bassi, and A. Mazzanti, "8.3 A power-scalable 7-tap FIR equalizer with tunable active delay line for 10-to-25Gb/s multi-mode fiber EDC in 28nm LP-CMOS," in *2014 IEEE International Solid-State Circuits Conference Digest of Technical Papers (ISSCC)*, 2014, pp. 142-143.
[62] A. G. Bell, "Upon the production and reproduction of sound by light," *Telegraph Engineers, Journal of the Society of*, vol. 9, pp. 404-426, 1880.
[63] D. Killinger, "Free space optics for laser communication through the air," *Optics and Photonics News*, vol. 13, pp. 36-42, 2002.
[64] J. Hawkes and I. Latimer, *Lasers: theory and practice*: Prentice Hall, 1995.
[65] F. E. Goodwin, "A review of operational laser communication systems," *Proceedings of the IEEE*, vol. 58, pp. 1746-1752, 1970.
[66] K. C. Kao and G. A. Hockham, "Dielectric-fibre surface waveguides for optical frequencies," *Proceedings of the Institution of Electrical Engineers*, vol. 113, pp. 1151-1158, 1966.
[67] S. Nandi, S. Thota, A. Nag, S. Divyasukhananda, P. Goswami, A. Aravindakshan, R. Rodriguez, and B. Mukherjee, "Computing for rural empowerment: enabled by last-mile telecommunications," *IEEE Communications Magazine*, vol. 54, pp. 102-109, 2016.

[68] C. Lin, *Broadband Optical Access Networks and Fiber-to-the-Home: Systems Technologies and Deployment Strategies*: Wiley, 2006.
[69] W. Jiang Jr, C.-T. Lin, P.-T. Shih, J. J. Chen, P.-C. Peng, and S. Chi, "A full duplex radio-over-fiber link with multi-level OFDM signal via a single-electrode MZM and wavelength reuse with a RSOA," *Optics Express*, vol. 18, pp. 2710-2718, 2010.
[70] H. Kaushal and G. Kaddoum, "Optical Communication in Space: Challenges and Mitigation Techniques," *IEEE Communications Surveys & Tutorials*, vol. PP, pp. 1-1, 2016.
[71] S. Yan, M. Morant, C. Okonkwo, R. Llorente, E. Tangdiongga, and A. M. J. Koonen, "Multistandard Wireless Transmission Over SSMF and Large-Core POF for Access and In-Home Networks," *Photonics Technology Letters, IEEE*, vol. 24, pp. 736-738, 2012.
[72] W. P. Ng, T. Kanesan, Z. Ghassemlooy, and C. Lu, "Theoretical and experimental optimum system design for LTE-RoF over varying transmission span and identification of system nonlinear limit," *Photonics Journal, IEEE*, vol. 4, pp. 1560-1571, 2012.
[73] A. Shami, M. Maier, and C. Assi, *Broadband access networks : technologies and deployments*, 1st ed. New York: Springer, 2009.
[74] R. E. Schuh, "Hybrid fiber radio for second and third generation wireless systems," in *MWP '99. International Topical Meeting on Microwave Photonics*, 1999, pp. 213-216 vol.1.
[75] A. M. J. Koonen, M. G. Larrode, A. Ng'oma, K. Wang, H. Yang, Y. Zheng, and E. Tangdiongga, "Perspectives of radio over fiber technologies," *2008 Conference on Optical Fiber Communication/National Fiber Optic Engineers Conference, Vols 1-8*, pp. 2005-2007, 2008.
[76] R. Yuen and X. N. Fernando, "Enhanced Wireless Hotspot Downlink Supporting IEEE802.11 and WCDMA," in *2006 IEEE 17th International Symposium on Personal, Indoor and Mobile Radio Communications*, 2006, pp. 1-6.
[77] P. Hartmann, Q. Xin, A. Wonfor, R. V. Penty, and I. H. White, "1-20 GHz Directly Modulated Radio over MMF Link," in *MWP 2005. International Topical Meeting on Microwave Photonics*, 2005, pp. 95-98.
[78] Z. Bouhamri, Y. Le Guennec, J. Duchamp, G. Maury, A. Schimpf, V. Dobremez, L. Bidaux, and B. Cabon, "Multistandard Transmission Over Plastic Optical Fiber," *IEEE Transactions on Microwave Theory and Techniques*, vol. 58, pp. 3109-3116, 2010.
[79] F. Forni, Y. Shi, H. v. d. Boom, E. Tangdiongga, and T. Koonen, "Multiband LTE-A and 4-PAM Signals Over Large-Core Plastic Fibers for In-Home Networks," *IEEE Photonics Technology Letters*, vol. 28, pp. 2281-2284, 2016.
[80] C. H. Chang, W. Y. Lin, H. H. Lu, C. Y. Chen, P. Y. Wu, and Y. P. Lin, "An Integrated Long-Reach PON and GI-POF In-House Network Architecture for Hybrid CATV/OFDM Signals Transmission," *Journal of Lightwave Technology*, vol. 30, pp. 3247-3251, 2012.
[81] http://www.commscope.com. (20/01/2017).
[82] http://www.zinwave.com. (20/01/2017).
[83] http://www.te.com. (20/01/2017).
[84] A. Antonino, D. Zeolla, and R. Gaudino, "Experimental Proof-of-Concept of Bidirectional Gigabit Transmission Over Single Step-Index Plastic Optical Fiber," *Photonics Technology Letters, IEEE*, vol. 22, pp. 923-925, 2010.

[85] H. Willebrand and B. S. Ghuman, *Free Space Optics: Enabling Optical Connectivity in Today's Networks*: Sams, 2002.
[86] I. E. Lee, "Free space optical communication systems with a partially coherent gaussian beam and media diversity," Doctoral thesis, Northumbria University, 2014.
[87] W. O. Popoola, "Subcarrier intensity modulated free-space optical communication systems," Doctoral thesis, Northumbria University, Newcastle upon Tyne, UK, 2009.
[88] Ofcom, "Study on the future UK spectrum demand for terrestrial mobile broadband applications," *Realwireless, report,* vol. 3.1, April 2014.
[89] M. Uysal, C. Capsoni, Z. Ghassemlooy, A. Boucouvalas, and E. Udvary, *Optical Wireless Communications: An Emerging Technology*: Springer International Publishing, 2016.
[90] P. V. Trinh, N. T. Dang, and A. T. Pham, "All-optical relaying FSO systems using EDFA combined with optical hard-limiter over atmospheric turbulence channels," *Journal of Lightwave Technology,* vol. 33, pp. 4132-4144, 2015.
[91] G. Parca, A. Shahpari, V. Carrozzo, G. M. T. Beleffi, and A. L. Teixeira, "Optical wireless transmission at 1.6-Tbit/s (16× 100 Gbit/s) for next-generation convergent urban infrastructures," *Optical Engineering,* vol. 52, pp. 116102-116102, 2013.
[92] K. Biesecker, "The promise of broadband wireless," *IT Professional,* vol. 2, pp. 31-39, 2000.
[93] A. K. Majumdar, *Advanced Free Space Optics (FSO): A Systems Approach*: Springer New York, 2015.
[94] X. Tang, "Polarisation shift keying modulated free-space optical communication systems," Doctoral thesis, Northumbria University, Newcastle upon Tyne, UK, 2012.
[95] A. Morea, J. Perell, x00F, S. Spadaro, D. Verch, x00E, re, and M. Vigoureux, "Protocol enhancements for "greening" optical networks," *Bell Labs Technical Journal,* vol. 18, pp. 211-230, 2013.
[96] I. E. Lee, Z. Ghassemlooy, W. P. Ng, and A. Khalighi, "Green-inspired hybrid FSO/RF wireless backhauling and basic access signalling for next generation metrozones," presented at the 2nd International Symposium on Environment Friendly Energies and Applications (EFEA), 2012.
[97] M. Ijaz, "Experimental characterisation and modelling of atmospheric fog and turbulence in FSO," Doctoral thesis, Northumbria University, Newcastle upon Tyne, UK, 2013.
[98] M. Mitsuji, K. Kamugisha, P. Dat, A. Shah, O. Kazunori, S. Toshiji, W. Kazuhiko, H. Takeshi, T. Katsutoshi, and K. Shozo, "An alternative access technology for next generation networks based on full-optical wireless communication links," presented at the Innovations in NGN: Future Network and Services, 2008. K-INGN 2008. First ITU-T Kaleidoscope Academic Conference, 2008.
[99] D. Chadha, *Terrestrial Wireless Optical Communication*: McGraw-Hill Education, 2013.
[100] D. A. Rockwell and G. S. Mecherle. (2016, 17/08/2016). *Optical wireless: Low-cost, broadband, optical access*. Available: http://www.fsona.com/tech/white_papers/optical_wireless.pdf
[101] M. A. Esmail, A. Ragheb, H. Fathallah, and M. S. Alouini, "Experimental demonstration of outdoor 2.2 Tbps super-channel FSO transmission system,"

presented at the 2016 IEEE International Conference on Communications Workshops (ICC), 2016.
[102] H. A. Fadhil, A. Amphawan, H. A. Shamsuddin, T. H. Abd, H. M. Al-Khafaji, S. Aljunid, and N. Ahmed, "Optimization of free space optics parameters: An optimum solution for bad weather conditions," *Optik-International Journal for Light and Electron Optics*, vol. 124, pp. 3969-3973, 2013.
[103] N. A. M. Nor, J. Bohata, Z. Ghassemlooy, S. Zvanovec, P. Pesek, M. Komanec, J. Libich, and M. A. Khalighi, "10 Gbps all-optical relay-assisted FSO system over a turbulence channel," in *4th International Workshop on Optical Wireless Communications (IWOW)*, 2015, pp. 69-72.
[104] S. V. Kartalopoulos, *Free space optical networks for ultra-broad band services*. Hoboken, N.J.: Wiley ; IEEE Press, 2011.
[105] V. H. Tanzil, P. Farkas, and D., "Cost Optimized Planning of Fixed-Wireless Hybrid Access Networks," in *Broadband Coverage in Germany; 10. ITG-Symposium*, 2016, pp. 1-5.
[106] J. Bohata, S. Zvanovec, M. M. Abadi, and Z. Ghassemlooy, "Channel characterization of a last-mile access radio over combined fibre and free-space optics system," in *2015 International Conference on Automation, Cognitive Science, Optics, Micro Electro-Mechanical System, and Information Technology (ICACOMIT)*, 2015, pp. 27-30.
[107] J. Libich, M. Mudroch, P. Dvorak, and S. Zvanovec, "Performance analysis of hybrid FSO/RF link," in *2012 6th European Conference on Antennas and Propagation (EUCAP)*, 2012, pp. 1235-1238.
[108] Y. Tang, M. Brandt-Pearce, and S. G. Wilson, "Link adaptation for parallel channels with encoder rate and modem symbol rate constraints," in *2010 IEEE Globecom Workshops*, 2010, pp. 1000-1004.
[109] F. Nadeem, V. Kvicera, M. S. Awan, E. Leitgeb, S. S. Muhammad, and G. Kandus, "Weather effects on hybrid FSO/RF communication link," *IEEE Journal on Selected Areas in Communications*, vol. 27, pp. 1687-1697, 2009.
[110] H. Moradi, H. H. Refai, and P. G. LoPresti, "Spatial Diversity for Fiber-Bundled FSO Nodes With Limited Mobility," *Journal of Lightwave Technology*, vol. 30, pp. 175-183, 2012.
[111] S. Vangala and H. Pishro-Nik, "A Highly Reliable FSO/RF Communication System Using Efficient Codes," in *IEEE GLOBECOM 2007 - IEEE Global Telecommunications Conference*, 2007, pp. 2232-2236.
[112] A. Abdulhussein, A. Oka, T. T. Nguyen, and L. Lampe, "Rateless coding for hybrid free-space optical and radio-frequency communication," *IEEE Transactions on Wireless Communications*, vol. 9, pp. 907-913, 2010.
[113] N. Letzepis, K. D. Nguyen, A. Guill, x00E, F. n i, bregas, and W. G. Cowley, "Hybrid free-space optical and radio-frequency communications: Outage analysis," in *2010 IEEE International Symposium on Information Theory*, 2010, pp. 2048-2052.
[114] G. Nykolak, P. F. Szajowski, G. Tourgee, and H. Presby, "2.5 Gbit/s free space optical link over 4.4 km," *Electronics Letters*, vol. 35, pp. 578-579, 1999.
[115] C. Pei-Lin, C. Shenq-Tsong, J. Shuen-Te, L. Shu-Chuan, L. Han-Hsuan, T. Ho-Lin, H. Po-Hsuan, C. Wei-Chieh, L. Wei-Cheng, L. San-Liang, T. Hen-Wai, W. Jin-Pu, and W. Jingshown, "Demonstration of 16 channels 10 Gb/s WDM free space transmission over 2.16 km," in *2008 Digest of the IEEE/LEOS Summer Topical Meetings*, 2008, pp. 235-236.

[116] Y. Arimoto, M. Presi, V. Guarino, A. D. Errico, G. Contestabile, M. Matsumoto, and E. Ciaramella, "320 Gbit/s (8x40 Gbit/s) double-pass terrestrial free-space optical link transparently connected to optical fibre lines," in *2008 34th European Conference on Optical Communication*, 2008, pp. 1-2.
[117] C. B. Naila, K. Wakamori, M. Matsumoto, A. Bekkali, and K. Tsukamoto, "Transmission analysis of digital TV signals over a radio-on-FSO channel," *IEEE Communication Magazine*, vol. 50, pp. 137-144, 2012.
[118] M. A. Khalighi and M. Uysal, "Survey on free space optical communication: A communication theory perspective," *IEEE Communications Surveys & Tutorials*, vol. 16, pp. 2231-2258, 2014.
[119] H. K. Al-Musawi, T. Cseh, M. M. Abadi, W. P. Ng, Z. Ghassemlooy, E. Udvary, and T. Berceli, "Experimental demonstration of transmitting LTE over FSO for in-building POF networks," in *17th International Conference on Transparent Optical Networks (ICTON)*, 2015, pp. 1-4.
[120] H. K. Al-Musawi, T. Cseh, J. Bohata, P. Pesek, W. P. Ng, Z. Ghassemlooy, E. Udvary, S. Zvanovec, and M. Ijaz, "Fundamental investigation of extending 4G-LTE signal over MMF/SMF-FSO under controlled turbulence conditions," in *2016 International Symposium on Communication Systems, Networks and Digital Signal Processing (CSNDSP)*, 2016, pp. 1-6.
[121] H. K. Al-Musawi, T. Cseh, J. Bohata, W. P. Ng, Z. Ghassemlooy, S. Zvanovec, E. Udvary, and P. Pesek, "Adaptation of Mode Filtering Technique in 4G-LTE Hybrid RoMMF-FSO for Last-mile Access Network," *Journal of Lightwave Technology*, vol. PP, pp. 1-1, 2017.
[122] J. E. Barg, X. Jin, M. Wiltshire, M. Abolhasani, and J. F. Holzman, "Photoconductive sensors for distributed optical sensing," in *23rd Canadian Conference on Electrical and Computer Engineering (CCECE)*, 2010, pp. 1-4.
[123] N. Agrawal, C. C. Davis, and S. D. Milner, "Free space optical sensor networking for underwater sensing applications," in *Intelligent Sensors, Sensor Networks and Information Processing (ISSNIP), 2009 5th International Conference on*, 2009, pp. 475-480.
[124] W. Boubakri, W. Abdallah, and N. Boudriga, "A light-based communication architecture for smart city applications," in *2015 17th International Conference on Transparent Optical Networks (ICTON)*, 2015, pp. 1-6.
[125] A. Bekkali, C. B. Naila, K. Kazaura, K. Wakamori, and M. Matsumoto, "Transmission analysis of OFDM-based wireless services over turbulent radio-on-FSO links modeled by gamma-gamma distribution," *IEEE Photonics Journal*, vol. 2, pp. 510-520, 2010.
[126] G. S. D. Gordon, M. J. Crisp, R. V. Penty, T. D. Wilkinson, and I. H. White, "Feasibility demonstration of a mode-division multiplexed MIMO-enabled radio-over-fiber distributed antenna system," *Journal of Lightwave Technology*, vol. 32, pp. 3521-3528, 2014.
[127] A. Koonen, A. Pizzinat, E. O. Martinez, J. Faller, B. Lannoo, H. van den Boom, C. Okonkwo, Y. Shi, E. Tangdiongga, and P. Guignard, "A look into the future of in-building networks: Roadmapping the fiber invasion," 2011.
[128] R. Gindera, Mo, x, I. llers, M. Bulters, D. Kalinowski, Ja, x, and D. ger, "Recent Developments in Polymer Optical Fiber (POF) Transceivers," in *Transparent Optical Networks, 2007. ICTON '07. 9th International Conference on*, 2007, pp. 54-57.

[129] I. B. Djordjevic and H. G. Batshon, "LDPC-Coded OFDM for Heterogeneous Access Optical Networks," *IEEE Photonics Journal*, vol. 2, pp. 611-619, 2010.
[130] D. Wake, A. Nkansah, N. J. Gomes, G. De Valicourt, R. Brenot, M. Violas, L. Zhansheng, F. Ferreira, and S. Pato, "A Comparison of Radio Over Fiber Link Types for the Support of Wideband Radio Channels," *Lightwave Technology, Journal of*, vol. 28, pp. 2416-2422, 2010.
[131] Y. H. Kho, L. Yong, K. L. Lau, and K. P. Kiu, "Design of an Indoor Wireless Optical Transceiver System with Source and Channel Coding," in *2012 IEEE Symposium on Industrial Electronics and Applications (ISIEA)*, 2012, pp. 45-49.
[132] G. Keiser, *Optical communications essentials*. New York: McGraw-Hill, 2003.
[133] K. Vahala, *Optical microcavities*. Singapore ; Hackensack, N.J.: World Scientific, 2004.
[134] G. Keiser, *Optical fiber communications*, 4th ed. New York, NY: McGraw-Hill Companies, 2011.
[135] J. M. Senior and M. Y. Jamro, *Optical fiber communications : principles and practice*, 3rd ed. Harlow, England ; New York: Financial Times/Prentice Hall, 2009.
[136] L. Hai-Han, C. Ching-Hung, P. Peng-Chun, S. Heng-Sheng, and H. Hsuan-Wen, "A Radio-Over-GI-POF Transport System," *Journal of Lightwave Technology*, vol. 28, pp. 1917-1921, 2010.
[137] M. Faugeron, M. Chtioui, A. Enard, O. Parillaud, F. Lelarge, M. Achouche, J. Jacquet, A. Marceaux, and F. Van Dijk, "High Optical Power, High Gain and High Dynamic Range Directly Modulated Optical Link," *Journal of Lightwave Technology*, vol. 31, pp. 1227-1233, 2013.
[138] E. Leitgeb, T. Plank, M. S. Awan, P. Brandl, W. Popoola, Z. Ghassemlooy, F. Ozek, and M. Wittig, "Analysis and evaluation of optimum wavelengths for free-space optical transceivers," in *2010 12th International Conference on Transparent Optical Networks*, 2010, pp. 1-7.
[139] E. Leitgeb, S. S. Muhammad, B. Flecker, C. Chlestil, M. Gebhart, and T. Javornik, "The Influence of Dense Fog on Optical Wireless Systems, Analysed by Measurements in Graz for Improving the Link-Reliability," in *2006 International Conference on Transparent Optical Networks*, 2006, pp. 154-159.
[140] K. Tsukamoto, A. Hashimoto, Y. Aburakawa, and M. Matsumoto, "The case for free space," *Microwave Magazine, IEEE*, vol. 10, pp. 84-92, 2009.
[141] S. Mohrdiek, H. Burkhard, F. Steinhagen, H. Hillmer, R. Losch, W. Schlapp, and R. Gobel, "10-Gb/s standard fiber transmission using directly modulated 1.55-μm quantum-well DFB lasers," *IEEE Photonics Technology Letters*, vol. 7, pp. 1357-1359, 1995.
[142] R. Michalzik, *VCSELs: Fundamentals, Technology and Applications of Vertical-Cavity Surface-Emitting Lasers*: Springer, 2013.
[143] Z. Toffano, A. Gholami, M. Fez, A. Destrez, and M. Marec, "VCSEL short reach communications: Behavioural modelling of high speed optoelectronic modules," in *Proceedings of the 4th International Conference on Numerical Simulation of Optoelectronic Devices, 2004. NUSOD '04.* , 2004, pp. 49-50.
[144] A. Tapetado, P. J. Pinzón, J. Zubia, and C. Vázquez, "Polymer Optical Fiber Temperature Sensor With Dual-Wavelength Compensation of Power Fluctuations," *Journal of Lightwave Technology*, vol. 33, pp. 2716-2723, 2015.

[145] M. B. Othman, L. Deng, X. Pang, J. Caminos, W. Kozuch, K. Prince, J. B. Jensen, and I. T. Monroy, "Directly-modulated VCSELs for 2 x 2 MIMO-OFDM radio over fiber in WDM-PON," in *2011 37th European Conference and Exhibition on Optical Communication*, 2011, pp. 1-3.
[146] A. Brillant, *Digital and Analog Fiber Optic Communications for CATV and FTTx Applications*: Wiley-Interscience, 2008.
[147] L. N. Binh, *Advanced Digital Optical Communications, Second Edition*: CRC Press, 2015.
[148] W. Shieh and I. Djordjevic, *OFDM for Optical Communications*: Academic Press/Elsevier, 2010.
[149] A. M. J. Koonen and E. Tangdiongga, "Photonic Home Area Networks," *Journal of Lightwave Technology*, vol. 32, pp. 591-604, 2014.
[150] S. F. Yu, "Nonlinear dynamics of vertical-cavity surface-emitting lasers," *IEEE Journal of Quantum Electronics*, vol. 35, pp. 332-341, 1999.
[151] M. Asai, Y. Inuzuka, K. Koike, S. Takahashi, and Y. Koike, "High-Bandwidth Graded-Index Plastic Optical Fiber With Low-Attenuation, High-Bending Ability, and High-Thermal Stability for Home-Networks," *Journal of Lightwave Technology*, vol. 29, pp. 1620-1626, 2011.
[152] A. Rissons and J.-C. Mollier, "The Vertical-Cavity Surface Emitting Laser (VCSEL) and Electrical Access Contribution," in *Optoelectronics - Devices and Applications*, P. P. Predeep, Ed., ed: InTech Europe, 2011, pp. 227-254.
[153] N. J. Gomes, A. Nkansah, and D. Wake, "Radio-Over-MMF Techniques-Part I: RF to Microwave Frequency Systems," *Journal of Lightwave Technology*, vol. 26, pp. 2388-2395, 2008.
[154] H. Boom, W. Li, and G. Khoe, "CWDM Technology for Polymer Optical Fiber Networks," in *Proceedings Symposium IEEE/LEOS Benelux Chapter, Delft, The Netherlnads*, 2000.
[155] A. M. J. Koonen, H. Yang, H. D. Jung, S. C. J. Lee, E. Tangdiongga, C. Okonkwo, and H. P. A. Van den Boom, "Optical in-building network techniques," in *LEOS Annual Meeting Conference Proceedings, 2009. LEOS '09. IEEE*, 2009, pp. 622-623.
[156] S. Shimazaki, D. Hanawa, and K. Oguchi, "Cost evaluation analysis for next generation home network using optical fiber," in *Photonics Global Conference (PGC), 2012*, 2012, pp. 1-5.
[157] A. Méndez and T. F. Morse, *Specialty optical fibers handbook*. Amsterdam ; Boston: Academic Press, 2007.
[158] O. Ziemann, H. Poisel, and J. Vinogradov, "Potential of High Speed, Short Distance Optical Data Communication on Large Diameter Optical Fibers," in *Electronics Systemintegration Technology Conference, 2006. 1st*, 2006, pp. 409-414.
[159] H. P. A. Van den Boom, W. Li, P. K. Van Bennekom, I. T. Monroy, and G. D. Khoe, "High-capacity transmission over polymer optical fiber," *IEEE Journal of Selected Topics in Quantum Electronics*, vol. 7, pp. 461-470, 2001.
[160] T. Ishigure, E. Nihei, and Y. Koike, "Optimum refractive-index profile of the graded-index polymer optical fiber, toward gigabit data links," *Applied Optics*, vol. 35, pp. 2048-2053, Apr 20 1996.
[161] G. Yabre, "Theoretical investigation on the dispersion of graded-index polymer optical fibers," *Journal of Lightwave Technology*, vol. 18, pp. 869-877, 2000.

[162] S. Louvros and A. C. Iossifides, "Impulse response analysis of graded index polymer optical fiber," *Optical Fiber Technology*, vol. 12, pp. 262-264, Jul 2006.
[163] J. Siuzdak, "RF Carrier Frequency Selection for Incoherent MIMO Transmission Over MM Fibers," *Journal of Lightwave Technology*, vol. 27, pp. 4960-4963, 2009.
[164] GigaPOF Cable Datasheet [Online]. Available: http://chromisfiber.com
[165] T. Cseh and T. Berceli, "Modeling and Simulation of Mode Filtered Radio over Multimode Fiber Links," *INFOCOMMUNICATIONS JOURNAL*, vol. 7, pp. 20-27, 2015.
[166] L. C. Andrews and R. L. Phillips, *Laser beam propagation through random media*, 2nd ed. Bellingham, Wash.: SPIE Press, 2005.
[167] M. Ijaz, Z. Ghassemlooy, J. Pesek, O. Fiser, H. Le Minh, and E. Bentley, "Modeling of fog and smoke attenuation in free space optical communications link under controlled laboratory conditions," *Journal of Lightwave Technology*, vol. 31, pp. 1720-1726, 2013.
[168] S. Arnon, J. Barry, G. Karagiannidis, R. Schober, and M. Uysal, *Advanced Optical Wireless Communication Systems*: Cambridge University Press, 2012.
[169] C. Liu, Y. Yao, Y. X. Sun, J. J. Xiao, and X. H. Zhao, "Average capacity optimization in free-space optical communication system over atmospheric turbulence channels with pointing errors," *Optics Letters*, vol. 35, pp. 3171-3173, Oct 1 2010.
[170] Z. Ghassemlooy, H. Le Minh, S. Rajbhandari, J. Perez, and M. Ijaz, "Performance analysis of ethernet/fast-ethernet free space optical communications in a controlled weak turbulence condition," *Journal of Lightwave Technology*, vol. 30, pp. 2188-2194, Jul 1 2012.
[171] D. Sadot and N. S. Kopeika, "Forecasting optical turbulence strength on the basis of macroscale meteorology and aerosols: models and validation," *Optical Engineering*, vol. 31, pp. 200-212, 1992.
[172] R. Pernice, A. Parisi, A. And, xf, S. Mangione, G. Garbo, A. C. Busacca, J. Perez, and Z. Ghassemlooy, "Error mitigation using RaptorQ codes in an experimental indoor free space optical link under the influence of turbulence," *IET Communications*, vol. 9, pp. 1800-1806, 2015.
[173] M. A. Khalighi, N. Aitamer, N. Schwartz, and S. Bourennane, "Turbulence mitigation by aperture averaging in wireless optical systems," in *10th International Conference on Telecommunications. ConTEL 2009.* , 2009, pp. 59-66.
[174] V. Weerackody, A. R. Hammons, and D. J. Tebben, "Multi-Input Multi-Output Free Space Optical Satellite Communication Links," in *41st Annual Conference on Information Sciences and Systems, CISS '07.* , 2007, pp. 679-683.
[175] M. A. Jarajreh, Z. Ghassemlooy, and W. P. Ng, "Improving the chromatic dispersion tolerance in long-haul fibre links using the coherent optical orthogonal frequency division multiplexing," *IET Microwaves, Antennas & Propagation*, vol. 4, pp. 651-658, 2010.
[176] M. A. Jarajreh, J. L. Wei, J. M. Tang, Z. Ghassemlooy, and W. P. Ng, "Effect of number of sub-carriers, cyclic prefix and analogue to digital converter parameters on coherent optical orthogonal frequency division multiplexing modem's transmission performance," *IET Communications*, vol. 4, pp. 213-222, 2010.

[177] T. Kobayashi, A. Sano, E. Yamada, Y. Miyamoto, H. Takara, and A. Takada, "Electro-optically multiplexed 110 Gbit/s optical OFDM signal transmission over 80 km SMF without dispersion compensation," *Electronics Letters*, vol. 44, pp. 225-226, 2008.
[178] T. Nguyen, S. Mhatli, E. Giacoumidis, L. V. Compernolle, M. Wuilpart, and P. Mégret, "Fiber Nonlinearity Equalizer Based on Support Vector Classification for Coherent Optical OFDM," *IEEE Photonics Journal*, vol. 8, pp. 1-9, 2016.
[179] A. Nagate, K. Hoshino, M. Mikami, and T. Fujii, "A field trial of multi-cell cooperative transmission over LTE system," in *2011 IEEE International Conference on Communications (ICC)*, 2011, pp. 1-5.
[180] CommScope, "In-Building Wireless Solutions," 2012.
[181] R. E. Freund, C. Bunge, N. N. Ledentsov, D. Molin, and C. Caspar, "High-speed transmission in multimode fibers," *Journal of Lightwave Techenology*, vol. 28, pp. 569-586, 2010.
[182] H. Samimi and M. Uysal, "End-to-End performance of mixed RF/FSO transmission systems," *Journal of Optical Communications and Networking*, vol. 5, pp. 1139-1144, 2013/11/01 2013.
[183] D. Visani, G. Tartarini, M. N. Petersen, L. Tarlazzi, and P. Faccin, "Link design rules for cost-effective short-range radio over multimode fiber systems," *Microwave Theory and Techniques, IEEE Transactions on*, vol. 58, pp. 3144-3153, 2010.
[184] 3GPP, "Evolved universal terrestrial radio access (E-UTRA);physical channels and modulation," vol. 3GPP TS36.211 V10.4.0, Rel-10, 2011.
[185] L. N. Binh, *Optical fiber communications systems : theory and practice with MATLAB and Simulink models*. Boca Raton, FL: CRC Press, 2010.
[186] G. P. Agrawal, *Nonlinear Fiber Optics*: Academic Press, 2013.
[187] M. G. Larrode and A. M. J. Koonen, "Theoretical and experimental demonstration of OFM robustness against modal dispersion impairments in radio over multimode fiber links," *Journal of Lightwave Technology*, vol. 26, pp. 1722-1728, 2008.
[188] J. Siuzdak and M. Kowalczyk, "3x3 incoherent MIMO transmission over MM fiber," in *2011 2nd International Conference on Photonics*, 2011, pp. 1-4.
[189] A. A. Farid and S. Hranilovic, "Outage capacity optimization for free-space optical links with pointing errors," *Journal of Lightwave Technology*, vol. 25, pp. 1702-1710, 2007.
[190] I. E. Lee, Z. Ghassemlooy, W. P. Ng, and M.-A. Khalighi, "Joint optimization of a partially coherent Gaussian beam for free-space optical communication over turbulent channels with pointing errors," *Optics Letters*, vol. 38, pp. 350-352, 2013.
[191] H. K. Al-Musawi, W. P. Ng, Z. Ghassemlooy, C. Lu, and N. Lalam, "Experimental analysis of EVM and BER for indoor radio-over-fibre networks using polymer optical fibre," in *2015 20th European Conference on Networks and Optical Communications*, 2015, pp. 1-6.
[192] H. A. Mahmoud and H. Arslan, "Error vector magnitude to SNR conversion for nondata-aided receivers," *IEEE Transactions on Wireless Communications*, vol. 8, pp. 2694-2704, May 2009.
[193] J. Nagar, S. D. Campbell, and D. H. Werner, "Multi-objective optimization for GRIN lens design," in *2015 IEEE Intern. Symp. on Antennas and Propagation & USNC/URSI National Radio Science Meeting*, 2015, pp. 1326-1327.

[194] Rohde&Schwarz, "R&S FSW-K70 vector signal analysis user manual," ed. Munchen, Germany, 2015.
[195] S. Y. Sun, Y. L. Hu, H. H. Chen, and W. X. Meng, "Joint pre-equalization and adaptive combining for CC-CDMA systems over asynchronous frequency-selective fading channels," *IEEE Transactions on Vehicular Technology*, vol. 65, pp. 5175-5184, 2016.
[196] 3GPP, "LTE; Evolved universal terrestrial radio access (E-UTRA); Base station (BS) radio transmission and reception (3GPP TS 36.104 Release 12)," vol. 12.6.0, 2015.
[197] N. A. M. Nor, Z, J. Bohata, P. Saxena, M. Komanec, S. Zvanovec, M. R. Bhatnagar, and M. A. Khalighi, "Experimental investigation of all-optical relay-assisted 10 Gb/s FSO link over the atmospheric turbulence channel," *Journal of Lightwave Technology*, vol. 35, pp. 45-53, 2017.
[198] M. Pavlu and J. Poliak, "Modeling of the multichannel optical wireless link," in *2013 Conference on Microwave Techniques (COMITE)*, 2013, pp. 79-82.
[199] P. A. Haigh, A. Burton, K. Werfli, H. L. Minh, E. Bentley, P. Chvojka, W. O. Popoola, I. Papakonstantinou, and S. Zvanovec, "A Multi-CAP Visible-Light Communications System With 4.85-b/s/Hz Spectral Efficiency," *IEEE Journal on Selected Areas in Communications*, vol. 33, pp. 1771-1779, 2015.
[200] T. Cseh and T. Berceli, "Efficient compensation methods for modal dispersion in radio over multimode fiber links," in *2014 20th International Conference on Microwaves, Radar, and Wireless Communication (MIKON)*, 2014, pp. 1-3.
[201] T. Cseh, H. K. Al-Musawi, M. M. Abadi, Z. Ghassemlooy, W. P. Ng, E. Udvary, T. Berceli, and S. Zvanovec, "Improvements in combined radio over multimode fibre and radio over FSO systems by applying mode filtering," in *2015 17th International Conference on Transparent Optical Networks (ICTON)*, 2015, pp. 1-4.
[202] J. Pesek, O. Fiser, J. Svoboda, and V. Schejbal, "Modeling of 830 nm FSO Link Attenuation in Fog or Wind Turbulence," *Radio Engineering*, vol. 19, pp. 237-241, Jun 2010.
[203] I. I. Kim, B. McArthur, and E. J. Korevaar, "Comparison of laser beam propagation at 785 nm and 1550 nm in fog and haze for optical wireless communications," in *Information Technologies 2000*, 2001, pp. 26-37.
[204] M. Grabner and V. Kvicera, "Multiple Scattering in Rain and Fog on Free-Space Optical Links," *Journal of Lightwave Technology*, vol. 32, pp. 513-520, 2014.
[205] I. E. Lee, Z. Ghassemlooy, W. P. Ng, V. Gourdel, M. A. Khalighi, S. Zvanovec, and M. Uysal, "Practical implementation and performance study of a hard-switched hybrid FSO/RF link under controlled fog environment," in *2014 9th International Symposium on Communication Systems, Networks & Digital Sign (CSNDSP)*, 2014, pp. 368-373.
[206] M. Al Naboulsi, F. de Fornel, H. Sizun, M. Gebhart, E. Leitgeb, S. S. Muhammad, B. Flecker, and C. Chlestil, "Measured and predicted light attenuation in dense coastal upslope fog at 650, 850, and 950 nm for free-space optics applications," *Optical Engineering*, vol. 47, Mar 2008.
[207] T. Kanesan, W. P. Ng, Z. Ghassemlooy, and C. Lu, "Theoretical and experimental design of an alternative system to 2x2 MIMO for LTE over 60 km directly modulated RoF link," in *2012 IEEE Global Communications Conference (GLOBECOM)*, 2012, pp. 2959-2964.

[208] C. Johnson, *Long Term Evolution in Bullets*: Johnson, 2012.
[209] D. Gilstrap, "Ericsson mobility report: on the pulse of the networked society," 2014.
[210] T. Kamisaka, T. Kuri, and K. Kitayama, "Simultaneous modulation and fiber-optic transmission of 10-Gb/s baseband and 60-GHz-band radio signals on a single wavelength," *IEEE Transactions on Microwave Theory and Techniques,* vol. 49, pp. 2013-2017, 2001.
[211] I. Gasulla and J. Capmany, "Simultaneous baseband and radio over fiber signal transmission over a 5 km MMF link," in *International Topical Meeting on Microwave Photonics, 2008. jointly held with the 2008 Asia-Pacific Microwave Photonics Conference. MWP/APMP 2008.* , 2008, pp. 209-212.
[212] C. Lethien, C. Loyez, J.-P. Vilcot, N. Rolland, and P. A. Rolland, "10 GbE and radio over fiber dual transmission through polymer optical fiber," *Applied Physics Express,* vol. 4, p. 112502, 2011.
[213] T. Ishigure, Y. Koike, and J. W. Fleming, "Optimum index profile of the perfluorinated polymer-based GI polymer optical fiber and its dispersion properties," *Journal of Lightwave Technology,* vol. 18, pp. 178-184, 2000.
[214] I. Djordjevic, W. Ryan, and B. Vasic, *Coding for Optical Channels*: Springer US, 2010.
[215] J. Siuzdak, G. Stepniak, M. Kowalczyk, and L. Maksymiuk, "Instability of the Multimode Fiber Frequency Response Beyond the Baseband for Coherent Sources," *Photonics Technology Letters, IEEE,* vol. 21, pp. 993-995, 2009.
[216] R. A. Shafik, M. S. Rahman, and A. H. M. R. Islam, "On the extended relationships among EVM, BER and SNR as performance metrics," *ICECE 2006: Proceedings of the 4th International Conference on Electrical and Computer Engineering,* pp. 408-411, 2006.
[217] D. Hillerkuss, *Single-Laser Multi-Terabit/s Systems* vol. 9: KIT Scientific Publishing, 2013.
[218] B. Nebendahl, W. Freude, C. Koos, J. Leuthold, M. Huebner, R. Schmogrow, A. Josten, D. Hillerkuss, S. Koenig, M. Winter, W. Freude, C. Koos, J. Leuthold, J. Meyer, M. Dreschmann, M. Huebner, D. Hillerkuss, J. Leuthold, and M. Winter, "EVM as New Quality Metric for Optical Modulation Analysis," *2013 Saudi International Electronics, Communications and Photonics Conference (Siecpc),* 2013.
[219] T. Kanesan, W. P. Ng, Z. Ghassemlooy, and C. Lu, "Experimental Verification of Optimized LTE-RoF System for eNB Cell Radius Improvement," *IEEE Photonics Technology Letters,* vol. 24, pp. 2210-2213, 2012.
[220] F. Barrami, Y. Le Guennec, E. Novakov, and P. Busson, "Impact of VCSEL nonlinearity on discrete MultiTone modulation: Quasi-static approach," in *2014 21st International Conference on Telecommunications (ICT)*, 2014, pp. 113-118.
[221] L. Maoliu, Z. Qijun, and X. Qinghua, "EVM simulation and its comparison with BER for different types of modulation," in *TENCON 2007 - 2007 IEEE Region 10 Conference*, 2007, pp. 1-4.